

# Operational Nonclassicality in Quantum Communication Networks

Brian Doolittle,<sup>1,2</sup> Felix Leditzky,<sup>3</sup> and Eric Chitambar<sup>4</sup>

<sup>1</sup>*Aliro Quantum Technologies, Brighton, Massachusetts, 02135, USA*

<sup>2</sup>*Department of Physics, University of Illinois Urbana-Champaign, Urbana, Illinois, 61801, USA*

<sup>3</sup>*Department of Mathematics, University of Illinois Urbana-Champaign, Urbana, Illinois, 61801, USA*

<sup>4</sup>*Department of Electrical and Computer Engineering, Coordinated Science Laboratory, University of Illinois Urbana-Champaign, Urbana, Illinois, 61801, USA*

(Dated: March 6, 2024)

To quantify quantum advantage in communication networks, we apply an operational framework for witnessing quantum nonclassicality. Following previous approaches in the field, this framework first computes linear constraints on the input/output probabilities that arise in classical networks when the amount of communication is bounded. We then apply variational quantum algorithms to optimize these probabilities when quantum communication resources are introduced. Any violation of the classical constraints indicates that extra classical communication is needed to simulate the comparable quantum network, thereby demonstrating an explicit quantum advantage. We demonstrate nonclassicality in many basic networks such as entanglement-assisted point-to-point and multi-point channels. In all examples, we find that equipping classical or quantum channels with entanglement leads to nonclassicality, whereas networks having multiple senders do not require entanglement to achieve nonclassicality. Finally, we discuss how our approaches could be implemented on quantum networking hardware and used to automatically establish certain protocols.

## I. INTRODUCTION

Quantum networks promise to revolutionize science and technology by enhancing communication systems with entanglement and quantum communication resources. Quantum communication networks are necessary for scaling quantum technologies such as distributed quantum sensing, distributed quantum computing, and long-distance quantum secure communications [1–4]. Although large-scale fault tolerant quantum systems demonstrate a clear non-classical advantage, there is still much to learn about what advantages can be realized in near-term quantum networks. Indeed, characterizing and demonstrating near-term quantum advantages is crucial for justifying the continued development of quantum networks, as well as gaining insight into fundamental physics.

The advantages of quantum networks are a product of their communication resources, the units of currency consumed to share and correlate information between parties in the network. *Dynamic* resources pass information from one party to another, *e.g.* one bit or qubit of communication, whereas *static* resources correlate two or more parties, *e.g.* classical shared randomness or quantum entanglement. From weakest to strongest the resources are ordered as shared randomness, entanglement, classical communication, and quantum communication.

Quantum advantage is typically expressed in terms of communication or computational complexity [5, 6], in which the number of quantum resources needed to execute a distributed information processing is shown to scale more efficiently than what is classically possible. Unfortunately, demonstrating communication complexity advantages often requires extensive quantum resources [6], a requirement that existing quantum hardware cannot easily realize.

An alternative and less demanding form of quantum advantage can be framed in terms of simulating the behavior of some device that has classical inputs and outputs. In information-theoretic terms, this is known as the channel simulation problem [7–9], and in this work we focus on the zero-error version of this problem [10]. If the channel can be simulated using fewer dynamic quantum resources than what is classically necessary (*i.e.* fewer qubits than bits), then a quantum advantage is realized. This line of research builds on prior work investigating quantum advantages in the Bell nonlocality scenario [11–19], point-to-point communication channels [20–28], random-access codes [29–33], and more complex scenarios [25, 34]. A general *nonclassicality* framework that captures all of these settings was introduced by Bowles *et al.* [35] where this framework extends the idea of local hidden variable models [36] to causal models with limited signaling.

In this work, we build on this framework and develop a formal method with accompanying software [37] for witnessing and maximizing nonclassicality in quantum networks. Taking a hardware-agnostic approach, we consider a communication network composed of independent black box devices that communicate with each other in a fixed causal structure using a fixed amount of communication resources. Such signaling black box systems are sometimes referred to as Bayesian networks [38], which are studied in fields such as causal inference [39]. These black box communication networks may be depicted as a directed acyclic graph (DAG) showing the network’s causal structure where each directed link in the DAG represents one-way noiseless communication capable of transmitting  $d$  bits (for classical networks) or  $d$  qubits (for quantum networks).

In a single shot, the network accepts a discrete classical input  $\vec{x} \in \mathcal{X}$  and returns a discrete classical output

$\vec{y} \in \vec{\mathcal{Y}}$  where the black box devices independently process their local information and use their allocated resources to communicate and correlate their information. After many shots, the network can be characterized by its *behavior*, the probability distribution  $\{P(\vec{y}|\vec{x})\}_{\vec{x},\vec{y}}$  describing the classical input-output data. Similar to Bell nonlocality, the classical constraints of locality, causality, and realism impose bounds on the classical network’s behaviors. When an unlimited amount of randomness is shared globally amongst all devices, these bounds correspond to linear inequalities. When a behavior violates such classicality inequalities, it is referred to as *nonclassical*.

A quantum network can realize this type of nonclassicality by allowing for shared entanglement between certain devices or using directed quantum communication in place of classical communication. Such quantum violations of classicality inequalities are not just mathematical artifacts, as they have practical uses such as semi-device-independent entanglement witnessing [40] and providing advantages in nonlocal games [6, 41, 42] and network communication tasks [43–45].

Our goal is to demonstrate a simulation advantage across a range of quantum resource configurations in networks. To this end, we apply the nonclassicality framework introduced by Bowles *et al.* [35] to complex signaling scenarios, deriving a large range of nonclassicality witnesses and demonstrating quantum violations to these bounds. We then follow the variational quantum optimization applied by Doolittle *et al.* [46–48] to maximize nonclassicality in quantum communication networks. Our main contributions include demonstrating quantum violations of classicality broadly across quantum communication networks and the development of variational quantum algorithms for establishing quantum network protocols.

We begin with an overview of our applied methods. In Section II A, we introduce our semi-device-independent approach to characterizing the behaviors of communication networks. Then in Section II B, we discuss how to derive linear constraints that bound the behaviors of classical communication networks. Next in Section II C we show how violations to these classicality constraints serve as operational tests for witnessing nonclassicality. In Section II D we characterize the behaviors of quantum networks. Finally, in Section II E, we discuss how variational quantum optimization methods can be applied maximize nonclassicality in quantum communication networks.

Our main results apply our methods across a wide range of network scenarios, producing numerical evidence that identifies causal structures and resource configurations that admit nonclassicality. In Section III A, we consider bipartite signaling scenarios, showing that our numerical results are consistent with similar results in the literature. In Section III B, we investigate nonclassicality in *multiaccess networks* that have multiple senders and one receiver. We identify cases where quantum resources yield significant operational advantages over classical re-

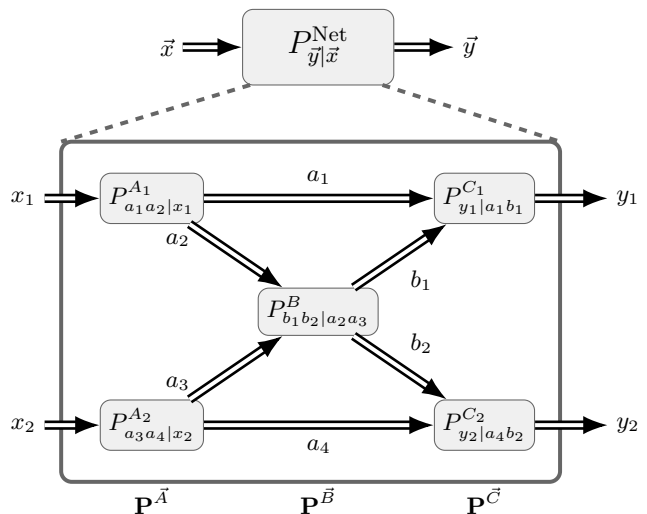


**FIG. 1:** The internal structure of a device with classical input  $\vec{x} \in \vec{\mathcal{X}}$  and output  $\vec{y} \in \vec{\mathcal{Y}}$  are exposed to show a classical communication network. The directed acyclic graph (DAG) depicts the causal structure and information flow through the network. Each device operates independently from the others. The DAG also describes the tensor decomposition for the network’s behavior as  $\mathbf{P}^{\text{Net}} = (\mathbf{P}^{C_1} \otimes \mathbf{P}^{C_2})(\mathbb{I}_{d_1} \otimes \mathbf{P}^B \otimes \mathbb{I}_{d_4})(\mathbf{P}^{A_1} \otimes \mathbf{P}^{A_2})$ .

sources. In Section III C, we investigate nonclassicality in broadcast networks in which one sender signals to multiple receivers. Remarkably, we find no violations for assisted quantum communication, however, when entanglement is present, quantum advantages can be witnessed. Finally, in Section III D, we investigate nonclassicality in multipoint communication networks having two senders, two receivers, and intermediate processing devices. We find that unassisted quantum communication is sufficient for demonstrating nonclassicality in all considered multipoint cases. Furthermore, our results indicate that entanglement shared between senders leads to greater advantages than when entanglement is shared between the receivers.

## II. METHODS

### A. Communication Networks

At the highest level of abstraction, a communication network can be treated as a “black box” that receives inputs  $\vec{x} \in \vec{\mathcal{X}}$  from its users and generates some output  $\vec{y} \in \vec{\mathcal{Y}}$  (see Fig. 1). More structure is added to the problem by assuming that the inputs and outputs are linked by a specific type of causal network that reflects the physical structure and flow of information in the network. These communication networks can be represented by a directed acyclic graph (DAG), denoted as Net, in which each node corresponds to a different party who can locally process the received information, and the

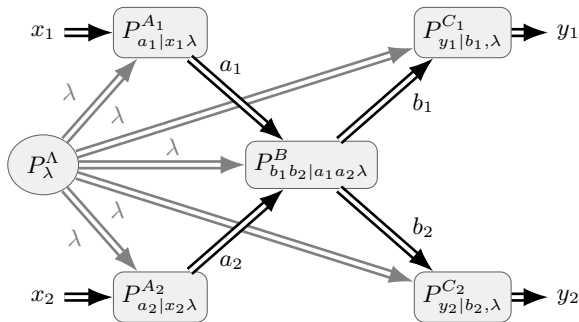


**FIG. 2:** Classical Network assisted by global shared randomness. A source  $\Lambda$  emits a shared random value  $\lambda \in \{0, 1, 2, \dots\}$  drawn from a discrete set of infinite length. The light gray double arrows show that each device receives the value  $\lambda$ .

edges represent noiseless communication channels with the dimension of each channel specified by the elements of a vector  $\vec{d}$ . The entire network communication setup can then be denoted by  $\text{Net}(\vec{\mathcal{X}} \xrightarrow{\vec{d}} \vec{\mathcal{Y}})$ , where we have fixed the input and output alphabets,  $\vec{\mathcal{X}}$  and  $\vec{\mathcal{Y}}$ , the network structure  $\text{Net}$ , and edge capacities  $\vec{d}$ .

The overall objective is to determine what type of network behaviors  $\mathbf{P}^{\text{Net}}: \vec{\mathcal{X}} \rightarrow \vec{\mathcal{Y}}$  are achievable for a given  $\text{Net}(\vec{\mathcal{X}} \xrightarrow{\vec{d}} \vec{\mathcal{Y}})$  when the underlying components are classical versus quantum. In this notation, the network behavior  $\mathbf{P}^{\text{Net}} \in \mathbb{R}^{|\vec{\mathcal{Y}}| \times |\vec{\mathcal{X}}|}$  refers to a classical channel represented as the column stochastic matrix

$$\mathbf{P}^{\text{Net}} \equiv \sum_{\vec{y} \in \vec{\mathcal{Y}}} \sum_{\vec{x} \in \vec{\mathcal{X}}} P_{\vec{y}|\vec{x}}^{\text{Net}} \langle \vec{y} | \vec{x} \rangle \quad (1)$$

where  $P_{\vec{y}|\vec{x}}^{\text{Net}}$  denotes the channel's transition probabilities. We then denote the set of all such behaviors as  $\mathbb{P}_{\vec{\mathcal{Y}}|\vec{\mathcal{X}}}$ . More details on black box behaviors can be found in Appendix B.

**Remark.** The dimension  $d$  of a noiseless channel in our framework equivalently refers to the size of its Hilbert space, the number of classical messages it can transmit, and its signaling dimension. For any classical channel  $\mathbf{P}^{\text{Net}}$ , its *signaling dimension* is the minimum amount of noiseless classical communication needed between a sender and receiver who share randomness so that they can perfectly simulate the channel  $\mathbf{P}^{\text{Net}}$  [22, 26]. It has been proven that if  $\mathbf{P}^{\text{Net}}$  is built using the communication of  $\log d$  qubits, then its signaling dimension is  $d$ ; i.e. one could also build the channel by sending  $\log d$  bits [20]. Consequently, we can realize nonclassicality in a communication setup only when that channel is used in concert with other quantum resources.

## B. Classical Network Polytopes

We begin by characterizing fully classical networks. As shown in Fig. 2, we consider the scenario in which randomness  $\lambda$  with probability mass function  $P_\lambda^\Lambda$  is distributed from some source  $\Lambda$  to all the devices on the network. The assumption of globally shared randomness (GSR) is not always justified, and it is an active area of research to consider its relaxation [49]. However, we consider it here since there are many scenarios in which global shared randomness is a reasonably accessible classical resource, and it enables us to identify many instances of nonclassicality.

We let  $\mathbb{C}^{\text{Net}}$  denote the collection of all behaviors  $\mathbf{P}^{\text{Net}}$  for a given network  $\text{Net}(\vec{\mathcal{X}} \xrightarrow{\vec{d}} \vec{\mathcal{Y}})$ . Due to the shared randomness,  $\mathbb{C}^{\text{Net}}$  forms a convex polytope referred to as the *classical network polytope*. The vertices of this polytope are the set of deterministic behaviors [35],

$$\mathbb{V}^{\text{Net}} \equiv \{\mathbf{V} \in \mathbb{C}^{\text{Net}} \mid \mathbf{V} \in \mathbb{B}^{|\vec{\mathcal{Y}}| \times |\vec{\mathcal{X}}|}\} \quad (2)$$

that the classical network can implement. A deterministic behavior  $\mathbf{V} \in \mathbb{V}^{\text{Net}}$  is formed when each local node performs a deterministic function on its received data. Note that the domain and range of these functions are determined entirely by the sizes of the input/output sets  $\vec{\mathcal{X}}/\vec{\mathcal{Y}}$  and the dimensions of the connecting channels  $\vec{d}$ . More details on the behavior of classical communication networks can be found in Appendix C.

Convex polytopes can equivalently be expressed as the intersection of linear half-spaces [50]. In this representation, the classical network polytope can be written as

$$\mathbb{C}^{\text{Net}} = \bigcap_{i=1}^{|\mathbb{F}^{\text{Net}}|} \left\{ \mathbf{P} \in \mathbb{P}_{\vec{\mathcal{Y}}|\vec{\mathcal{X}}} \mid \gamma_i \geq \langle \mathbf{F}_i, \mathbf{P} \rangle \right\}, \quad (3)$$

where  $\langle \mathbf{F}, \mathbf{P} \rangle \equiv \sum_{\vec{y} \in \vec{\mathcal{Y}}} \sum_{\vec{x} \in \vec{\mathcal{X}}} F_{\vec{y}, \vec{x}} P_{\vec{y}|\vec{x}}$  and the set of facet inequalities is defined as

$$\mathbb{F}^{\text{Net}} \equiv \left\{ \left( \gamma_k \in \mathbb{Z}_{>0}, \mathbf{F}_k \in \mathbb{Z}_{\geq 0}^{|\vec{\mathcal{Y}}| \times |\vec{\mathcal{X}}|} \right) \right\}_{k=1}^{|\mathbb{F}^{\text{Net}}|}. \quad (4)$$

Here, each tuple  $(\gamma, \mathbf{F})$  denotes a linear half-space inequality  $\gamma \geq \langle \mathbf{F}, \mathbf{P} \rangle$  that tightly bounds the classical network polytope  $\mathbb{C}^{\text{Net}}$ .

It is also important to note that classical network polytopes can exhibit a considerable amount of symmetry [51]. First, the local input and output alphabets can be relabeled without altering the classical network polytope. Hence, the classical network polytope is invariant to local permutations of its input or output sets. Second, indistinguishable devices in the network may be swapped without altering the classical network polytope. Note that two devices are indistinguishable if they have the same number of inputs, number of outputs, and the causal structure of the network is unchanged upon swapping the two devices. These symmetries are important because they can be used to simplify the description of classical network polytopes.

### C. Witnessing Nonclassicality

We define a nonclassicality witness as any linear black box game  $(\gamma, \mathbf{G})$  satisfying  $\gamma \geq \langle \mathbf{G}, \mathbf{P} \rangle$  for all  $\mathbf{P} \in \mathbb{C}^{\text{Net}}$ . That is, no behavior in the classical network polytope can win the game, however, there exist nonclassical behaviors that achieve winning scores. Hence, a winning score, or *violation*, of the inequality  $\langle \mathbf{G}, \mathbf{P} \rangle > \gamma$  implies that the behavior  $\mathbf{P} \notin \mathbb{C}^{\text{Net}}$  is nonclassical. Thus, nonclassicality witnesses serve as operational tests of nonclassicality. The facet inequalities  $\mathbb{F}^{\text{Net}}$  that tightly bound the classical network polytope are nonclassicality witnesses, however, we do not require nonclassicality witnesses to be tight (see. Fig. 5).

In this work, we consider two types of nonclassicality witnesses. The first being facet inequalities of the classical network polytope  $(\gamma, \mathbf{F}) \in \mathbb{F}^{\text{Net}}$  as defined in Eq. (4). The advantage of using facet inequalities to witness nonclassicality is that they tightly bound the classical network polytope. Hence facet inequalities are more sensitive to witnessing nonclassicality than other witnesses that are not tight. The drawback of using facet inequalities is that they are difficult to compute in general.

The second type of nonclassicality witness are *simulation games* defined as any linear black box  $(\gamma, \mathbf{V})$  where  $\mathbf{V}$  is a deterministic behavior (see Eq. 2). The advantage of using simulation games as nonclassicality witnesses is that they can be derived with relative ease, they correspond to clear information processing tasks, and as shown in Lemma 6 of Appendix B, the average score of a simulation game corresponds directly to how much the given behavior deviates from  $\mathbf{V}$  in variational distance as

$$D(\mathbf{V}, \mathbf{P}) \equiv \frac{1}{2|\mathcal{X}|} \sum_{\vec{x}, \vec{y}} |V_{\vec{y}|\vec{x}} - P_{\vec{y}|\vec{x}}| = 1 - \frac{1}{|\mathcal{X}|} \langle \mathbf{V}, \mathbf{P} \rangle \quad (5)$$

where the sum is over all  $\vec{x} \in \mathcal{X}$  and  $\vec{y} \in \mathcal{Y}$ . If  $D(\mathbf{V}, \mathbf{P}) = 0$ , then  $\mathbf{P} = \mathbf{V}$  and a zero-error simulation has been achieved.

Unfortunately, both the number of vertices and the dimension of behaviors scale exponentially with the number of devices in the network, causing challenges in computing the facet inequalities of classical network polytopes. In the simplest networks, the complete set of facet inequalities can be efficiently computed using a software such as the Polytope Representation Transformation Algorithm (PoRTA) [52]. As classical networks become more complex, the facets of their polytopes cannot efficiently be computed in full. In These cases, the facet inequalities can be derived using linear programming. In this approach, a test behavior  $\mathbf{P} \in \mathbb{P}_{\mathcal{Y}|\mathcal{X}}$  is provided where  $\mathbf{P} \notin \mathbb{C}^{\text{Net}}$ , then the following linear program obtains a facet inequality that is violated by the

test behavior [16]

$$(\gamma^*, \mathbf{G}^*) = \arg \max_{\substack{\gamma \in \mathbb{R} \\ \mathbf{G} \in \mathbb{R}^{|\mathcal{Y}| \times |\mathcal{X}|}}} \langle \mathbf{G}, \mathbf{P} \rangle - \gamma \quad (6)$$

$$\text{s.t. } \langle \mathbf{G}, \mathbf{P} \rangle - \gamma \leq 1 \quad (7)$$

$$\langle \mathbf{G}, \mathbf{V} \rangle - \gamma \leq 0 \quad \forall \mathbf{V} \in \mathbb{V}^{\text{Net}}. \quad (8)$$

Note that if the test behavior is classical  $\mathbf{P} \in \mathbb{C}^{\text{Net}}$ , then the optimal value is  $\langle \mathbf{G}^*, \mathbf{P} \rangle - \gamma^* = 0$ , otherwise the optimal value is one. Naturally, the linear program in Eq. (6) lends way to an interesting algorithm for deciding whether or not a behavior  $\mathbf{P}$  can be simulated by a classical network  $\text{Net}(\vec{\mathcal{X}} \xrightarrow{\vec{\mathcal{A}}} \vec{\mathcal{Y}})$ .

**Algorithm 1.** Given a behavior  $\mathbf{P} \in \mathbb{P}_{\vec{\mathcal{Y}}|\vec{\mathcal{X}}}$  and the set of vertices  $\mathbb{V}^{\text{Net}}$  for the classical network polytope, decide whether  $\mathbf{P} \in \mathbb{C}^{\text{Net}}$ .

1. Solve the linear program in Eq. 6.
2. If  $\langle \mathbf{G}^*, \mathbf{P} \rangle - \gamma^* = 0$ , then  $\mathbf{P} \in \mathbb{C}^{\text{Net}}$ .
3. Otherwise,  $\mathbf{P} \notin \mathbb{C}^{\text{Net}}$  and  $(\gamma^*, \mathbf{G}^*) \in \mathbb{F}^{\text{Net}}$  constitutes a facet inequality of  $\mathbb{C}^{\text{Net}}$ .
4. **Return:** A boolean value indicating whether  $\mathbf{P} \in \mathbb{C}^{\text{Net}}$  and the nonclassicality witness  $(\gamma^*, \mathbf{G}^*)$ .

Notably Algorithm 1 provides a means to upper bound the classical simulation cost. That is, the optimization program returns a maximal value  $\gamma = 0$  when the behavior is contained by the classical network polytope. Thus, if the vertices of the classical network polytope can be enumerated, then classical simulability can be certified by the linear programming.

In our supplemental software [37], facet inequalities of classical network polytopes are computed using both methods. We apply PoRTA via the Julia programming language using the XPORTA.jl wrapper [53] exposed through Polyhedra.jl interface [54]. To solve the linear programs, we apply the HiGHS [55] mathematical programming solver exposed via the Julia Mathematical Programming toolbox (JuMP.jl) [56].

Finally, it is important to discuss how we present the violations of nonclassicality witnesses that we obtain in this work. First, in Lemma 3 of Appendix B we show that for a given nonclassicality witness  $(\gamma, \mathbf{G})$ , the maximal score possible is

$$\hat{\gamma} = \sum_{\vec{x} \in \mathcal{X}} \max_{\vec{y} \in \mathcal{Y}} G_{\vec{y}, \vec{x}} \geq \langle \mathbf{G}, \mathbf{P} \rangle. \quad (9)$$

Furthermore, without loss of generality, we may use Lemma 4 in Appendix B to rescale the maximal possible score as  $\hat{\gamma} = 1$  and the classical bound as  $\gamma = 0$ . In doing so, the violations of different inequalities can be compared with greater consistency.

### D. Quantum Communication Networks

We investigate the behaviors of communication networks in which classical communication resources are replaced or assisted by quantum communication resources. As in the classical case, we assume that an unlimited amount of randomness is shared globally across the network, which ensures the convexity of the sets of behaviors that characterize quantum networks. Since our non-classicality framework bounds the amount of signaling, the quantum network may only replace classical channels with quantum channels of equivalent signaling dimension. However, we allow multi-party entanglement across network network devices because it is a static resource that could have been distributed prior to the network receiving its classical input  $\vec{x} \in \vec{\mathcal{X}}$ . We view each unique configuration of entanglement, quantum communication, and classical communication as a distinct *resource configuration* for a given network.

Like classical communication networks, a DAG depicts the causal structure and communication resources used to produce a quantum network's behavior  $\mathbf{P}^{\text{Net}}$ . A quantum network's DAG shows both classical and quantum communication resources as well as three distinct types of quantum network devices: preparation, processing, and measurement devices. A preparation device encodes an input  $x_j \in \mathcal{X}_j$  into a quantum state  $\rho_{x_j}^{A_j} \in D(\mathcal{H}_{\text{Tx}}^{A_j})$  where  $D(\mathcal{H})$  denotes the set of density operators acting on Hilbert space  $\mathcal{H}$ . A processing device  $B_j$  accepts as input a quantum state  $\rho_{\text{Rx}}^{B_j}$  and applies an operation  $\rho_{\text{Tx}}^{B_j} = \mathcal{E}(\rho_{\text{Rx}}^{B_j})$  where  $\mathcal{E}: D(\mathcal{H}_{\text{Rx}}^{B_j}) \rightarrow D(\mathcal{H}_{\text{Tx}}^{B_j})$  is a completely-positive trace-preserving map. A measurement device  $C_j$  measures the quantum state  $\rho_{\text{Rx}}^{C_j} \in D(\mathcal{H}_{\text{Rx}}^{C_j})$  to produce a classical output  $c_j \in \mathcal{C}_j^{\text{Tx}}$ . We assume that quantum communication is noiseless, hence, the identity map  $\text{id}^{A_j \rightarrow B_k}: D(\mathcal{H}_{\text{Tx}}^{A_j}) \rightarrow D(\mathcal{H}_{\text{Rx}}^{B_k})$  takes the output from device  $A_j$  and maps it to the input to device  $B_k$ . Any quantum or classical information that passes through a layer without being operated upon is understood to have an identity map applied to it.

Similarly to classical communication networks, a layered approach can be used to compute the conditional probabilities of the full network. Drawing from the three layer prepare-process-measure example shown in Fig. 3, the global state preparation is  $\rho_{\vec{x}^A}^{\vec{A}} = \bigotimes_{i=1}^{|\vec{A}|} \rho_{x_i^A}^{A_i}$ , the global processing is  $\bigotimes_{j=1}^{|\vec{B}|} \mathcal{E}_{x_j^B}^{\vec{B}}$ , and the global measurement is  $\Pi_{\vec{y}|\vec{x}^C}^{\vec{C}} = \bigotimes_{k=1}^{|\vec{C}|} \Pi_{y_k|x_k^C}^{C_k}$ . Note that  $\vec{x}^{\vec{A}}$ ,  $\vec{x}^{\vec{B}}$ , and  $\vec{x}^{\vec{C}}$  denote the classical inputs to each respective layer where  $\vec{x} \in \vec{\mathcal{X}}^A \times \vec{\mathcal{X}}^B \times \vec{\mathcal{X}}^C$ . The resulting probability is then calculated using the Born rule as

$$P_{\vec{y}|\vec{x}} = \text{Tr} \left[ \Pi_{\vec{y}|\vec{x}^C}^{\vec{C}} \mathcal{S}^{\vec{B} \rightarrow \vec{C}} \circ \mathcal{E}_{\vec{x}^B}^{\vec{B}} \circ \mathcal{S}^{\vec{A} \rightarrow \vec{B}}(\rho_{\vec{x}^A}^{\vec{A}}) \right] \quad (10)$$

where the noiseless channels  $\mathcal{S}^{\vec{A} \rightarrow \vec{B}}$  and  $\mathcal{S}^{\vec{B} \rightarrow \vec{C}}$  ensure that the outputs of one layer are correctly mapped to the

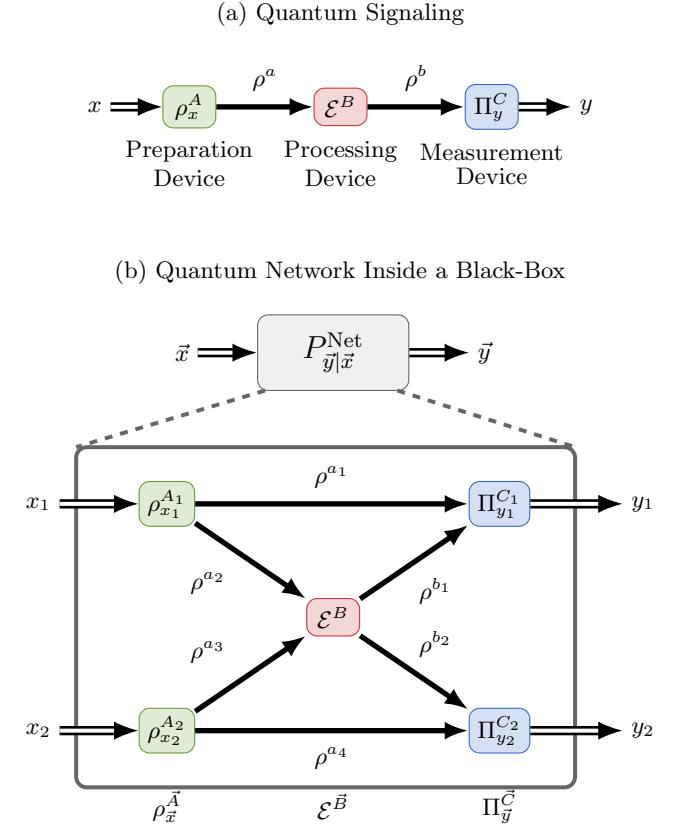


**FIG. 3:** Quantum network DAGs in which single lined arrows depict one-way noiseless quantum communication where double lined arrows show the classical inputs and outputs to the network. a) DAG showing quantum signaling through multiple layers. The network's transition probabilities are  $P_{y|x}^{\text{Net}} = \text{Tr} [\Pi_y^C \mathcal{E}^B(\rho_x^A)]$ . b) A quantum network is shown inside of a black-box. The first layer  $\vec{A}$  contains two preparation nodes (green), the second layer  $\vec{B}$  contains one processing device (red) and two pass through channels, and the third layer  $\vec{C}$  contains two measurement devices (blue).

$$P_{\vec{y}|\vec{x}}^{\text{Net}} = \text{Tr} [\Pi_{y_1}^{C_1} \otimes \Pi_{y_2}^{C_2} \text{id}^{A_1 \rightarrow C_1} \otimes \mathcal{E}^B \otimes \text{id}^{A_2 \rightarrow C_2}(\rho^{A_1} \otimes \rho^{A_2})]$$

next layer as indicated by the network's DAG. Although this is an overly simplistic example, a more thorough description is given in Section II E 1, and many examples are provided alongside our main results.

For a given network DAG  $\text{Net}(\vec{\mathcal{X}} \xrightarrow{\vec{Q}} \vec{\mathcal{Y}})$ , entanglement can assist communication in many ways (see Fig. 4). For a given entanglement structure, we distinguish between three different classes of behaviors that use quantum resources with a specific entanglement configuration where two or more devices share entanglement: (i)  $\mathbb{C}_{\text{EA}}^{\text{Net}}$  entanglement is used but all communication is classical; (ii)  $\mathbb{Q}^{\text{Net}}$  entanglement is not used all communication is quantum; and (iii)  $\mathbb{Q}_{\text{EA}}^{\text{Net}}$  entanglement is used and all communication is quantum. For any fixed entanglement configuration,  $\mathbb{Q}_{\text{EA}}^{\text{Net}}$  is clearly the largest of all, while both  $\mathbb{C}_{\text{EA}}^{\text{Net}}$  and  $\mathbb{Q}^{\text{Net}}$  contain  $\mathbb{C}^{\text{Net}}$ . The relationship between

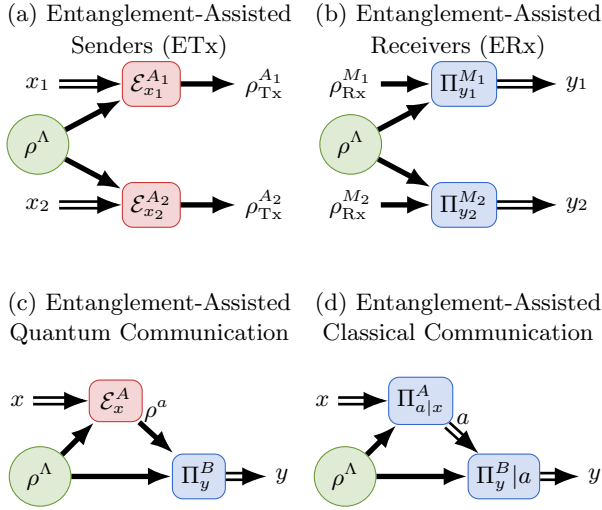


FIG. 4: DAGs for various entanglement-assisted signaling systems resources.

$\mathbb{C}_{\text{EA}}^{\text{Net}}$  and  $\mathbb{Q}^{\text{Net}}$  depends on the dimensions  $\vec{d}$  of the network's channels, the structure of entanglement, and the network's causal structure.

### E. Maximizing Quantum Nonclassicality

Our goal is to find the maximal violation of a nonclassicality witness  $(\gamma, \mathbf{G})$  for a given quantum network DAG, for which we aim to solve the optimization problem

$$\beta^* \equiv \max_{\mathbf{P} \in \mathbb{S}^{\text{Net}}} \langle \mathbf{G}, \mathbf{P} \rangle \quad (11)$$

where  $\mathbb{S}^{\text{Net}} \in \{\mathbb{C}_{\text{EA}}^{\text{Net}}, \mathbb{Q}^{\text{Net}}, \mathbb{Q}_{\text{EA}}^{\text{Net}}\}$  denotes the type of quantum network we are considering.

To solve the optimization problem in Eq. (11), we apply the variational quantum optimization (VQO) framework for quantum networks introduced by Doolittle *et al.* [46]. In general, this framework expresses a quantum network DAG as a parameterized quantum circuit that explicitly encodes the communication resources and the local operations at each device (see Fig. 7). Variational optimization techniques are then used to maximize the objective in Eq. (11). Our methods are applied in our supplementary codebase [37] using the Quantum Network Variational Optimizer (QNetVO) Python package [47] an extension of the PennyLane framework for quantum machine learning [57].

#### 1. A Parameterized Quantum Circuit Model of Quantum Communication Networks

Although our quantum circuit model is restricted to unitary operators applied across qubit subsystems, general quantum operations can be achieved using auxiliary qubits. Thus, our framework can simulate and optimized

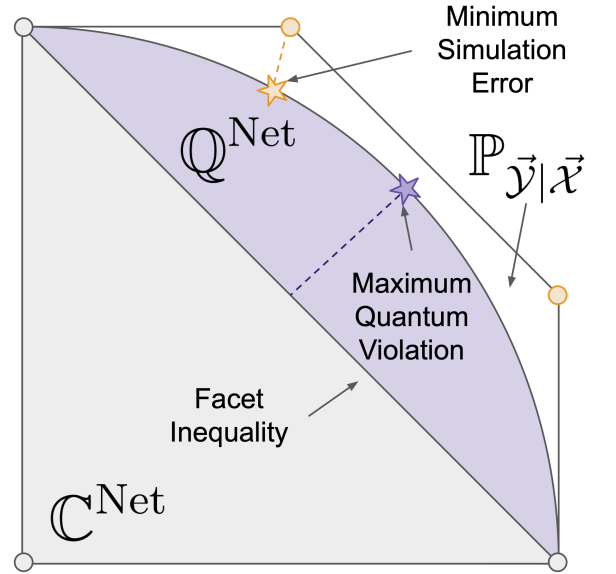


FIG. 5: A qualitative view of quantum nonclassicality as a 2D abstraction of the full probability polytope  $\mathbb{P}_{\vec{y}|\vec{x}}$  (outer pentagon) where the vertices represent deterministic behaviors. The gray shaded triangular region shows the classical network polytope  $\mathbb{C}^{\text{Net}}$ . The purple shaded region shows the set of nonclassical quantum network behaviors  $\mathbb{Q}^{\text{Net}}$  where the global shared randomness ensure convexity of the set. Note that  $\mathbb{C}^{\text{Net}} \subseteq \mathbb{Q}^{\text{Net}} \subseteq \mathbb{P}_{\vec{y}|\vec{x}}$ . The purple star shows the maximal quantum violation of the facet inequality of the classical network polytope. The orange star shows the minimal simulation error that can be achieved by the quantum set as it tries to simulate the nonclassical deterministic behavior (orange vertex).

over mixed state preparations, completely-positive trace-preserving (CPTP) maps, and positive operator-valued measure (POVM) measurements in networks. In addition, our framework accommodates local operations and classical communication (LOCC). As shown in Fig. 6 (d), the result of a midcircuit measurement can be used to condition a future gate operation. However, not all hardware platforms or simulators support midcircuit measurements. The alternative is to use the deferred measurement principle [58] (see Fig. 6(e)), by which a quantum circuit with midcircuit measurements can be recompiled such that measurements occur at the end (see Fig. 6(f)).

We can parameterize a general quantum circuit that simulates a quantum network as  $U^{\text{Net}}(\vec{\theta}_{\vec{x}})$  where the parameters  $\vec{\theta}_{\vec{x}} \subseteq \vec{\theta} \in \mathbb{R}^M$  vary the operations applied in the network where  $\vec{\theta}_{\vec{x}}$  denotes the network's parameters given the input  $\vec{x} \in \vec{\mathcal{X}}$ . Since only a subset of the qubits in the quantum circuit model will be measured, we can express the state prior to measurement as

$$\rho^{\text{Net}}(\vec{\theta}_{\vec{x}}) = \text{Tr}_E \left[ U^{\text{Net}}(\vec{\theta}_{\vec{x}}) |0\rangle\langle 0|^{\otimes N_S \times N_E} U^{\text{Net}}(\vec{\theta}_{\vec{x}})^\dagger \right] \quad (12)$$

where  $U^{\text{Net}}(\vec{\theta}_{\vec{x}})$  operates on the joint Hilbert space

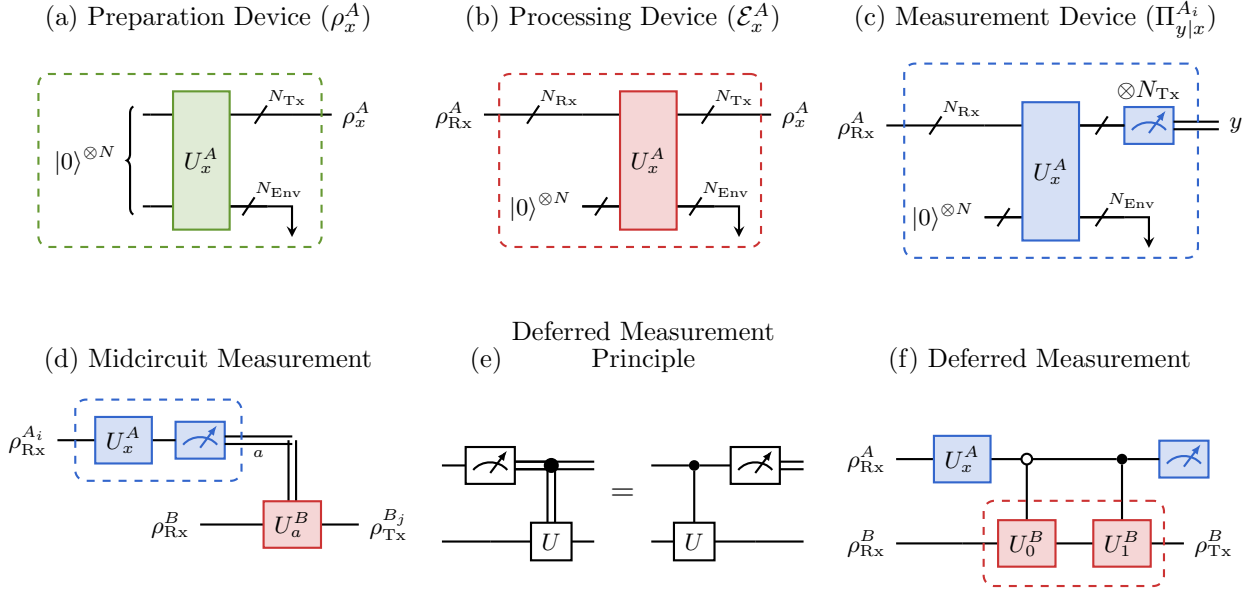


**FIG. 6:** Quantum circuit models of general quantum network devices. (a) State preparation device (green) that prepares the mixed state  $\rho_x^A$  using  $N_{\text{Env}}$  ancillary qubits. (b) Processing device (red) that uses  $N$  ancillary qubits to apply a general CPTP map  $\mathcal{E}_x^A$ . (c) Measurement device (blue) that uses ancillary  $N$  ancillary qubits to perform a POVM measurement  $\{\Pi_{y|x}^A\}_{y,x}$ . (d) Simulation of classical communication from  $A$  to  $B$  using midcircuit measurements. (e) The deferred measurement principle where controlled gate operation prior to measurement commutes with a gate operation controlled on the classical result. (f) Simulation of classical communication from  $A$  to  $B$  using deferred measurements.

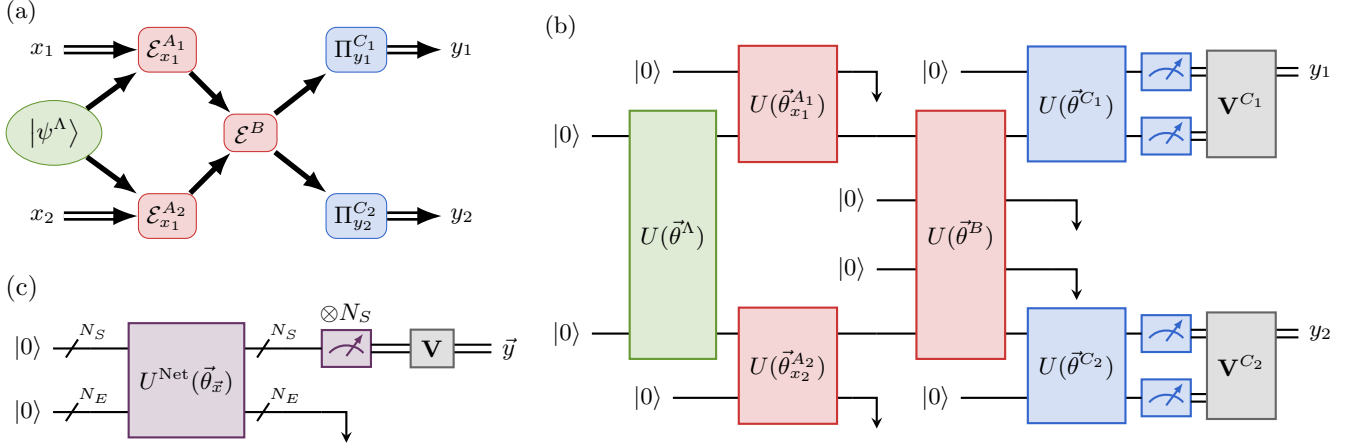


**FIG. 7:** (a) A DAG for an interference network with entangled senders. (b) A parameterized quantum circuit representation of the interference network DAG. (c) A general parameterized quantum circuit.

$\mathcal{H}^{\text{Net}} = \mathcal{H}^S \otimes \mathcal{H}^E$  with  $\mathcal{H}^S$  and  $\mathcal{H}^E$  respectively describe the  $N_S$  qubits that are measured and the  $N_E$  qubit that are discarded. The transition probabilities of the simulated network are then parameterized as

$$P_{\vec{y}|\vec{x}}^{\text{Net}}(\vec{\theta}_{\vec{x}}) = \sum_{\vec{z} \in \mathbb{B}^{N_S}} V_{\vec{y}|\vec{z}}^{\text{Post}} \text{Tr} \left[ |\vec{z}\rangle\langle\vec{z}| \rho_{\vec{x}}^{\text{Net}} \right] \quad (13)$$

where  $\mathbf{V}^{\text{Post}}$  designates a deterministic post-processing map that takes the  $|\vec{Z}| = 2^{N_S}$  outputs from the computational basis measurement into the appropriate output

alphabet  $|\vec{Y}| \leq |\vec{Z}|$  (see Fig. 7.c). As a result, a quantum network's behavior is parameterized as

$$\mathbf{P}^{\text{Net}}(\vec{\theta}) = \sum_{\vec{y} \in \vec{Y}} \sum_{\vec{x} \in \vec{X}} P_{\vec{y}|\vec{x}}^{\text{Net}}(\vec{\theta}_{\vec{x}}) |\vec{y}\rangle\langle\vec{x}|. \quad (14)$$

By locality constraints, the unitary operation  $U^{A_j}(\vec{\theta}_{x_j}^{A_j})$  applied by device  $A_j$  is then parameterized by  $\vec{\theta}_{x_j}^{A_j} \subset \vec{\theta}_{\vec{x}}$ , which is independent of the parameters for the other devices. Hence, the device  $A_j$  has  $|\vec{\theta}^{A_j}| =$

$|\mathcal{X}_j| \times |\vec{\theta}_{x_j}^{A_j}|$  parameters total. For a preparation device that acts on an  $N$ -qubit state (Fig. 6(a)), the number of settings is  $|\vec{\theta}_{x_j}^{A_j}| = 2^{N+1} - 2$  and achieved using the PennyLane's `ArbitraryStatePreparation` circuit ansatz. For both processing and measurement devices (Fig. 6(b,c)), the number of settings is  $|\vec{\theta}_{x_j}^{A_j}| = 4^N - 1$  and achieved using PennyLane's `ArbitraryUnitary` circuit ansatz [57]. As a result, the total number of settings in the network  $|\vec{\theta}|$  scales exponentially with the largest number of qubits used by any device in the network.

We remark that our quantum circuit model for quantum network simulation can be run using any quantum hardware or simulator thereof that can evaluate a quantum circuit. Throughout this work, we use PennyLane's "`default.qubit`" simulator, hence all data shown in this work is obtained on a classical computer.

## 2. Variational Optimization of Quantum Networks

A parameterized quantum network simulation circuit can be optimized using variational optimization (see Fig. 8). In variational optimization, the goal is to solve the optimization problem  $\max_{\vec{\theta} \in \mathbb{R}^M} \text{Gain}(\vec{\theta})$  for some function  $\text{Gain}: \mathbb{R}^M \rightarrow \mathbb{R}$ . Note that the gain function can be restated as a cost function  $-\text{Gain}(\vec{\theta}) = \text{Cost}(\vec{\theta})$  where  $\min_{\vec{\theta}} \text{Cost}(\vec{\theta}) = \max_{\vec{\theta}} \text{Gain}(\vec{\theta})$ . When using variational methods, the optimization is solved by evaluating the gradient vector of the gain function at a certain point  $\nabla_{\vec{\theta}} \text{Gain}(\vec{\theta}) \in \mathbb{R}^M$ . The gradient points in the direction of steepest ascent and can be followed to a (local) maximum. In practice, gradients can be calculated efficiently on classical hardware using backpropagation [59], or evaluated on quantum hardware using finite differences or parameter shift rules [60–63].

We use variational optimization to maximize the score of a linear black box game. In this case, the gain is written as

$$\text{Gain}(\vec{\theta}) = \langle \mathbf{G}, \mathbf{P}^{\text{Net}}(\vec{\theta}) \rangle \quad (15)$$

where the transition probabilities of  $\mathbf{P}^{\text{Net}}(\vec{\theta})$  are the measurement probabilities obtained when simulating the network with settings  $\vec{\theta}$ . We refer to the parameterized quantum network simulation circuit as the variational ansatz. Our goal is then to optimize the settings of the variational network ansatz to maximize the gain, and thereby, the score. We now describe our general variational optimization algorithm, which is a basic application of gradient descent [64].

### Algorithm 2. Maximizing a Quantum Network's Score in a Black Box Game:

**Goal:** For a black box game having reward matrix  $\mathbf{G}$ , solve  $\max_{\vec{\theta} \in \mathbb{R}^M} \langle \mathbf{G}, \mathbf{P}^{\text{Net}}(\vec{\theta}) \rangle$  for a given variational network ansatz  $\mathbf{P}^{\text{Net}}(\vec{\theta})$ . The algorithm is iterative and re-

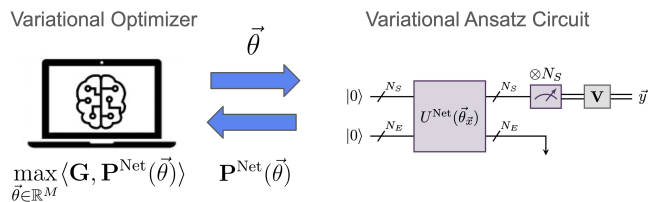


**FIG. 8:** A classical computer performs variational optimization of a parameterized quantum circuit.

quires a `num_steps` parameter specifying the number of iterations to take.

1. Select the input settings  $\vec{\theta}_0 \in \mathbb{R}^M$  at random and initialize a log of settings-cost tuples  $\text{LOG} = [(\vec{\theta}_0, \text{Gain}(\vec{\theta}_0))]$ .
2. For  $i$  in  $\{0, \dots, \text{num\_steps} - 1\}$ :
  - (a) For settings  $\vec{\theta}_i$ , evaluate the gradient  $\nabla \text{Gain}(\vec{\theta}_i)$ .
  - (b) Update the settings by taking a step of size  $\eta$  along the path of steepest ascent as  $\vec{\theta}_{i+1} = \vec{\theta}_i + \eta \nabla \text{Gain}(\vec{\theta}_i)$ .
  - (c) Append the tuple  $(\vec{\theta}_{i+1}, \text{Gain}(\vec{\theta}_{i+1}))$  to LOG.
3. Return the tuple  $(\vec{\theta}^*, \text{Gain}(\vec{\theta}^*))$  that has the minimum cost in LOG.

**Remark.** In practice, we use the Adam [65] optimizer to dynamically adjust the step-size  $\eta$  in step 2.b. Furthermore, different methods for approximating gradients can be applied.

**Remark.** There is no guarantee that the global optimum will be found and the maximal gain achieved in optimization will necessarily lower bound the true maximum. Therefore, it is best practice to repeat the gradient ascent procedure with randomized settings  $\vec{\theta}_{\text{init}}$  each time and to take the best optimization results.

Algorithm 2 serves as a useful tool throughout this work because when a linear inequality  $(\gamma, \mathbf{G})$  represents a nonclassicality witness its violation represents an explicit quantum advantage. This algorithm can be applied to maximize the violation of a facet inequality or minimize the error in a simulation game. For each case, provide an associated algorithm outlining the application.

### Algorithm 3. Establish Nonclassicality in a Quantum Network:

**Goal:** Given any nonclassicality witness  $(\gamma, \mathbf{G})$  and a variational ansatz circuit that simulates a quantum network as  $\mathbf{P}^{\text{Net}}(\vec{\theta})$ , establish a maximally nonclassical behavior.



1. Apply Algorithm 2 to obtain the optimal settings  $\vec{\theta}^*$  and the maximal score  $\langle \mathbf{G}, \mathbf{P}^{\text{Net}}(\vec{\theta}^*) \rangle$ .
2. If  $\langle \mathbf{G}, \mathbf{P}^{\text{Net}}(\vec{\theta}^*) \rangle > \gamma$ , the variational ansatz demonstrates nonclassicality for settings  $\vec{\theta}^*$ . Otherwise,  $\mathbf{P}^{\text{Net}}(\vec{\theta}^*)$  is classically simulable.

**Algorithm 4. Establishing a Deterministic Protocol in a Quantum Network:**

**Goal:** Given a target deterministic behavior  $\mathbf{V}$  to simulate and a variational ansatz circuit that simulates a quantum network as  $\mathbf{P}^{\text{Net}}(\vec{\theta})$ , establish a behavior that approximately simulates  $\mathbf{V}$  within an allowed tolerance  $\epsilon$ . As shown in Lemma 6 in Appendix B, the value  $\langle \mathbf{V}, \mathbf{P}^{\text{Net}} \rangle$  is related to the variational distance  $D(\mathbf{V}, \mathbf{P}^{\text{Net}})$  as shown in Eq. (5). Thus, we aim to minimize the simulation error

$$D(\mathbf{V}, \mathbf{P}^{\text{Net}}) = 1 - \frac{1}{|\mathcal{X}|} \langle \mathbf{V}, \mathbf{P}^{\text{Net}} \rangle = P_{\text{Error}} \leq \epsilon. \quad (16)$$

1. Apply Algorithm 2 to obtain the optimal settings  $\vec{\theta}^*$  and the maximal score  $\langle \mathbf{V}, \mathbf{P}^{\text{Net}}(\vec{\theta}^*) \rangle$ .
2. Using Eq. (16), if  $1 - \frac{1}{|\mathcal{X}|} \langle \mathbf{V}, \mathbf{P}^{\text{Net}}(\vec{\theta}^*) \rangle \leq \epsilon$ , then, for settings  $\vec{\theta}^*$ , the network approximately simulates the target deterministic behavior  $\mathbf{V}$ . Otherwise, the network fails to perform the task encoded by  $\mathbf{V}$  within the allowed tolerance  $\epsilon$ .
3. **Return:** The optimal settings  $\vec{\theta}^*$  and the simulation error  $P_{\text{Error}}^* = 1 - \frac{1}{|\mathcal{X}|} \langle \mathbf{V}, \mathbf{P}^{\text{Net}}(\vec{\theta}^*) \rangle$ .

**Remark.** Upon failure to surpass the specified threshold in either Algorithm 3 or Algorithm 4, the variational optimization in Algorithm 2 can be rerun for another set of randomized initial setting  $\vec{\theta}_{\text{init}}$ . After a set number of retry attempts, the algorithm exits indicating that no violation of classicality or simulation within the allowed tolerance  $\epsilon$  has been found.

It is important to note that our variational optimization methods are compatible with both quantum computing and quantum networking hardware [66]. However, our results are obtained using classical computers to evaluate quantum circuits and their gradients. In doing so, we are able to perform optimizations of quantum circuits in a noiseless setting. Future work can extend our optimizations to quantum networking systems to certify their quantum communication resources, or establish protocols between nodes.

The applied variational quantum optimization techniques offer many advantages. First, the network’s causal structure, communication resources, and free operations are encoded explicitly into the variational ansatz circuit. As a result, a successful optimization returns the settings  $\vec{\theta}^*$  that achieve the minimum cost, thereby providing an example quantum circuit that achieves the desired behavior. Moreover, when applied on quantum hardware, these

methods have shown the capability of optimizing network architectures around unknown noise models, evaluating quantum information properties such as von Neumann entropy, and establishing protocols on uncharacterized hardware [46–48, 67, 68].

### III. RESULTS

#### A. Point-to-Point Communication Scenarios

We first discuss the simplest communication scenario in which a sender device  $A$  communicates to a receiver device  $B$ . We consider the three configurations in Fig. 9 when there is only one bit of one-way communication from the sender to the receiver, that is,  $a \in \mathbb{B}$ . In each scenario, we obtain nonclassicality witnesses that bound the classical network polytope  $\mathbb{C}^{\text{Net}}$  and consider the behaviors of three quantum resource configurations: unassisted quantum communication ( $\mathbb{Q}^{\text{Net}}$ ), entanglement-assisted classical communication ( $\mathbb{C}_{\text{EA}}^{\text{Net}}$ ), and entanglement-assisted quantum communication ( $\mathbb{Q}_{\text{EA}}^{\text{Net}}$ ). We then apply Algorithm 2 to maximize the violation of the classical bounds using variational optimization. Overall, we find that our numerical results are consistent with the results of previous works, while we also find new examples of nonclassicality that have not been reported to our knowledge. These simple examples of nonclassicality demonstrate the advantage of quantum signaling systems in the simplest and most fundamental settings.

##### 1. Point-to-Point Networks

The point-to-point network is a bipartite signaling scenario as shown in Fig. 9(a)). The sender  $A$  is given the input  $x_1 \in \mathcal{X}_1$  and the receiver  $B$  outputs the value  $y_2 \in \mathcal{Y}_2$  where we use  $\mathcal{X}_1 \xrightarrow{d} \mathcal{Y}_2$  to denote this scenario. The point-to-point network describes a classical channel where the sender encodes the input into a compressed message and transmits it to the receiver who decodes the message into a classical output.

The facet inequalities that bound the classical point-to-point network polytope  $\mathbb{C}^{\mathcal{X} \xrightarrow{d} \mathcal{Y}}$  witness the signaling dimension of the communication channel. In Ref. [26], the complete set of facet inequalities bounding the signaling dimension for  $d = 2$  were derived (see Table I).

Additionally, inequality  $b$  of Table I,  $\mathbf{G}_b^{4 \rightarrow 4} = \mathbb{I}_4 = \mathbf{V}^{\text{CV}}$  describes an important simulation game, which we refer to as the *communication value* (CV) game. This simulation game is significant because its score relates to the state discrimination success probability as  $\langle \mathbf{V}^{\text{CV}}, \mathbf{P} \rangle = |\mathcal{X}| P_{\text{Success}}$ . Furthermore, the quantity  $\max_{\mathbf{P} \in \mathbb{Q}^{\text{Net}}} \langle \mathbf{V}^{\text{CV}}, \mathbf{P} \rangle$  is precisely the communication value of a quantum channel as defined in reference [69]. In general, the communication value game is expressed

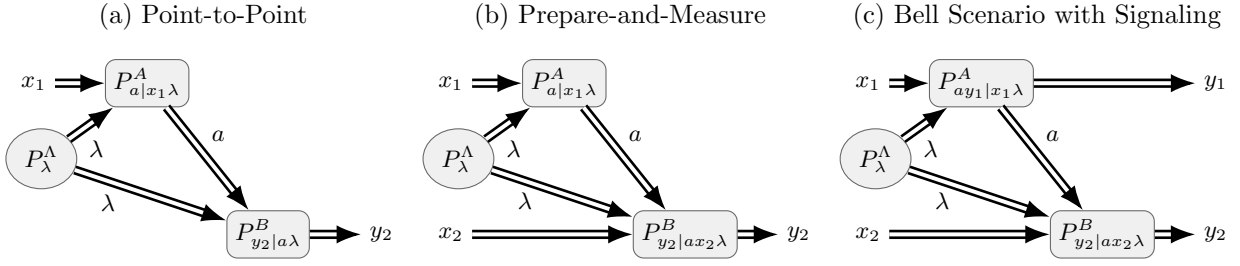


**FIG. 9:** DAGs for bipartite classical signaling scenarios in which a source  $\Lambda$  distributes a shared random value  $\lambda$  to the sender device  $A$  and the receiver device  $B$ . a) Point-to-point signaling  $\mathcal{X}_1 \xrightarrow{d} \mathcal{Y}_2$ , b) prepare-and-measure signaling  $\text{PM}(\mathcal{X}_1 \mathcal{X}_2 \xrightarrow{d} \mathcal{Y}_2)$ , and c) Bell scenario assisted by bounded communication  $\text{BS}(\mathcal{X}_1 \mathcal{X}_2 \xrightarrow{d} \mathcal{Y}_1 \mathcal{Y}_2)$ .

<p>(a) <math>2 \geq \begin{bmatrix} 1 &amp; 0 &amp; 0 \\ 1 &amp; 0 &amp; 0 \\ 0 &amp; 1 &amp; 0 \\ 0 &amp; 0 &amp; 1 \end{bmatrix}</math></p>	<p>(e) <math>4 \geq \begin{bmatrix} 2 &amp; 0 &amp; 0 &amp; 0 \\ 0 &amp; 2 &amp; 0 &amp; 0 \\ 0 &amp; 0 &amp; 1 &amp; 1 \\ 1 &amp; 1 &amp; 1 &amp; 0 \end{bmatrix}</math></p>
<p>(b) <math>2 \geq \begin{bmatrix} 1 &amp; 0 &amp; 0 &amp; 0 \\ 0 &amp; 1 &amp; 0 &amp; 0 \\ 0 &amp; 0 &amp; 1 &amp; 0 \\ 0 &amp; 0 &amp; 0 &amp; 1 \end{bmatrix}</math></p>	<p>(f) <math>4 \geq \begin{bmatrix} 2 &amp; 0 &amp; 0 &amp; 0 &amp; 0 \\ 0 &amp; 1 &amp; 0 &amp; 1 &amp; 0 \\ 0 &amp; 0 &amp; 1 &amp; 0 &amp; 1 \\ 1 &amp; 1 &amp; 1 &amp; 0 &amp; 0 \end{bmatrix}</math></p>
<p>(c) <math>3 \geq \begin{bmatrix} 1 &amp; 1 &amp; 0 &amp; 0 \\ 1 &amp; 0 &amp; 1 &amp; 0 \\ 0 &amp; 1 &amp; 1 &amp; 0 \\ 0 &amp; 0 &amp; 0 &amp; 1 \end{bmatrix}</math></p>	<p>(g) <math>4 \geq \begin{bmatrix} 1 &amp; 0 &amp; 0 &amp; 1 &amp; 0 &amp; 0 \\ 0 &amp; 1 &amp; 0 &amp; 0 &amp; 1 &amp; 0 \\ 0 &amp; 0 &amp; 1 &amp; 0 &amp; 0 &amp; 1 \\ 1 &amp; 1 &amp; 1 &amp; 0 &amp; 0 &amp; 0 \end{bmatrix}</math></p>
<p>(d) <math>4 \geq \begin{bmatrix} 2 &amp; 0 &amp; 0 \\ 0 &amp; 2 &amp; 0 \\ 0 &amp; 0 &amp; 2 \\ 1 &amp; 1 &amp; 1 \end{bmatrix}</math></p>	<p>(h) <math>5 \geq \begin{bmatrix} 1 &amp; 1 &amp; 1 &amp; 0 &amp; 0 &amp; 0 \\ 1 &amp; 0 &amp; 0 &amp; 1 &amp; 1 &amp; 0 \\ 0 &amp; 1 &amp; 0 &amp; 1 &amp; 0 &amp; 1 \\ 0 &amp; 0 &amp; 1 &amp; 0 &amp; 1 &amp; 1 \end{bmatrix}</math></p>

**TABLE I:** [26] Classical upper bounds and reward matrices ( $\gamma \geq \mathbf{G}$ ) for all nonclassicality witnesses bounding the  $d = 2$  point-to-point signaling scenario. Note that all witnesses have four outputs and no more than six inputs. Equivalent witnesses are obtained by relabeling the input and outputs.

as  $(d, \mathbf{V}^{\text{CV}})$  where  $\mathbf{V}^{\text{CV}} \in \mathbb{R}^{d^2 \times d^2}$  and  $V_{y,x}^{\text{CV}} = \delta_{y,x}$ . Note that this game was introduced in reference [26] as the maximum likelihood game and shown to be a facet inequality for all classical point-to-point network polytopes  $\mathbb{C}^{\mathcal{X} \xrightarrow{d} \mathcal{Y}}$  where  $1 < d < |\mathcal{X}| = |\mathcal{Y}|$ .

To demonstrate nonclassicality in the point-to-point signaling scenario, it is insufficient to just replace the classical communication with quantum communication (i.e.  $\mathbb{C}^{\mathcal{X} \xrightarrow{d} \mathcal{Y}} = \mathbb{Q}^{\mathcal{X} \xrightarrow{d} \mathcal{Y}}$ ) [20]. However, nonclassical behaviors are found when using entanglement-assisted classical communication (EACC) or entanglement-assisted quantum communication (EAQC) resource configurations,  $\mathbb{C}_{\text{EA}}^{\mathcal{X} \xrightarrow{d} \mathcal{Y}}$  and  $\mathbb{Q}_{\text{EA}}^{\mathcal{X} \xrightarrow{d} \mathcal{Y}}$ , respectively.

For the case  $d = 2$ , we use variational optimization to maximize the violation of the signaling dimension witnesses in Table I, plotting the results in Fig. 10. The behaviors in the set  $\mathbb{Q}_{\text{EA}}^{\mathcal{X} \xrightarrow{2} \mathcal{Y}}$  are able to achieve the maximal possible violation for each nonclassicality witness. In

general, EAQC resources can achieve the maximal score since entanglement plus one qubit communication allows for the transmission of two bits due to dense coding [70]. Interestingly, a trit ( $d = 3$ ) of classical communication is sufficient to achieve the maximal possible violation for all facet inequalities in Table I except  $\mathbf{G}_b^{4 \rightarrow 4}$ . Thus, a sufficiently large violation of this inequality can witness EAQC of a qubit from a trit of classical communication ( $d = 3$ ).

For EACC, we find no violations for the inequalities  $\mathbf{G}_a^{3 \rightarrow 4}$  and  $\mathbf{G}_b^{4 \rightarrow 4}$ , confirming that entanglement cannot improve the communication value of a classical channel [69]. Nonetheless there still EACC resources still show an operational advantage because all remaining nonclassicality witnesses can be violated. Moreover, we find that these violations require that the sender only uses entanglement in the encoding for certain values of  $x \in \mathcal{X}$  while the entanglement is otherwise discarded. For the game  $\mathbf{G}_h^{6 \rightarrow 4}$ , our methods successfully reproduces the maximal violation derived by Frenkel *et al.* [21].

One practical application of these entanglement-assisted nonclassical behaviors is to certify the presence of entanglement between sender and receiver in a semi-device-independent manner. Suppose that it is known that a bit (or qubit) of communication is used between sender and receiver in a point-to-point network. Then, a violation of any signaling dimension witness bounding the (qu-)bit signaling case witnesses the presence of entanglement between the two parties. Furthermore, entanglement-assisted quantum communication can be discerned from entanglement-assisted classical communication by optimizing the communication value. Indeed, such violations serve as a minimal example of a semi-device-independent tests that can certify LOCC and LOQC resources.

Finally, our results demonstrate that dense-coding protocols can be optimized into a variational circuit ansatz that simulates entanglement-assisted quantum communication in a point-to-point network. Since  $\mathbf{V}^{\text{CV}}$  corresponds to a simulation game, it can be optimized using Algorithm 4. Upon completion of the algorithm, a variational ansatz is optimized such that  $\mathbf{P}(\hat{\theta}^*)$  minimizes the state discrimination error, or equivalently, yields the communication value of the channel. Remarkably, if the

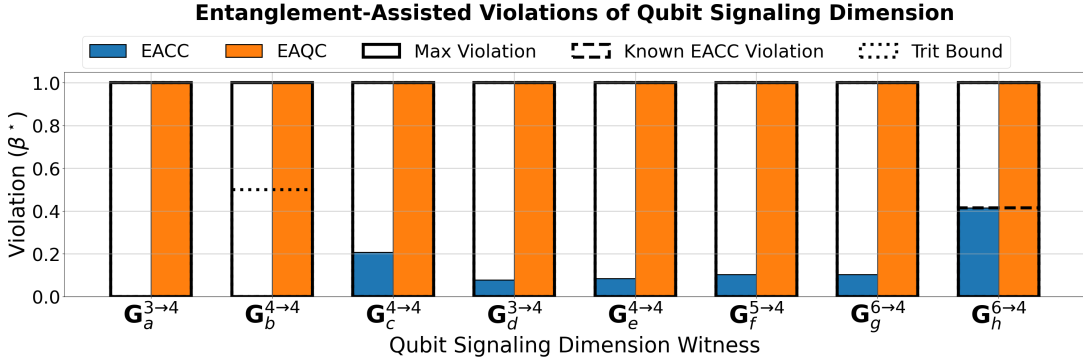


**FIG. 10:** VQO is used to maximize the violation of the nonclassicality witnesses in Table I. The variational ansatz used is the same as in Fig. 11 (b) and (c) except with  $x_2$  being constant. The solid black outline shows the maximal possible violation for each nonclassicality witness, the dotted line shows the maximal violation for unassisted classical signaling of dimension  $d = 3$  where we note that all inequalities but  $\mathbf{G}_b^{4 \rightarrow 4}$  can be maximally violated by a trit. The black dashed line shows the EACC violation of  $\mathbf{G}_h^{6 \rightarrow 4}$  reported in Ref. [21].

ansatz encodes entanglement-assisted quantum communication resources, then the resulting minimized simulation error  $D(\mathbf{V}^{\text{CV}}, \mathbf{P}(\tilde{\theta}^*)) = P_{\text{Error}}$  characterizes precisely the quality of the dense-coded channel established between the sender and receiver. Thus, our variational quantum algorithm automatically establishes a dense-coding protocol using the quantum network’s available resources.

## 2. Prepare-and-Measure Networks

The natural extension of the point-to-point network is the prepare-and-measure network (see Fig. 9(b)). This setting has been widely studied in literature and the presence of nonclassicality for QC, EACC, and EAQC resources is well-established. Nonclassical behaviors in the prepare-and-measure network have known applications in quantum dimensionality witnessing [71], random access coding [72], and other semi-device-independent protocols for key distribution [73], randomness generation [74], and certification tasks testing quantum resources and operations [75, 76]. Furthermore, it was shown in References [77, 78] that  $\mathbb{Q}^{\text{PM}}(\vec{\mathcal{X}} \xrightarrow{2} \mathcal{Y}_2) \subseteq \mathbb{C}_{\text{EA}}^{\text{PM}}(\vec{\mathcal{X}} \xrightarrow{2} \mathcal{Y}_2)$ , meaning that one entanglement-assisted bit of communication can simulate one qubit of communication with zero error.

Using our framework we reproduce known violations in dimensionality witnessing and random access coding. In Table II, we list the nonclassicality witnesses considered for the prepare-and-measure network. In some cases these witnesses have previously been derived, although we are unable to find references for each example witness.

A notable nonclassicality witness for prepare-and-measure networks is the random access coding (RAC) game [31, 72]. Random access coding corresponds to a simulation game that admits a quantum advantage for all quantum resource configurations. In the classical set-

ting of this game, the sender  $A$  is given an  $n$ -bit input  $\vec{x}_1 = (b_i)_{i=1}^n$ , and signals one bit ( $d = 2$ ) to the receiver  $B$ . Meanwhile, the receiver is given an input  $x_2 \in \{0, \dots, n-1\}$ . The objective of the game is for the receiver to output the value  $y = b_{x_2}$ , the  $x_2^{\text{th}}$  bit of the  $n$ -bit string  $\vec{x}_1$ . The maximal probability of winning the RAC game using one-way classical communication of a bit is [72]

$$P_{\text{Success}}^{\text{RAC}(n)} = \frac{1}{2} + \frac{1}{2^n} \binom{n-1}{\lfloor \frac{n-1}{2} \rfloor} \quad (17)$$

When a qubit of communication is used instead in the  $n = 2$  and  $n = 3$  cases, then the maximal winning probability is [30]

$$P_{\text{Success}}^{\text{RAC}(n)} = \frac{1}{2} \left( 1 + \frac{1}{\sqrt{n}} \right), \quad (18)$$

which exceeds the classical bound in Eq. (17) and demonstrates nonclassicality. The RAC task can be encoded into a simulation game

$$\gamma^{\text{RAC}(n)} = |\vec{\mathcal{X}}| P_{\text{Success}}^{\text{RAC}}, \quad V_{y|\vec{x}_1, x_2}^{\text{RAC}(n)} = \delta_{y, b_{x_2}}. \quad (19)$$

A violation of the inequality  $(\gamma^{\text{RAC}(n)}, \mathbf{V}^{\text{RAC}(n)})$  demonstrates nonclassicality and an explicit advantage in the RAC task.

Turning to quantum networks, we use the variational ansätze for the QC, EACC, and EAQC scenarios as depicted in Fig. 11. When we optimize these ansätze, we find the violations shown in Fig. 12. Furthermore, our data suggests that EACC resources are not fully simulable by QC resources, suggesting that EACC resources are stronger than QC resources in this scenario. However, our numerical results are lower bounds and do not fully prove a separation between the blue (left) and orange (middle) bars for the cases of  $\mathbf{G}_c^{\text{PM}}$  and  $\mathbf{G}_e^{\text{PM}}$  in Fig. 12.

$$\begin{aligned}
\text{(a)} \quad 4 &\geq \begin{bmatrix} 0 & 0 & 0 & 1 & 1 & 0 \\ 1 & 1 & 1 & 0 & 0 & 0 \end{bmatrix} & \text{(c)} \quad 5 &\geq \begin{bmatrix} 0 & 0 & 1 & 0 & 1 & 0 & 0 & 0 & 1 \\ 1 & 0 & 0 & 1 & 0 & 0 & 0 & 1 & 0 \end{bmatrix} & \text{(e)} \quad 7 &\geq \begin{bmatrix} 0 & 0 & 1 & 0 & 1 & 0 & 0 & 1 & 1 \\ 1 & 1 & 0 & 1 & 0 & 1 & 1 & 0 & 0 \end{bmatrix} \\
\text{(b)} \quad 7 &\geq \begin{bmatrix} 1 & 0 & 0 & 0 & 1 & 0 & 0 & 0 & 1 \\ 0 & 1 & 1 & 1 & 0 & 1 & 1 & 1 & 0 \end{bmatrix} & \text{(d)} \quad 5 &\geq \begin{bmatrix} 0 & 0 & 1 & 0 & 1 & 0 & 1 & 0 & 0 \\ 1 & 0 & 0 & 0 & 0 & 1 & 0 & 1 & 0 \end{bmatrix} & \text{(f)} \quad 6 &\geq \begin{bmatrix} 1 & 1 & 1 & 0 & 0 & 1 & 0 & 0 \\ 0 & 0 & 0 & 1 & 1 & 0 & 1 & 1 \end{bmatrix} \\
\text{(g)} \quad 18 &\geq \begin{bmatrix} 1 & 1 & 1 & 1 & 1 & 0 & 1 & 0 & 1 & 1 & 0 & 0 & 0 & 1 & 1 & 0 & 1 & 0 & 0 & 0 & 1 & 0 & 0 & 0 \\ 0 & 0 & 0 & 0 & 0 & 1 & 0 & 1 & 0 & 0 & 1 & 1 & 1 & 0 & 0 & 1 & 0 & 1 & 1 & 1 & 0 & 1 & 1 & 1 \end{bmatrix} \\
\text{(h)} \quad 8 &\geq \begin{bmatrix} 0 & 0 & 1 & 1 & 0 & 0 & 0 & 0 & 0 & 0 & 0 & 0 & 0 & 0 & 0 & 1 & 0 & 0 & 0 & 0 & 0 & 0 & 0 \\ 0 & 0 & 0 & 0 & 0 & 1 & 0 & 0 & 0 & 0 & 1 & 1 & 0 & 0 & 0 & 1 & 0 & 1 & 1 & 1 & 0 & 0 & 0 & 0 \end{bmatrix}
\end{aligned}$$

**TABLE II:** Nonclassicality witnesses for prepare-and-measure networks  $\text{PM}(\mathcal{X}_1, \mathcal{X}_2 \xrightarrow{2} \mathcal{Y}_2)$ . (a) Qubit dimensionality witness for  $\text{PM}(3, 2 \xrightarrow{2} 2)$  network [71] (b) Finger printing nonclassicality witness for  $\text{PM}(3, 3 \xrightarrow{2} 2)$  network. (c,d,e) Nonclassicality witnesses for  $\text{PM}(3, 3 \xrightarrow{2} 2)$  network. (f) Two-bit random access code for  $\text{PM}(4, 2 \xrightarrow{2} 2)$ . (g) Three-bit random access code for  $\text{PM}(8, 3 \xrightarrow{2} 2)$  (not a facet inequality). (h) Qubit dimensionality witness for  $\text{PM}(8, 3 \xrightarrow{2} 2)$ .

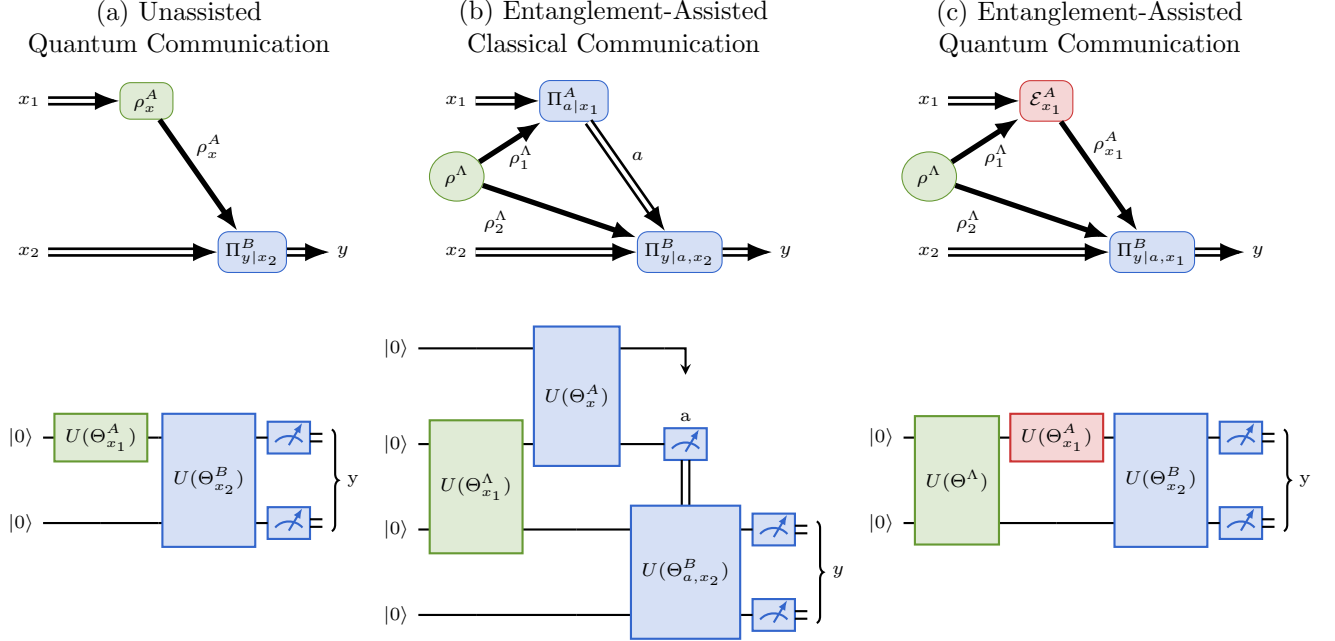


**FIG. 11:** DAGs and variational ansatz circuits for point-to-point and prepare-and-measure scenarios. (a) Quantum communication, (b) entanglement-assisted classical communication, and (c) entanglement-assisted quantum communication. Note that in figure (b) the classical measurement result  $a$  is used to condition the applied measurement.

We find that EAQC resources are sufficient in all but one case to achieve the maximal possible violation. The exception being  $\mathbf{G}_g^{\text{PM}}$ , the three-bit RAC having signaling dimension  $d = 2$ . Naturally, dense coding only boosts the classical communication to  $d^2 = 4$ , meaning that in the case where  $|\mathcal{X}_1| = 8$ , the complete input cannot be communicated to the receiver, preventing the prepare-and-measure network from achieving the maximal possible score in the three-bit RAC.

### 3. Bell Scenarios Assisted with Auxiliary Communication

Consider the case where the two devices  $A$  and  $B$  have the respective inputs  $x_1 \in \mathcal{X}_1$  and  $x_2 \in \mathcal{X}_2$  and outputs  $y_1 \in \mathcal{Y}_1$  and  $y_2 \in \mathcal{Y}_2$  with one-way communication from either  $A$  to  $B$ , or  $B$  to  $A$ . This setting is an example of a Bell scenario assisted by auxiliary communication, for which the classical polytopes have been derived in Refs. [12, 15] for two and three inputs to each device. In Table III, we express these inequalities in our notation.

In Fig. 14 we plot the maximal violations of the inequalities in Table III obtained using VQO. We find that only the inequalities for the  $|\mathcal{X}_1| = |\mathcal{X}_2| = 3$  case have violations, suggesting that quantum resources provide no

## Quantum Violations of Prepare and Measure Nonclassicality Witnesses

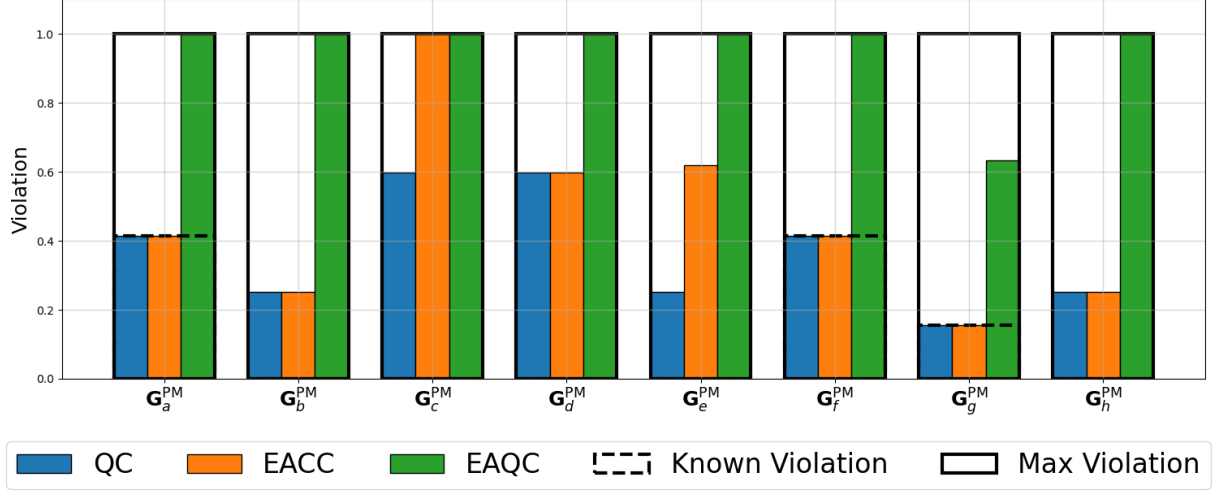


**FIG. 12:** For each nonclassicality witness in Table II we numerically optimize the classically violation for each quantum resources configuration. From left to right, the blue bars show QC resources, the orange bars show EACC resources, and the green bars show EAQC resources. The dashed lines show the theoretical upper bounds on the QC case for  $G_a^{\text{PM}}$  [71] and the two-bit and three-bit RACs,  $G_f^{\text{PM}}$  and  $G_g^{\text{PM}}$  respectively (see Eq. (18)) [30].

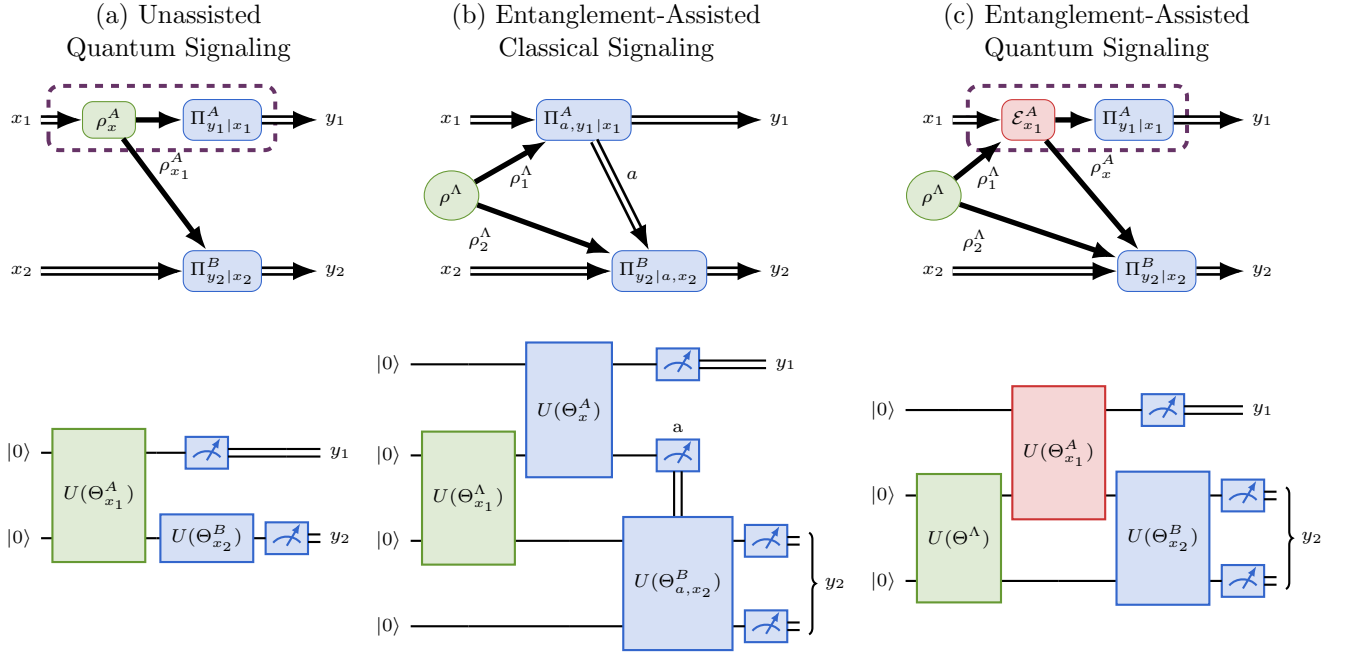


**FIG. 13:** DAGs and variational ansatz circuits for quantum resource configurations in feedforward networks and Bell scenarios assisted with auxiliary communication. (a) Unassisted quantum communication, (b) entanglement-assisted classical communication, and (c) entanglement-assisted quantum communication. Note that in figure (b) the classical measurement result  $a$  is used to condition the applied measurement. Furthermore, note that all networks having  $|x_2| = 1$  are feedforward networks.

$$\begin{aligned}
\text{(a)} \quad 2 &\geq \begin{bmatrix} 1 & 0 & 0 & 0 \\ 0 & 0 & 1 & 0 \\ 0 & 1 & 0 & 0 \\ 0 & 0 & 0 & 1 \end{bmatrix} & \text{(c)} \quad 7 &\geq \begin{bmatrix} 0 & 0 & 1 & 0 & 1 & 1 & 1 & 1 & 1 \\ 0 & 1 & 0 & 1 & 0 & 0 & 0 & 0 & 0 \\ 0 & 1 & 0 & 1 & 0 & 0 & 0 & 0 & 0 \\ 0 & 0 & 1 & 0 & 1 & 1 & 1 & 1 & 1 \end{bmatrix} \\
\text{(b)} \quad 2 &\geq \begin{bmatrix} 1 & 0 & 0 & 0 \\ 0 & 0 & 1 & 0 \\ 1 & 0 & 0 & 1 \\ 0 & 0 & 0 & 1 \end{bmatrix} & \text{(d)} \quad 13 &\geq \begin{bmatrix} 1 & 2 & 0 & 2 & 1 & 2 & 0 & 2 & 1 \\ 0 & 0 & 2 & 0 & 0 & 0 & 2 & 0 & 0 \\ 0 & 0 & 2 & 0 & 0 & 0 & 2 & 0 & 0 \\ 1 & 2 & 0 & 2 & 1 & 2 & 0 & 2 & 1 \end{bmatrix}
\end{aligned}$$

**TABLE III:** Nonclassicality witnesses for the bipartite Bell scenario assisted by  $d = 2$  signaling from either device to the other [12]. (a, b) Tight nonclassicality witnesses for the case where  $|\mathcal{X}_1| = |\mathcal{X}_2| = |\mathcal{Y}_1| = |\mathcal{Y}_2| = 2$ . (c, d) Tight nonclassicality witnesses for the case where  $|\mathcal{X}_1| = |\mathcal{X}_2| = 3$  and  $|\mathcal{Y}_1| = |\mathcal{Y}_2| = 2$ .

### Quantum Violations of Bell Scenarios Assisted by Auxiliary Communication

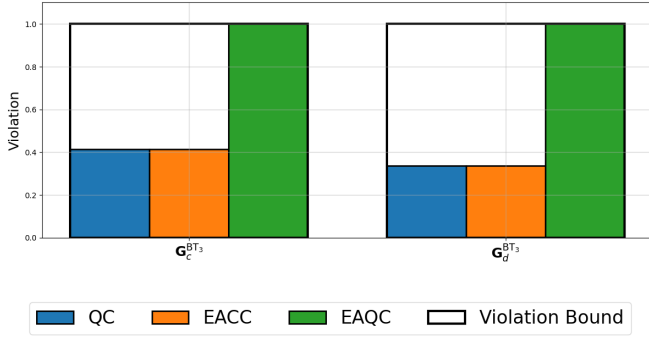


**FIG. 14:** The blue bar corresponds to QC resources, the orange bar EACC resources, and the green bar to EAQC resources.

advantage over one-bit of classical signaling in the two-input case. Furthermore, we observe that the violations of unassisted QC and EACC resources achieve similar values whereas EAQC resources approach the maximal possible violation of these inequalities.

### B. Nonclassicality in Multiaccess Networks

A multiaccess network  $\text{MA}(\vec{\mathcal{X}} \xrightarrow{\vec{d}} \mathcal{Y})$  has one receiver  $B$  and multiple independent senders  $\vec{A} = \{A_i\}_{i=1}^n$ . Each sender is given the classical input  $x_i \in \mathcal{X}_i$  where, in total, the network's input alphabet is  $\vec{\mathcal{X}} = \mathcal{X}_1 \times \dots \times \mathcal{X}_n$ . A noiseless communication channel  $\text{id}_{d_i}^{A_i \rightarrow B}$  having signaling dimension  $d_i$  connects sender  $A_i$  to the receiver where  $\vec{d} = (d_i)_{i=1}^n$ . The receiver  $B$  jointly processes the messages from all senders to produce the value  $y \in \mathcal{Y}$ .

We mainly focus on the bipartite multiaccess network having two senders  $A_1$  and  $A_2$ . This bipartite case generalizes the *prepare-and-measure* scenario discussed in Sec-

Set	Definition
a) $\mathbb{C}^{\text{MA}}$	$P_{y \vec{x}} = \sum_{\lambda} P_{\lambda}^A \prod_{\vec{a} \in \vec{\mathcal{A}}} P_{y \vec{a}, \lambda}^B \prod_{i=1}^n P_{a_i x_i, \lambda}^A$
b) $\mathbb{C}_{\text{ETx}}^{\text{MA}}$	$P_{y \vec{x}} = \sum_{\vec{a} \in \vec{\mathcal{A}}} P_{y \vec{a}}^B \text{Tr} \left[ \left( \bigotimes_{i=1}^n \Pi_{a_i x_i}^{A_i} \right) \rho^{\Lambda} \right]$
c) $\mathbb{C}_{\text{GEA}}^{\text{MA}}$	$P_{y \vec{x}} = \sum_{\vec{a} \in \vec{\mathcal{A}}} \text{Tr} \left[ \left( \Pi_{y \vec{a}}^B \otimes \bigotimes_{i=1}^n \Pi_{a_i x_i}^{A_i} \right) \rho^{\Lambda} \right]$
d) $\mathbb{Q}^{\text{MA}}$	$P_{y \vec{x}} = \text{Tr} \left[ \Pi_y^B \otimes_{i=1}^n \rho_{x_i}^{A_i} \right]$
e) $\mathbb{Q}_{\text{ETx}}^{\text{MA}}$	$P_{y \vec{x}} = \text{Tr} \left[ \Pi_y^B \left( \bigotimes_{i=1}^n \mathcal{E}_{x_i}^{A_i} \right) (\rho^{\Lambda}) \right]$
f) $\mathbb{Q}_{\text{GEA}}^{\text{MA}}$	$P_{y \vec{x}} = \text{Tr} \left[ \Pi_y^B \left( \mathbb{I}^{A_0} \otimes \bigotimes_{i=1}^n \mathcal{E}_{x_i}^{A_i} \right) (\rho^{\Lambda}) \right]$

**TABLE IV:** Sets of behaviors for multiaccess network resource configurations. From top to bottom we list a) classical signaling assisted by global shared randomness, b) classical signaling using entanglement-assisted senders, c) global entanglement-assisted classical signaling, d) unassisted quantum signaling, e) quantum signaling using entanglement-assisted senders, f) quantum signaling using global entanglement-assisted quantum signaling. The respective DAGs for each of these sets is shown in the two-sender case in Fig. 15.

tion III A 2 where

$$\text{MA}(\mathcal{X}_1, \mathcal{X}_2 \xrightarrow{d_1, |\mathcal{X}_2|} \mathcal{Y}) = \text{PM}(\mathcal{X}_1, \mathcal{X}_2 \xrightarrow{d_1} \mathcal{Y}_2). \quad (20)$$

Note that the multiaccess network restricts the amount of information between input  $\mathcal{X}_2$  and the output.

We begin by obtaining nonclassicality witnesses for the multiaccess networks having up to four inputs and outputs and one bit of communication from each sender to the receiver. These nonclassicality witnesses include both facet inequalities bounding the multiaccess network polytope  $\mathbb{C}^{\text{MA}}$  as well as simulation games  $(\gamma, \hat{\mathbf{V}})$  where  $\hat{\mathbf{V}}$  is a deterministic behavior not in the set  $\mathbb{C}^{\text{MA}}$ . We then apply variational optimization to obtain examples of quantum nonclassicality. Finally, we investigate the nonclassical quantum strategies that lead to advantages in simulation games corresponding to tasks including bit-wise XOR operations, calculating the distance between two inputs, and comparing two inputs.

#### 1. Nonclassicality Witnesses for Multiaccess Networks

In the classical signaling case, the behaviors decompose as

$$\mathbb{C}^{\text{MA}} \equiv \left\{ \mathbf{P} \in \mathbb{P}_{\mathcal{Y}|\vec{\mathcal{X}}} \mid \mathbf{P}^B \otimes_{i=1}^n \mathbf{P}^{A_i} \right\} \quad (21)$$

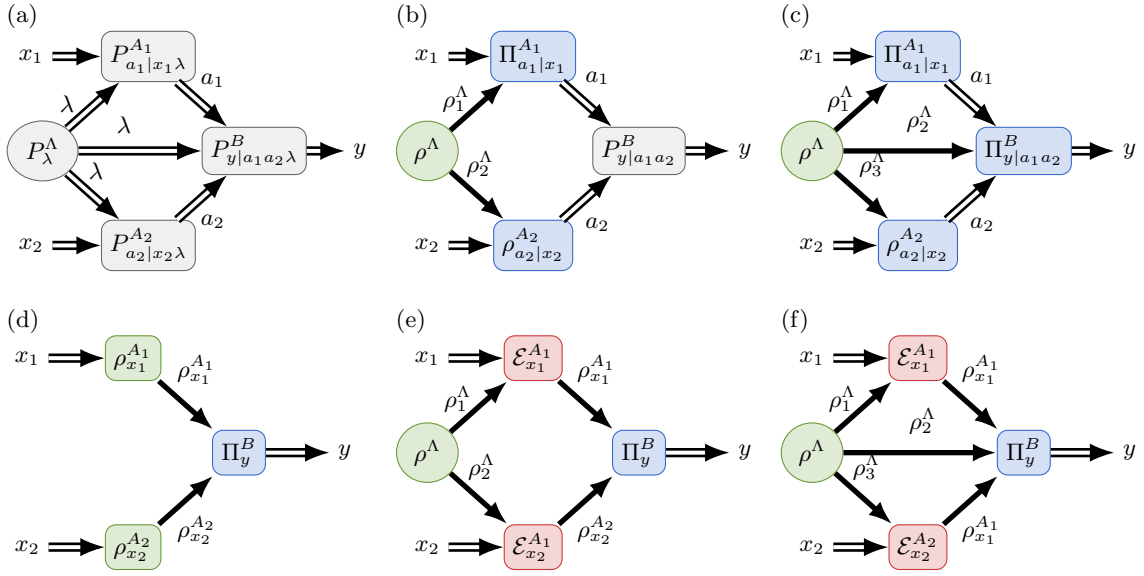


**FIG. 15:** Multiaccess network resource configuration DAGs. (a) Classical communication assisted by global shared randomness (CC). (b) Entanglement-assisted senders using classical communication (EATx CC). (c) Global entanglement-assisted classical communication (GEA CC). (d) Unassisted quantum communication (QC). (e) Entanglement-assisted senders using quantum communication (EATx QC). (f) Global entanglement-assisted quantum communication (GEA QC).

where  $\mathbf{P}^B \in \mathbb{P}_{\mathcal{Y}|\mathcal{A}_1 \times \dots \times \mathcal{A}_n}$  and  $\mathbf{P}^{A_i} \in \mathbb{P}_{\mathcal{A}_i|\mathcal{X}_i}$ . Note that  $|\mathcal{A}_i| = d_i$  is the message alphabet for signaling from sender  $A_i$  to receiver  $B$ . It follows that the classical multiaccess network polytope  $\mathbb{C}^{\text{MA}} \equiv \text{Conv}(\mathbb{C}^{\text{MA}})$ .

**Lemma 1.** Consider a classical multiaccess network having  $n$  senders. The relation  $\mathbb{C}^{\text{MA}} = \mathbb{P}_{\mathcal{Y}|\vec{\mathcal{X}}}$  holds if and only if  $|\mathcal{X}_i| \leq d_i$  for all  $i$  or if  $|\mathcal{Y}| = 1$ .

*Proof.* To prove the first condition, suppose that  $|\mathcal{X}_i| \leq d_i$  for all  $i$ . As a result all the complete input  $\vec{x}$  can be communicated without error to the receiver  $B$ . Since the receiver has the whole input, it can perform a black box map  $\mathbf{P}^B \in \mathbb{P}_{\mathcal{Y}|\vec{\mathcal{X}}}$ , implying that any behavior can be implemented. For the second case, suppose that  $|\mathcal{Y}| = 1$ , then  $\mathbf{P} \in \mathbb{P}_{\mathcal{Y}|\vec{\mathcal{X}}}$  is simply a row vector of ones because each column must be normalized.  $\square$

As a result of Lemma 1, we find that nonclassicality can only occur in multiaccess networks that have  $|\mathcal{Y}| \geq 2$  and  $d_i \leq |\mathcal{X}_i|$  for at least one sender. Therefore, to demonstrate nonclassicality in multiaccess networks in a simple setting, we consider the case with two senders, each having signaling dimension  $d_1 = d_2 = 2$  while  $|\mathcal{X}_1| > 2$  and  $|\mathcal{X}_2| \geq 2$ . We first reproduce previous nonclassicality results regarding the prepare-and-measure scenario. Then we investigate examples of nonclassicality in multiaccess networks.

When  $|\mathcal{X}_1| = |\mathcal{X}_2| = 3$  and  $|\mathcal{Y}| = 2$ , we can use PoRTA [52] to compute the full multiaccess network polytopes for the case where  $\mathbb{C}^{\text{MA}(3,3 \xrightarrow{2,3} 2)}$  as shown in Table V. In

addition we compute the full multiaccess network polytope where either  $d_1$  or  $d_2$  equals three and the other equals two,

$$\mathbb{C}^{\text{MA}(3,3 \xrightarrow{\{2,3\}} 2)} = \text{Conv} \left( \mathbb{C}^{\text{MA}(3,3 \xrightarrow{2,3} 2)} \cup \mathbb{C}^{\text{MA}(3,3 \xrightarrow{3,2} 2)} \right) \quad (22)$$

where we use the curly braces in  $3, 3 \xrightarrow{\{2,3\}} 2$  to denote that either channel could send a trit while the other sends a bit (see Table VI). Note that for a behavior  $\mathbf{P} \notin \mathbb{C}^{\text{MA}(3,3 \xrightarrow{\{2,3\}} 2)}$ , each sender must use a trit of communication to simulate the behavior.

We also investigate a handful of simulation games  $(\gamma, \mathbf{V})$  where  $\mathbf{V}$  is a deterministic nonclassical behavior. Since multiaccess networks take two inputs  $x_1$  and  $x_2$  and map them to a single output  $y$ , it is natural to consider logical or arithmetic operations as tasks (see Table VII). Later, in Section III D, we consider multiaccess networks having up to  $|\mathcal{Y}| = 9$  outputs, allowing the consideration of more tasks including multiplication and addition.

## 2. Numerical Quantum Violations of Multiaccess Network Nonclassicality Witnesses

We consider the multiaccess network quantum resource configurations in Fig. 15. Using variational optimization, we maximize nonclassicality with respect to the nonclassicality witnesses introduced in the previous section.

In Figure 16, we plot the violations for each facet inequality bounding the classical network polytope  $\mathbb{C}^{\text{MA}(\mathcal{X}_1, \mathcal{X}_2 \xrightarrow{2,2} 2)}$  (see Table VII). Remarkably, all consid-

$$\begin{aligned}
(1) \quad 4 &\geq \begin{bmatrix} 1 & 1 & 0 & 1 & 0 & 0 & 0 & 0 \\ 0 & 0 & 0 & 0 & 1 & 0 & 1 & 0 \end{bmatrix} & (6) \quad 8 &\geq \begin{bmatrix} 0 & 0 & 0 & 0 & 1 & 1 & 2 & 0 \\ 2 & 2 & 0 & 1 & 0 & 0 & 0 & 1 \end{bmatrix} \\
(2) \quad 5 &\geq \begin{bmatrix} 0 & 0 & 0 & 0 & 0 & 1 & 1 & 0 \\ 1 & 1 & 0 & 1 & 0 & 0 & 0 & 1 \end{bmatrix} & (7) \quad 8 &\geq \begin{bmatrix} 0 & 0 & 0 & 0 & 2 & 0 & 1 & 0 \\ 2 & 2 & 0 & 1 & 0 & 1 & 0 & 0 \end{bmatrix} & (11) \quad 14 &\geq \begin{bmatrix} 0 & 0 & 2 & 0 & 2 & 0 & 2 & 0 \\ 3 & 1 & 0 & 1 & 0 & 3 & 0 & 3 \end{bmatrix} \\
(3) \quad 7 &\geq \begin{bmatrix} 0 & 0 & 1 & 0 & 1 & 0 & 1 & 0 \\ 2 & 1 & 0 & 1 & 0 & 1 & 0 & 1 \end{bmatrix} & (8) \quad 8 &\geq \begin{bmatrix} 0 & 0 & 1 & 0 & 1 & 0 & 2 & 0 \\ 2 & 1 & 0 & 0 & 0 & 1 & 0 & 2 \end{bmatrix} & (12) \quad 16 &\geq \begin{bmatrix} 0 & 0 & 2 & 0 & 3 & 0 & 2 & 0 \\ 5 & 3 & 0 & 3 & 0 & 1 & 0 & 1 \end{bmatrix} \\
(4) \quad 7 &\geq \begin{bmatrix} 0 & 0 & 1 & 0 & 1 & 0 & 1 & 0 \\ 2 & 2 & 0 & 1 & 0 & 0 & 0 & 1 \end{bmatrix} & (9) \quad 10 &\geq \begin{bmatrix} 0 & 0 & 1 & 0 & 2 & 0 & 1 & 0 \\ 3 & 2 & 0 & 2 & 0 & 1 & 0 & 0 \end{bmatrix} & (13) \quad 17 &\geq \begin{bmatrix} 0 & 0 & 2 & 1 & 2 & 0 & 5 & 0 \\ 4 & 2 & 0 & 0 & 0 & 1 & 0 & 4 \end{bmatrix} \\
(5) \quad 6 &\geq \begin{bmatrix} 0 & 0 & 0 & 0 & 1 & 1 & 1 & 0 \\ 1 & 1 & 0 & 1 & 0 & 0 & 0 & 1 \end{bmatrix} & (10) \quad 11 &\geq \begin{bmatrix} 0 & 0 & 2 & 0 & 1 & 0 & 2 & 0 \\ 3 & 1 & 0 & 1 & 0 & 2 & 0 & 2 \end{bmatrix}
\end{aligned}$$

**TABLE V:** Facet inequalities for the multiaccess network polytope  $\mathbb{C}^{\text{MA}(3,3 \xrightarrow{2,2})}$  also computed in Reference [35].

$$\begin{aligned}
(14) \quad 6 &\geq \begin{bmatrix} 0 & 0 & 0 & 0 & 1 & 0 & 1 & 0 \\ 1 & 1 & 0 & 1 & 0 & 1 & 0 & 0 \end{bmatrix} & (16) \quad 5 &\geq \begin{bmatrix} 0 & 0 & 1 & 0 & 1 & 0 & 1 & 0 \\ 1 & 1 & 0 & 1 & 0 & 0 & 0 & 0 \end{bmatrix} & (18) \quad 9 &\geq \begin{bmatrix} 0 & 0 & 2 & 0 & 1 & 0 & 2 & 0 \\ 2 & 1 & 0 & 1 & 0 & 1 & 0 & 1 \end{bmatrix} \\
(15) \quad 7 &\geq \begin{bmatrix} 1 & 0 & 0 & 0 & 1 & 0 & 0 & 0 \\ 0 & 1 & 1 & 1 & 0 & 1 & 1 & 1 \end{bmatrix} & (17) \quad 5 &\geq \begin{bmatrix} 0 & 0 & 1 & 0 & 1 & 0 & 1 & 0 \\ 1 & 0 & 0 & 0 & 0 & 1 & 0 & 1 \end{bmatrix} & (19) \quad 11 &\geq \begin{bmatrix} 0 & 0 & 1 & 1 & 0 & 0 & 2 & 0 \\ 2 & 1 & 0 & 0 & 1 & 2 & 0 & 1 \end{bmatrix}
\end{aligned}$$

**TABLE VI:** Facet inequalities for the multiaccess network polytope  $\mathbb{C}^{\text{MA}(3,3 \xrightarrow{\{2,3\}} 2)}$  as defined in Eq.(22).

Task	Symbol	Definition
Distance	$\mathbf{V}_{\mathcal{X}_1 \mathcal{X}_2 \rightarrow \mathcal{Y}}^-$	$V_{y, x_1, x_2}^- = \delta_{y,  x_1 - x_2 }$
Bitwise XOR	$\mathbf{V}_{4, 4 \rightarrow 4}^\oplus$	$V_{\vec{y}, \vec{x}_1, \vec{x}_2}^\oplus = \begin{cases} 1 & \text{if } y_j = x_{1j} \oplus x_{2j} \\ & \forall j \in \{0, 1\} \\ 0 & \text{otherwise} \end{cases}$
Compare	$\mathbf{V}_{\mathcal{X}_1 \mathcal{X}_2 \rightarrow 3}^\geq$	$V_{y, x_1, x_2}^\geq = \begin{cases} 1 & \text{if } y = 0 \text{ and } x_1 = x_2 \\ & \text{or } y = 1 \text{ and } x_1 > x_2 \\ & y = 2 \text{ and } x_1 < x_2 \\ 0 & \text{otherwise} \end{cases}$
Equals	$\mathbf{V}_{\mathcal{X}_1 \mathcal{X}_2 \rightarrow 2}^\equiv$	$V_{y, x_1, x_2}^\equiv = \begin{cases} 1 & \text{if } y = 0 \text{ and } x_1 = x_2 \\ & \text{or } y = 1 \text{ and } x_1 \neq x_2 \\ 0 & \text{otherwise} \end{cases}$

**TABLE VII:** Simulation games for multiaccess networks. The classical bound is computed for one-bit of communication from each sender.

ered quantum resource configurations can produce non-classical behaviors. In the top plot of Figure 17, we plot the violations for the multiaccess network polytope  $\mathbb{C}^{\text{MA}(3,3 \xrightarrow{\{2,3\}} 2)}$ . We find that unassisted qubit commu-

nication  $\mathbb{Q}^{\text{MA}}$  is unable to violate these bounds, indicating that qubits signaling is classically simulable as  $\mathbb{Q}^{\text{MA}} \subseteq \mathbb{C}^{\text{MA}(3,3 \xrightarrow{\{2,3\}} 2)}$  where only one bit and one trit are necessary. On the other hand, we find that entanglement-assisted senders are able to still violate these classical bounds, indicating that entanglement-assisted sender configurations require at least two-trits of classical communication to simulate.

In the bottom plot of Figure 17, we plot the violations of the classical bound for each of the simulation games in Table VII. We find that the entanglement-assisted senders using classical communication  $\mathbb{C}_{\text{ETx}}^{\text{MA}}$  is able demonstrate an advantage in the trit equality game  $\mathbf{V}_{3,3 \rightarrow 2}^-$ . We find that entanglement-assisted senders using quantum communication  $\mathbb{Q}_{\text{ETx}}^{\text{MA}}$  are able to achieve the maximal possible score for the games  $\mathbf{V}_{3,3 \rightarrow 3}^-$ ,  $\mathbf{V}_{4,4 \rightarrow 4}^\oplus$ ,  $\mathbf{V}_{3,3 \rightarrow 2}^-$ , and  $\mathbf{V}_{4,4 \rightarrow 2}^-$ . The strongest violations are achieved by the strongest resource configuration  $\mathbb{Q}_{\text{GEA}}^{\text{MA}}$  where entanglement is shared globally across all three parties. Note that the global entanglement-assisted quantum signaling setting does not admit the maximal possible scores for all games. In the games where the maximal possible score can be obtained as  $\gamma^* = \langle \mathbf{V}, \mathbf{P}^{\text{Net}}(\vec{\theta}^*) \rangle$ , Lemma 6 proves that  $\mathbf{V} \approx \mathbf{P}^{\text{Net}}(\vec{\theta}^*)$ . As a result, we show how variational optimization can be used in Algorithm (4) to establish a quantum network that implements a deterministic task.

Overall, our results suggest the resource simulation hi-



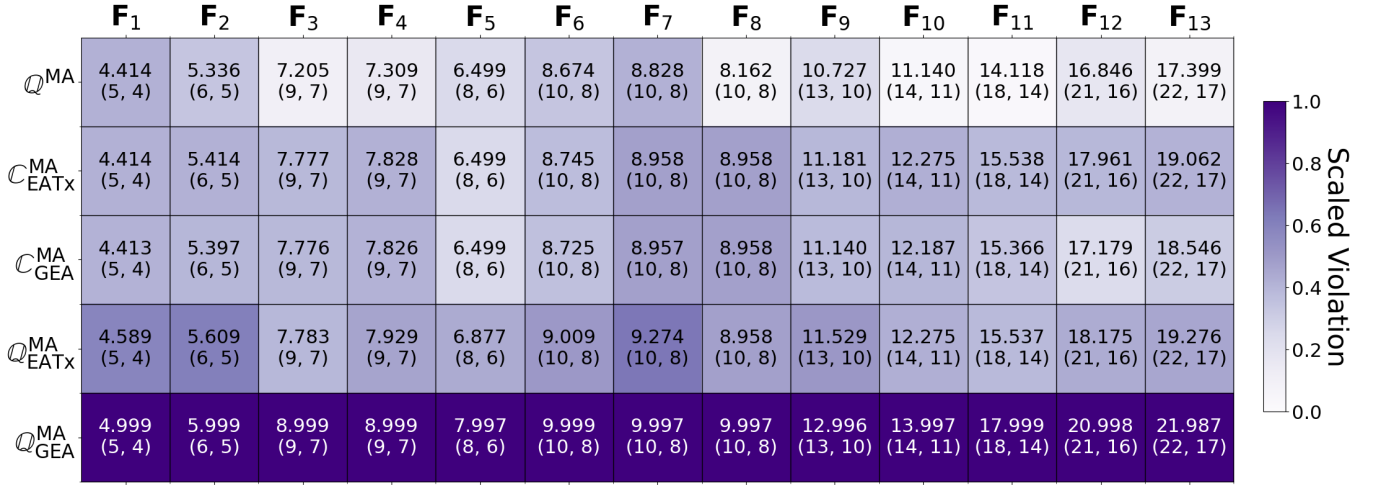


**FIG. 16: Quantum violations of classicality in  $3, 3^{2,2}$  multiaccess networks.** Each column corresponds to a facet inequality of  $C^{MA}$  listed in Table V. Each row corresponds to a quantum resource configuration in figure 15. Each cell plots a strict lower bound on the maximal violation for the given resource configuration where larger violations are shaded darker. For consistency across facets, the violations have been rescaled using Lemma 4 such that the classical bound is  $\gamma = 0$  and the maximal possible score is  $1 = \gamma^* \geq \langle F_i, P \rangle$ . The column of each plot corresponds to a different nonclassicality witness while each row corresponds to a different resource configuration. The top number in each cell shows the largest numerical violation obtained via variational optimization. The lower tuple,  $(\gamma^*, \gamma)$ , shows the largest possible score  $\gamma^*$  and the classical bound  $\gamma$  for each linear black box game.

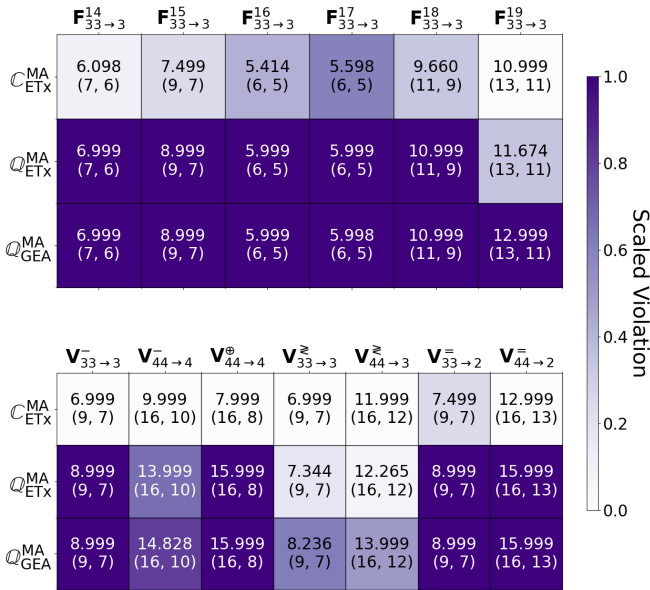


**FIG. 17: (Top)** Quantum violations of classicality in  $MA(3, 3^{2,3})$  multiaccess networks. The six facet inequalities in Table VI bounding  $C^{MA}$  multiaccess network polytope. **(Bottom)** Quantum advantages in simulating deterministic tasks. The quantum advantages achieved for simulating the deterministic behaviors in Table VII. The column of each plot corresponds to a different nonclassicality witness while each row corresponds to a different resource configuration. The top number in each cell shows the largest numerical violation obtained via variational optimization. The lower tuple,  $(\hat{\gamma}, \gamma)$ , shows the largest possible score  $\hat{\gamma}$  and the classical bound  $\gamma$  for each linear black box game.

erarchy

$$C^{MA} \subseteq Q^{MA} \subseteq C_{ETx}^{MA} \subseteq C_{GEA}^{MA} \subseteq Q_{ETx}^{MA} \subseteq Q_{GEA}^{MA} \quad (23)$$

where from left to right, each resource configuration achieves stronger violations of the classical bound. Although we do not prove this conjecture, our data indicates that not all resource configurations are compatible with a given violation. For instance, the violations of classicality shown in Fig. 17 cannot be achieved using unassisted quantum signaling, showing that these inequalities could serve as witnesses for entangled senders.

### 3. Protocols for Nonclassicality in Multiaccess Networks with Entanglement-Assisted Senders

We now present a few examples where entanglement-assisted senders achieve nonclassicality in multiaccess network simulation games. Since these games correspond to deterministic information processing tasks, the violations in Fig. 17 correspond to precise operations that can be implemented using quantum resources, but not classical resources for a given signaling dimension. Furthermore we focus on the cases where entanglement is shared between senders leading to new types of dense information processing. Notably, we find a significant advantage in the bitwise XOR simulation game  $V_{4,4}^{\oplus, 2,2}$ .

**Protocol 1.** Consider the set of multiaccess network behaviors  $Q_{ETx}^{MA(4,4^{2,2})}$  having entanglement-assisted senders that each transmit a qubit to the receiver. The

zero-error simulation  $D(\mathbf{V}_{4,4 \rightarrow 4}^\oplus, \mathbf{P}) = 0$  is achieved by the following protocol:

1. The source  $\Lambda$  prepares the maximally entangled state  $|\Phi^+\rangle = \frac{1}{\sqrt{2}}(|00\rangle + |11\rangle)$  and distributes it between two senders  $A_1$  and  $A_2$ .
2. Each sender applies a unitary

$$U_{\vec{x}_i}^{A_i} \in (\mathbb{I}_2, \sigma_z^{A_i}, \sigma_x^{A_i}, \sigma_y^{A_i}) \quad (24)$$

conditioned on the two-bit input  $\vec{x}_i \in \mathcal{X}_i = \mathbb{B}^2$ . The resulting quantum state is then

$$|\psi_{\vec{x}_1 \vec{x}_2}\rangle = U_{\vec{x}_1}^{A_1} \otimes U_{\vec{x}_2}^{A_2} |\Phi^+\rangle \quad (25)$$

$$= U_{\vec{x}_1}^{A_1} (U_{\vec{x}_2}^{A_2})^T \otimes \mathbb{I}_2 |\Phi^+\rangle, \quad (26)$$

for which we verify the following cases:

$$\text{when } 00 = \vec{x}_1 \oplus \vec{x}_2, \quad |\psi_{\vec{x}_1 \vec{x}_2}\rangle = \nu |\Phi^+\rangle \quad (27)$$

$$\text{when } 01 = \vec{x}_1 \oplus \vec{x}_2, \quad |\psi_{\vec{x}_1 \vec{x}_2}\rangle = \nu |\Phi^-\rangle \quad (28)$$

$$\text{when } 10 = \vec{x}_1 \oplus \vec{x}_2 \quad |\psi_{\vec{x}_1 \vec{x}_2}\rangle = \nu |\Psi^+\rangle \quad (29)$$

$$\text{when } 11 = \vec{x}_1 \oplus \vec{x}_2 \quad |\psi_{\vec{x}_1 \vec{x}_2}\rangle = \nu |\Psi^-\rangle \quad (30)$$

Note that  $\nu = \pm 1$  represents a global phase factor dependent on both  $\vec{x}_1$  and  $\vec{x}_2$ .

3. The receiver  $B$  jointly measures the two-qubits in the Bell basis  $\{|\Phi^+\rangle, |\Phi^-\rangle, |\Psi^+\rangle, |\Psi^-\rangle\}$  and the two-bit output  $y = \vec{x}_1 \oplus \vec{x}_2$  is obtained with zero error.

**Remark.** The classical bound for one bit of signaling is  $D(\mathbf{V}_{4,4 \rightarrow 4}^\oplus, \mathbf{P}) = P_{\text{Error}} = \frac{1}{2}$ , whereas two bits of signaling from each sender are needed to achieve the simulation error  $P_{\text{Error}} = 0$ .

Protocol 1 describes a quantum advantage similar to dense coding where the bitwise XOR operation is performed using two bits less signaling than an equivalent classical strategy. Furthermore, if  $N$  pairs of entangled states are shared between the two senders, then the XOR of two  $2N$ -bit strings can be evaluated by the multiaccess network where only  $2N$  qubits of communication are needed in total while  $4N$  classical bits are required in the classical case. This behavior could be employed as a cryptographic primitive for performing the bitwise XOR between two strings in a distributed manner.

We also find an interesting simulation advantage for entanglement-assisted senders using classical signaling. In the following protocol, we outline the quantum strategy that achieves a violation of the nonclassicality witness  $(7, \mathbf{V}_{3,3 \rightarrow 2}^-)$  (see inequality (15) in Table VI). Indeed, the following protocol achieves the score  $7.5 = \langle \mathbf{V}_{3,3 \rightarrow 2}^-, \mathbf{P} \rangle > 7$ . One application of this violation is demonstrating the use of entanglement between two senders.

**Protocol 2.** Consider the set of multiaccess network behaviors  $\mathbb{C}_{\text{ETx}}^{\text{MA}(3,3 \rightarrow 2)}$  that has entanglement-assisted classical senders each using one bit of classical signaling. For the equality game  $(7, \mathbf{V}_{3,3 \rightarrow 2}^-)$ , the nonclassical score  $7.5 > \gamma = 7$  is achieved by the following protocol:

1. The source prepares the maximally entangled state  $|\Phi^+\rangle = \frac{1}{\sqrt{2}}(|00\rangle + |11\rangle)$  and distributes it to the senders  $A_1$  and  $A_2$ .
2. Each sender measures their local qubit to obtain a one-bit outcome, with measurement bases  $\left\{ \left| \phi_{a_i | x_i}^{A_i} \right\rangle \right\}_{a_i \in \mathbb{B}}$  given as

$$\left\{ \left| \phi_{0|0}^{A_i} \right\rangle = |0\rangle, \left| \phi_{1|0}^{A_i} \right\rangle = |1\rangle \right\}, \quad (31)$$

$$\left\{ \left| \phi_{0|1}^{A_i} \right\rangle = \frac{1}{2} |0\rangle + \frac{\sqrt{3}}{2} |1\rangle, \left| \phi_{1|1}^{A_i} \right\rangle = \frac{\sqrt{3}}{2} |0\rangle - \frac{1}{2} |1\rangle \right\}, \quad (32)$$

$$\left\{ \left| \phi_{0|2}^{A_i} \right\rangle = \frac{1}{2} |0\rangle - \frac{\sqrt{3}}{2} |1\rangle, \left| \phi_{1|2}^{A_i} \right\rangle = \frac{\sqrt{3}}{2} |0\rangle + \frac{1}{2} |1\rangle \right\}. \quad (33)$$

Note that When  $x_1 = x_2$ , the senders  $A_1$  and  $A_2$  measure  $|\Phi^+\rangle$  in the same basis resulting in outcomes that have even parity,  $a_1 \oplus a_2 = 0$ . Otherwise, if  $x_1 \neq x_2$ , then we obtain even and odd parity results with probabilities

$$P(a_1 \oplus a_2 = 0 | x_1, x_2) = 0.25, \quad (34)$$

$$P(a_1 \oplus a_2 = 1 | x_1, x_2) = 0.75. \quad (35)$$

3. Each sender transmits their one-bit measurement result  $a_i$  via a classical channel to the receiver  $B$  who outputs the value  $y = a_1 \oplus a_2$ . The resulting behavior is then

$$\mathbf{P}^* = \begin{bmatrix} 1 & 0.25 & 0.25 & 0.25 & 1 & 0.25 & 0.25 & 0.25 & 1 \\ 0 & 0.75 & 0.75 & 0.75 & 0 & 0.75 & 0.75 & 0.75 & 0 \end{bmatrix}, \quad (36)$$

which achieves the score  $\langle \mathbf{V}_{3,3 \rightarrow 2}^-, \mathbf{P}^* \rangle = 7.5$ .

### C. Nonclassicality in Broadcast Networks

A broadcast network consists of one sender  $A$  and multiple receivers  $\vec{B} = (B_i)_{i=1}^n$  where a noiseless channel  $\text{id}_{d_i}^{A \rightarrow B_i}$  with signaling dimension  $d_i$  connects the sender to receiver  $B_i$ . The sender is given an input  $x \in \mathcal{X}$  while each receiver outputs  $y_i \in \mathcal{Y}_i$ , hence broadcast network behaviors belong to the probability polytope  $\mathbb{P}_{\vec{\mathcal{Y}} | \mathcal{X}}$  where  $\vec{\mathcal{Y}} \equiv \mathcal{Y}_1 \times \dots \times \mathcal{Y}_n$ . The classical broadcast DAG is shown in Fig. 18(a).

#### 1. Nonclassicality Witnesses for Broadcast Networks

To begin, we derive fundamental conditions for which the classical broadcast network polytope is equivalent to the full probability polytope. Indeed, we derive the necessary and sufficient conditions required by a classical broadcast to simulate any black box behavior.

$$\begin{array}{cccc}
\text{(a)} & \text{(b)} & \text{(d)} & \text{(e)} \\
2 \geq \begin{bmatrix} 0 & 0 & 1 \\ 0 & 0 & 0 \\ 1 & 0 & 0 \\ 0 & 0 & 0 \\ 0 & 1 & 0 \\ 1 & 0 & 0 \\ 1 & 0 & 0 \\ 1 & 0 & 0 \\ 1 & 0 & 0 \\ 1 & 0 & 0 \end{bmatrix} & 2 \geq \begin{bmatrix} 0 & 0 & 1 \\ 0 & 0 & 1 \\ 0 & 0 & 1 \\ 0 & 1 & 0 \\ 0 & 1 & 0 \\ 0 & 1 & 0 \\ 1 & 0 & 0 \\ 1 & 0 & 0 \\ 1 & 0 & 0 \\ 1 & 0 & 0 \end{bmatrix} & 2 \geq \begin{bmatrix} 0 & 0 & 1 \\ 0 & 0 & 0 \\ 0 & 0 & 0 \\ 0 & 0 & 0 \\ 1 & 0 & 0 \\ 0 & 1 & 0 \\ 0 & 0 & 0 \\ 0 & 1 & 0 \\ 1 & 0 & 0 \\ 1 & 0 & 0 \end{bmatrix} & 4 \geq \begin{bmatrix} 0 & 0 & 2 \\ 0 & 0 & 1 \\ 0 & 1 & 1 \\ 0 & 2 & 0 \\ 0 & 1 & 0 \\ 0 & 1 & 1 \\ 1 & 0 & 0 \\ 2 & 0 & 0 \\ 1 & 1 & 1 \end{bmatrix}
\end{array}$$

**TABLE VIII:** Canonical facet inequalities for the classical broadcast network polytope  $\mathbb{C}^{\text{BC}(3^{22}33)}$ .

**Lemma 2.** Consider a classical broadcast network that has  $n$  receivers and an unlimited amount of shared randomness. The relation  $\mathbb{C}^{\text{BC}} = \mathbb{P}_{\mathcal{Y}|\mathcal{X}}$  holds if and only if either  $|\mathcal{Y}_i| \leq d_i$  for all  $i \in [n]$  or  $|\mathcal{X}| \leq \min\{d_i\}_{i=1}^n$ .

*Proof.* We prove the first condition by asserting that, if  $|\mathcal{Y}_i| \leq d_i$  for all  $i \in [n]$ , then the sender can signal to each receiver any value  $y_i \in \mathcal{Y}_i$ . Since the sender can implement any behavior  $\mathbf{P}^A \in \mathbb{P}_{\mathcal{Y}|\mathcal{X}}$ , the entire probability polytope can be achieved. We prove the second condition by asserting that, if  $|\mathcal{X}| \leq \min\{d_i\}_{i=1}^n$ , then the entire input can be signaled to each receiver. If an unlimited amount of shared randomness is available, then the receivers can coordinate their operations to achieve any black box behavior  $\mathbf{P} \in \mathbb{P}_{\mathcal{Y}|\mathcal{X}}$ .  $\square$

In the simple case of two senders and signaling dimension  $d_1 = d_2 = 2$ , we can compute the complete classical network polytope  $\mathbb{C}^{\text{BC}}$  when  $|\mathcal{X}| = |\mathcal{Y}_1| = |\mathcal{Y}_2| = 3$  (see Table VIII). This setting constitutes the simplest broadcast network in which the network polytope is neither equivalent to the probability polytope nor the signaling polytope.

We also compute the facet inequalities of  $\text{Conv}(\mathbb{C}^{\text{BC}(3^{22}33)} \cup \mathbb{C}^{\text{BC}(3^{32}33)})$ , the case where one trit and one bit of communication are used in the network. The resulting facet inequality corresponds to an interesting simulation game, which we refer to as the broadcast communication value (BCV). The simulation game is  $(\gamma = d, \mathbf{V}^{\text{BCV}})$  where the deterministic behavior is

$$V_{y_1, y_2, x}^{\text{BCV}} = \begin{cases} 1 & \text{if } y_1 = y_2 = x \\ 0 & \text{otherwise.} \end{cases} \quad (37)$$

The maximal possible score for the inequality is  $\gamma^* = |\mathcal{X}|$  while the classical bound is  $\gamma = \min\{d_1, d_2\}$ . The broadcast communication value nonclassicality witness tightly bounds the broadcast network polytope.

Set	Definition
$\mathbb{C}^{\text{BC}}$	$P_{\mathcal{Y} x} = \sum_{\lambda} P_{\lambda}^A \sum_{\vec{a} \in \vec{\mathcal{A}}} (\prod_{i=1}^{ \vec{\mathcal{A}} } P_{y_i a_i, \lambda}^{B_i}) P_{\vec{a} x, \lambda}^A$
$\mathbb{C}_{\text{ERx}}^{\text{BC}}$	$P_{\mathcal{Y} x} = \sum_{\vec{a} \in \vec{\mathcal{A}}} \text{Tr} \left[ \prod_{y_1 a_1}^{B_1} \otimes \prod_{y_2 a_2}^{B_2} \rho^{B_1 B_2} \right] P_{\vec{a} x}^A$
$\mathbb{C}_{\text{GEA}}^{\text{BC}}$	$P_{\mathcal{Y} x} = \sum_{\vec{a} \in \vec{\mathcal{A}}} \text{Tr} \left[ \bigotimes_{i=1}^n \prod_{y_i a_i}^{B_i} \text{Tr}_A \left[ \prod_{\vec{a} x}^A \otimes \mathbb{I}^{\vec{B}} \rho^A \right] \right]$
$\mathbb{C}_{\text{EA}}^{\text{BC}}$	$P_{\mathcal{Y} x} = \text{Tr} \left[ \bigotimes_{i=1}^n \sum_{\vec{a} \in \vec{\mathcal{A}}} \prod_{y_i a_i}^{B_i} \text{Tr}_A \left[ \prod_{\vec{a} x}^A \otimes \text{id}^{\vec{B}} \bigotimes_{j=1}^n \rho^{\Lambda_j} \right] \right]$
$\mathbb{Q}^{\text{BC}}$	$P_{\mathcal{Y} x} = \text{Tr} \left[ \bigotimes_{i=1}^n \prod_{y_i}^{B_i} \rho_x^A \right]$
$\mathbb{Q}_{\text{ERx}}^{\text{BC}}$	$P_{\mathcal{Y} x} = \text{Tr} \left[ \bigotimes_{i=1}^n \prod_{y_i}^{B_i} \text{id}^{A, \Lambda \rightarrow \vec{B}} (\rho_x^A \otimes \rho^{\Lambda}) \right]$
$\mathbb{Q}_{\text{GEA}}^{\text{BC}}$	$P_{\mathcal{Y} x} = \text{Tr} \left[ \bigotimes_{i=1}^n \prod_{y_i}^{B_i} \text{id}^{A, \text{Tx} \rightarrow \vec{B}} (\mathcal{E}_x^A \otimes \text{id}^{\vec{B}} (\rho^{\Lambda})) \right]$
$\mathbb{Q}_{\text{EA}}^{\text{BC}}$	$P_{\mathcal{Y} x} = \text{Tr} \left[ \bigotimes_{i=1}^n \prod_{y_i}^{B_i} \mathcal{E}_x^A \otimes \text{id}^{\vec{B}} \left( \bigotimes_{j=1}^n \rho^{\Lambda_j} \right) \right]$

**TABLE IX:** Sets of behaviors for general broadcast networks. From top to bottom, the resource configurations are classical signaling assisted by unlimited global shared randomness, classical signaling using entanglement-assisted receivers, classical signaling assisted by global entanglement, entanglement-assisted classical signaling, quantum signaling, quantum communication using entanglement-assisted receivers, quantum signaling assisted by global entanglement, and entanglement-assisted quantum signaling.

## 2. Numerical Quantum Violations of Broadcast Nonclassicality Witnesses

We consider several quantum resource configurations (see Fig. 18). To simplify our analysis, we consider the case where there are two receivers and the signaling dimension of all channels is  $d_1 = d_2 = 2$ . In this setting, we upgrade the classical broadcast network DAG with quantum resources and study the resulting nonclassical behaviors. The respective behavior sets for each resource configuration are given in Table IX.

In Figure 19 plot our variational optimization results as we maximize the violation for each nonclassicality witness in Table VIII over each quantum resource configuration in Fig. 18. Remarkably, we obtain nonclassicality for only the case of entanglement-assisted quantum signaling resources. When entanglement-assisted quantum signaling is used, *i.e.*, dense-coding signaling, the maximal score for each nonclassicality witness is obtained.

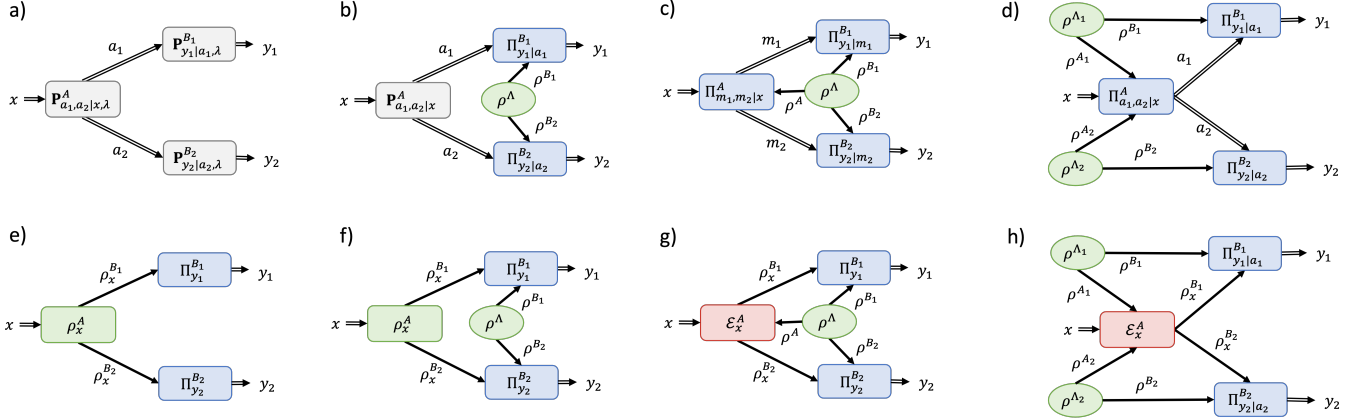


**FIG. 18:** DAGs featuring resource configurations of broadcast networks that have two receivers. a) Classical signaling assisted by global shared randomness. b) Classical signaling using entanglement-assisted receivers. c) Global entanglement-assisted classical signaling. d) Entanglement-assisted classical signaling. e) Unassisted quantum signaling. f) Quantum signaling using entanglement-assisted receivers. g) Global entanglement-assisted quantum signaling. h) Entanglement-assisted quantum signaling.

This result aligns with the fact that dense-coding allows for two bits of information to be encoded in the entanglement-assisted qubit communication. Since the entire input  $x$  can be communicated to each receiver, Lemma 2 shows that  $\mathbb{C}_{EA}^{BC} = \mathbb{P}_{\bar{y}|x}$  for the considered scenario, implying that all broadcast behaviors having  $|\mathcal{X}| = |\mathcal{Y}_1| = |\mathcal{Y}_2| = 3$  can be simulated. A more nuanced result is perhaps the case where a 3-qubit entangled state shared amongst all parties shows violations proving that  $\mathbb{C}^{BC} \subset \mathbb{Q}_{G\text{EA}3}^{BC}$ . However, we do not observe that the 3-qubit entangled states can achieve as strong of a violation as the entanglement-assisted signaling case where each qubit of communication is paired with a two-qubit entangled state. Indeed, we find that entanglement-assisted qubit communication on one side can achieve similar scores to the tripartite entanglement case, raising the question of whether 3-qubit entanglement can increase the nonclassicality over a single maximally entangled state. Furthermore, we find for all inequalities that a single two-qubit maximally entangled state is sufficient for achieving the maximal violation in the probability polytope. However, the entangled sender-receiver pair depends on the considered nonclassicality witness.

In the  $\text{BC}(3 \xrightarrow{2,2} 3, 3)$  broadcast network scenario, we find only one quantum resource configuration that requires the simulation of two trits ( $d_1 = d_2 = 3$ ). The relevant broadcast communication value (BCV) nonclassicality witness is expressed as the simulation game ( $\gamma = 2, \mathbf{V}^{\text{BCV}}$ ) where the simulated deterministic behavior is given by Eq. (37). When considering quantum resources in the  $\text{BC}(3 \xrightarrow{2,2} 3, 3)$  case, we find that only two-sided entanglement-assisted qubit signaling can violate the classical bound. This result should not be surprising as dense-coding can be independently applied on each side resulting in two bits of communica-

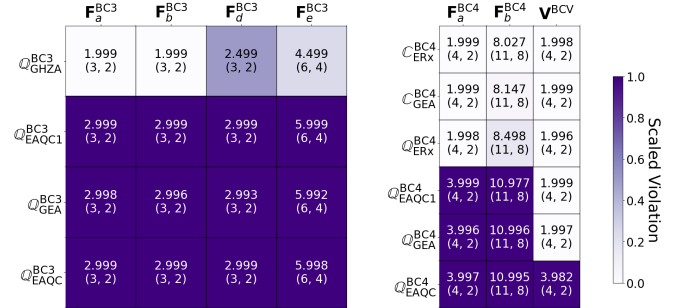


**FIG. 19:** (Left) We plot the entanglement-assisted violations of the facet inequalities listed in Table VIII for the BC3 network polytope. (Right) We plot the entanglement-assisted violations of the BC4 network polytope facet inequalities in Eq. (38) and the  $\mathbf{V}^{\text{BCV}}$  game described in Eq. (37). The column of each plot corresponds to a different nonclassicality witness while each row corresponds to a different resource configuration. The top number in each cell shows the largest numerical violation obtained via variational optimization. The lower tuple,  $(\gamma^*, \gamma)$ , shows the largest possible score  $\gamma^*$  and the classical bound  $\gamma$  for each linear black box game.

tion from the sender to each receiver. The  $d^2$  signaling dimension of entanglement-assisted quantum communication allows for the entire input to be communicated to each receiver, thus enabling perfect coordination between the outputs of the two receivers. Remarkably, we find no other violations of this inequality for signaling dimensions  $d_1 = d_2 = 2$ , further indicating numerically that entanglement-assisted receivers, entanglement-assisted classical communication, and tripartite entanglement-assisted quantum signaling resources are all insufficient for boosting the amount of information that can be communicated from the sender to the two receivers. Hence, we argue that violations of

the broadcast communication value nonclassicality witness can serve as a semi-device-independent test for two-sided entanglement-assisted quantum communication.

To consider scenarios with more inputs and outputs, we apply linear programming to find nonclassicality witnesses. In the following equation, we show a facet inequality of  $\mathbb{C}^{\text{BC}}$  where  $|\mathcal{X}| = |\mathcal{Y}_1| = |\mathcal{Y}_2| = 4$ . This was derived from a nonclassical test behavior obtained using a Popescu-Rohrlich (PR) box [79] between the receivers and tasking the receivers with achieving the maximal possible violation of the CHSH inequality [80] where each device outputs a two-bit value containing their measurement result and their measurement basis. The derived inequality is

$$(a) \ 2 \geq \begin{bmatrix} 1 & 0 & 0 & 0 \\ 0 & 1 & 0 & 0 \\ 0 & 0 & 0 & 0 \\ 0 & 0 & 0 & 0 \\ 0 & 1 & 0 & 0 \\ 1 & 0 & 0 & 0 \\ 0 & 0 & 0 & 0 \\ 0 & 0 & 0 & 0 \\ 0 & 0 & 0 & 0 \\ 0 & 0 & 0 & 0 \\ 0 & 0 & 1 & 0 \\ 0 & 0 & 0 & 1 \\ 0 & 0 & 0 & 1 \\ 0 & 0 & 1 & 0 \end{bmatrix} \quad (b) \ 8 \geq \begin{bmatrix} 3 & 0 & 0 & 0 \\ 0 & 3 & 0 & 0 \\ 0 & 0 & 0 & 3 \\ 1 & 1 & 0 & 2 \\ 1 & 1 & 0 & 2 \\ 1 & 1 & 0 & 2 \\ 2 & 1 & 0 & 2 \\ 1 & 3 & 0 & 2 \\ 1 & 0 & 2 & 0 \\ 0 & 1 & 2 & 0 \\ 0 & 0 & 0 & 3 \\ 1 & 1 & 0 & 2 \\ 2 & 1 & 0 & 2 \\ 1 & 2 & 0 & 2 \\ 1 & 1 & 1 & 2 \\ 2 & 2 & 1 & 2 \end{bmatrix}. \quad (38)$$

Remarkably, nonclassicality can be witnessed when the two receivers share quantum entanglement. The strongest violation we find for the inequality in Eq. (38).b is  $8.5 = \max_{\mathbf{P} \in \mathbb{Q}_{\text{ERX}}^{\text{BC}}} \langle \mathbf{G}_b, \mathbf{P} \rangle \geq \gamma = 8$ . To achieve this violation, we find the minimal necessary variational ansatz shown in Fig. 20. The optimal settings for each of the unitaries are as follows:

$$\vec{\theta}_x^A = \left( (0, \frac{\pi}{2}), (0, \frac{3\pi}{2}), (\pi, \frac{3\pi}{2}), (\pi, \frac{\pi}{2}) \right), \quad (39)$$

$$\vec{\theta}^{B_1} = \left( \frac{3\pi}{2}, \frac{\pi}{2}, \frac{\pi}{2}, \frac{\pi}{4} \right), \quad \vec{\theta}^{B_2} = \left( \vec{\theta}_0^{B_2}, \pi, \frac{\pi}{4}, \frac{\pi}{2} \right), \quad (40)$$

where  $\vec{\theta}_0^{B_2} \approx -2.498091860$ . Rounded to the eighth dec-

imal place, we estimate the optimal behavior to be

$$\mathbf{P}^{\text{BC}}(\vec{\theta}^*) = \begin{bmatrix} 0.45000005 & 0. & 0. & 0. \\ 0. & 0.45000005 & 0. & 0. \\ 0.04999995 & 0. & 0. & 0. \\ 0. & 0.04999995 & 0. & 0. \\ 0.04999995 & 0. & 0. & 0. \\ 0. & 0.04999995 & 0. & 0. \\ 0.45000005 & 0. & 0. & 0. \\ 0. & 0.45000005 & 0. & 0. \\ 0. & 0. & 0. & 0.10000006 \\ 0. & 0. & 0.39999994 & 0. \\ 0. & 0. & 0. & 0.39999994 \\ 0. & 0. & 0.10000006 & 0. \\ 0. & 0. & 0. & 0.39999994 \\ 0. & 0. & 0.10000006 & 0. \\ 0. & 0. & 0. & 0.10000006 \\ 0. & 0. & 0.39999994 & 0. \end{bmatrix}. \quad (41)$$

When the unrounded behavior is played against the game  $\mathbf{G}_b^{\text{BC}}$ , we find the score  $8.5 = \langle \mathbf{G}_b^{\text{BC}}, \mathbf{P}^{\text{BC}}(\vec{\theta}^*) \rangle + \epsilon$  where  $\epsilon < 10^{-12}$ . With the rounded behavior from Eq. (41), a score of 8.5 is obtained up to seven decimal places.

Overall, we observe that quantum signaling is an insufficient resource for demonstrating nonclassicality in a broadcast network. We conjecture that there exists a no-go theorem restricting broadcast network behaviors to the classical broadcast network polytope, much in a similar manner to the classicality of unassisted quantum communication in the point-to-point network [20]. On the other hand, we find that entanglement-assisted classical and quantum communication are both sufficient resources to demonstrate nonclassicality as well as entanglement-assisted receivers.

One application of these novel broadcast nonclassicality witnesses is to apply them as semi-device-independent tests that certify the presence of entanglement-assisted resources: Suppose that no entanglement-assisted signaling is used. Then a violation of a broadcast nonclassicality witness shows that the receivers must share a resource stronger than shared randomness, such as entanglement. We expect a further investigation of broadcast nonclassicality witnesses and their associated violations to uncover interesting tests for verifying entangled measurement devices and entanglement-assisted communication in communication networks.

#### D. Nonclassicality in Multipoint Networks

A multipoint network consists of multiple senders and multiple receivers and may also contain intermediate processing devices, creating a complex causal structure. We consider the case where two senders  $A_1$  and  $A_2$  are given

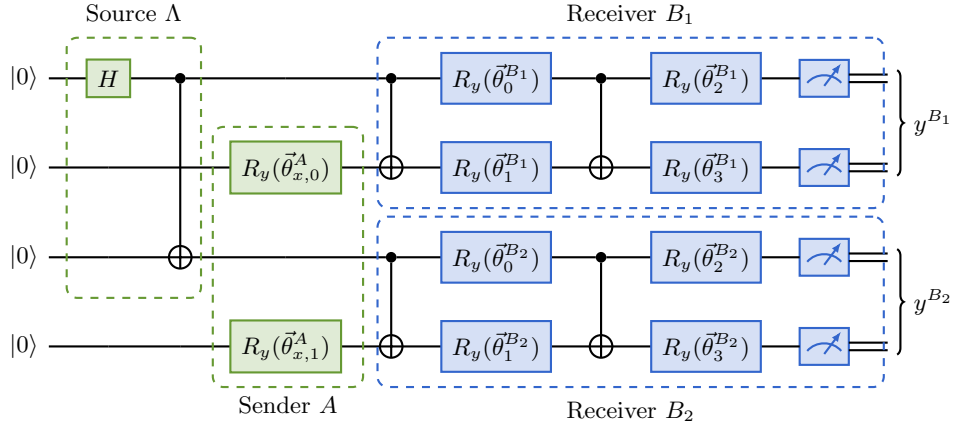


**FIG. 20:** Minimal variational ansatz circuit for entanglement-assisted receivers that achieves the maximal nonclassicality score. All rotations are about the  $y$ -axis on Bloch sphere such that  $R_y(\vec{\theta}) = e^{-i\vec{\theta}\sigma_y/2}$ . Note that the source  $\Lambda$  operates upon the first and third qubits whereas the sender  $A$  operates on the second and fourth qubits. The receivers each get one qubit from the sender and one qubit from the source. Furthermore, note that the sender does not prepare an entangled state.

Set	Definition
$\mathbb{C}^{\text{IF}}$	$\mathbf{P}^{\text{IF}} = \sum_{\lambda} P_{\lambda}(\mathbf{P}_{\lambda}^{C_1} \otimes \mathbf{P}_{\lambda}^{C_2}) \mathbf{P}_{\lambda}^B(\mathbf{P}_{\lambda}^{A_1} \otimes \mathbf{P}_{\lambda}^{A_2})$
$\mathbb{C}^{\text{CIF}}$	$\mathbf{P}^{\text{CIF}} = \sum_{\lambda} P_{\lambda}(\mathbf{P}_{\lambda}^{D_1} \otimes \mathbf{P}_{\lambda}^{D_2}) \mathbf{P}_{\lambda}^C \mathbf{P}_{\lambda}^B(\mathbf{P}_{\lambda}^{A_1} \otimes \mathbf{P}_{\lambda}^{A_2})$
$\mathbb{C}^{\text{HG}}$	$\mathbf{P}^{\text{HG}} = \sum_{\lambda} P_{\lambda}(\mathbf{P}_{\lambda}^{B_1} \otimes \mathbf{P}_{\lambda}^{B_2}) \times (\mathbb{I}_2 \otimes \mathbf{V}^{\leftrightarrow} \otimes \mathbb{I}_2)(\mathbf{P}_{\lambda}^{A_1} \otimes \mathbf{P}_{\lambda}^{A_2})$
$\mathbb{C}^{\text{BF}}$	$\mathbf{P}^{\text{BF}} = \sum_{\lambda} P_{\lambda}(\mathbf{P}_{\lambda}^{D_1} \otimes \mathbf{P}_{\lambda}^{D_2}) \times (\mathbb{I}_2 \otimes \mathbf{P}_{\lambda}^C \mathbf{P}_{\lambda}^B \otimes \mathbb{I}_2)(\mathbf{P}_{\lambda}^{A_1} \otimes \mathbf{P}_{\lambda}^{A_2})$

**TABLE X:** Classical multipoint network polytope definitions (see Fig. 21 for DAG representations). Listed from top to bottom are the interference (IF) network, compressed interference (CIF) network, hourglass (HG) network, and butterfly (BF) network. Note that in the hourglass and butterfly  $2 \times 2$  identity matrices are used to pass data through an intermediate layer. Moreover, in the hourglass network, an explicit swap  $\mathbf{V}^{\leftrightarrow}$  is needed to model the communication from  $A_1 \rightarrow B_2$  and  $A_2 \rightarrow B_1$ .

the inputs  $x_1 \in \mathcal{X}_1$  and  $x_2 \in \mathcal{X}_2$  respectively. After the information flows through the network, two independent receivers  $M_1$  and  $M_2$  output the values  $y_1 \in \mathcal{Y}_1$  and  $y_2 \in \mathcal{Y}_2$ , respectively. Note that  $M_i$  is used as a placeholder for nodes in the final network layer, which we refer to as the measurement layer. Although, we restrict ourselves to two senders and two receivers, there are a range of signaling configurations that can be considered (see Fig. 21). Note that the considered multipoint networks are not exhaustive, but serve as important examples.

### 1. Nonclassicality Witnesses for Multipoint Networks

In general, the enumeration of deterministic behaviors for the classical network polytope is difficult due to the number of independent devices. Given the memory constraints of a typical laptop computer, we are only able to calculate the full set of vertices  $\mathbb{V}^{\text{Net}}$  in the simplest non-trivial case where  $|\mathcal{X}_1| = |\mathcal{X}_2| = |\mathcal{Y}_1| = |\mathcal{Y}_2| = 3$  for each of the networks in Fig. 21. Using this set of vertices, we take two approaches to derive nonclassicality witnesses.

We first derive simulation games  $(\gamma, \mathbf{V})$  where the game's objective is to minimize the error of simulating a deterministic behavior  $\mathbf{V} \in \mathbb{V}_{\vec{y}|\vec{x}}^{\text{Net}}$  such that  $\mathbf{V} \notin \mathbb{C}^{\text{Net}}$ . By Lemma 6 there is a direct correspondence between simulation error and game score where  $D(\mathbf{V}, \mathbf{P}) = P_{\text{Error}} = 1 - \frac{1}{|\mathcal{X}|} \langle \mathbf{V}, \mathbf{P} \rangle$ . A simulation game can be derived from any deterministic behavior that is excluded from the classical network polytope such that  $\mathbf{V} \notin \mathbb{C}^{\text{Net}}$ . The classical bound is then calculated as

$$\gamma = \max_{\mathbf{V}' \in \mathbb{V}_{\vec{y}|\vec{x}}^{\text{Net}}} \langle \mathbf{V}, \mathbf{V}' \rangle. \quad (42)$$

A complete list of considered simulation games is provided in Table XI.

Our second approach to deriving nonclassicality witnesses for multipoint networks applies the linear programming technique in Algorithm 1. That is, we apply each of the deterministic behaviors in Table XI as a test behavior used to derive a facet inequality that tightly bounds the classical network polytope  $\mathbb{C}^{\text{Net}}$ . Each deterministic test behavior yields a distinct facet  $(\gamma, \mathbf{F})$  that witnesses its violation. Note that the facets calculated for each network are distinct from that network. Furthermore, we use  $\mathbf{F}$  to distinguish the facets from the simulation games where the same superscript labels as in Table XI are used. In Appendix D, we present the

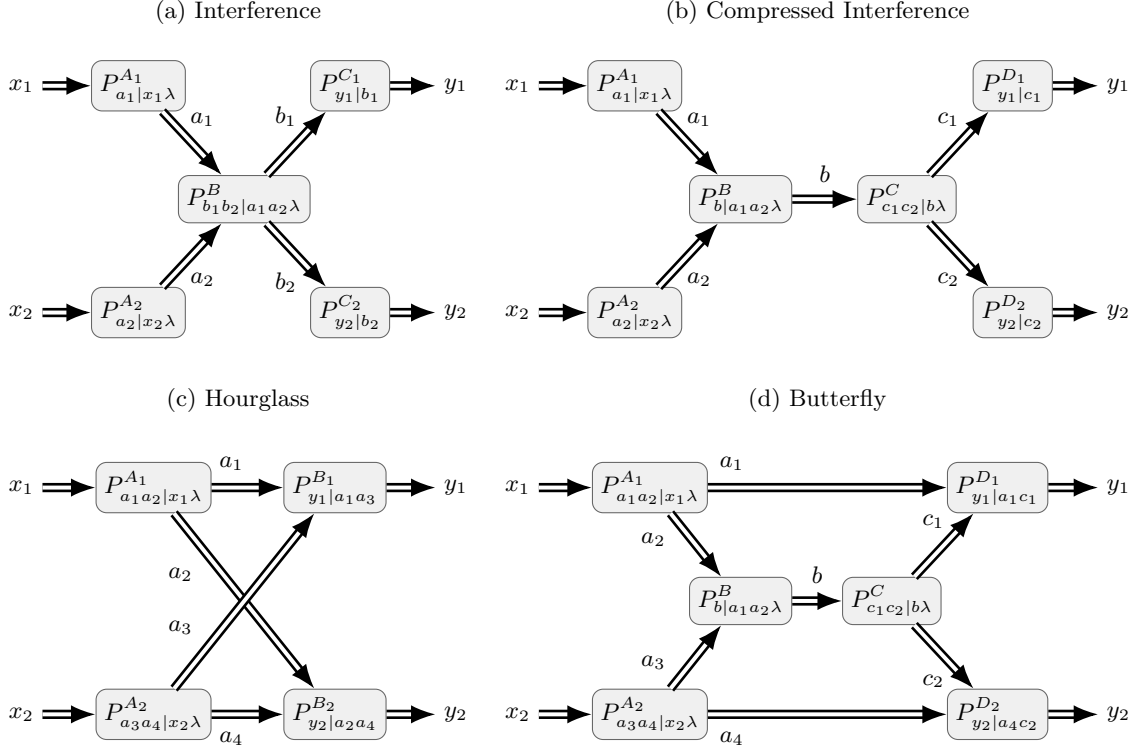


**FIG. 21:** Classical multipoint network DAGs. (a) Interference (IF) network, (b) compressed interference (CIF) network, (c) hourglass (HG) network, and (d) butterfly (BF) network.

facet inequalities that we obtain for each of the multipoint communication networks.

## 2. Numerical Quantum Violations of Nonclassicality in Multipoint Networks

For each multipoint network shown in Fig. 21 we consider the three distinct quantum resource configurations shown in Fig. 22. In all three quantum resource configurations, quantum signaling replaces all classical communication. Furthermore, we investigate the added advantage of the two senders or two receivers sharing a single maximally entangled state.

Within our variational ansatz circuit the free operations for each network device span the complete set of unitaries for a fixed number of qubits. Preparation devices (green rectangles) are assumed to prepare pure states. It follows that the number of qubits at each preparation device is equivalent to the number of arrows exiting the devices in the DAG. For processing devices (red rectangles) we permit at least one ancillary qubit in addition to number of qubits received from upstream devices. As a result, our free operations extend beyond the unitary evolution of the initialized pure state, allowing for a broader class of quantum channels to be considered. Similarly, measurement devices (blue rectangles) each perform a projective on the received qubits plus an

ancilla qubit, meaning that they can implement POVM measurements on the received qubits. In our numerical examples we consider  $|\mathcal{Y}_1| = |\mathcal{Y}_2| = 3$  hence we apply a deterministic postprocessing map that takes each local two-bit measurement result to a trit.

In the majority of cases we consider the post-processing map

$$\mathbf{V}^{\text{Post}} = \begin{bmatrix} 1 & 0 & 0 & 1 \\ 0 & 1 & 0 & 0 \\ 0 & 0 & 1 & 0 \end{bmatrix}, \quad (43)$$

but alternative postprocessing maps can achieve better scores in some cases. In particular, we found that the classical bound of a certain simulation game  $\gamma = \langle \mathbf{V}, \mathbf{P} \rangle$  can only be achieved by certain post-processing maps.

As consider quantum resources configurations that replace classical communication with quantum communication. In particular, we study quantum communication without entanglement assistance (QC), entanglement-assisted senders (ETx), and entanglement-assisted receivers (ERx). In each network, we optimize each resource configuration against the respective network's nonclassicality witnesses. As nonclassicality witnesses, we consider the simulation games listed in Table XI as well as the associated facet inequalities of the classical network polytope  $\mathcal{C}^{\text{Net}}$  obtained using the linear program in Eq. (6).

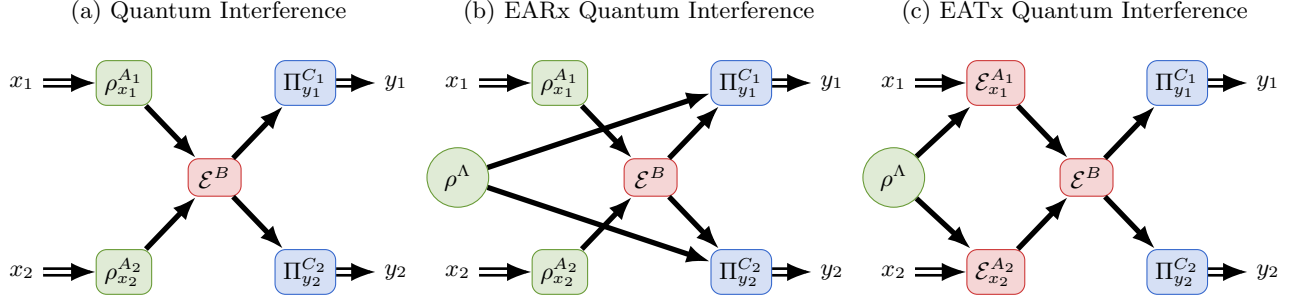


**FIG. 22:** Quantum interference network DAGs considered in this work. Each of the DAGs in Fig. 21 can have their classical signaling replaced with quantum communication (a). Similarly, entanglement can be used to assist either the receivers (EARx) (b) or senders (EATx) (c). Note that many alternative resource configurations could be considered, but we restrict ourselves to the three resource configurations for brevity.

Name	Sym.	Definition
Multiplication (0,1,2)	$\mathbf{V}^{\times_0}$	$V_{\vec{y} \vec{x}}^{\times_0} = \begin{cases} 1 & \text{if } \vec{y} = x_1 \times x_2 \\ 0 & \text{otherwise} \end{cases}$
Multiplication (1,2,3)	$\mathbf{V}^{\times_1}$	$V_{\vec{y} \vec{x}}^{\times_1} = \begin{cases} 1 & \text{if } \vec{y} = x_1 \times x_2 \\ 0 & \text{otherwise} \end{cases}$
Swap	$\mathbf{V}^{\leftrightarrow}$	$V_{\vec{y} \vec{x}}^{\leftrightarrow} = \begin{cases} 1 & \text{if } y_1 = x_2 \text{ and } y_2 = x_1 \\ 0 & \text{otherwise} \end{cases}$
Addition (0,1,2)	$\mathbf{V}^+$	$V_{\vec{y} \vec{x}}^+ = \begin{cases} 1 & \text{if } \vec{y} = x_1 + x_2 \\ 0 & \text{otherwise} \end{cases}$
Equality	$\mathbf{V}^=$	$V_{y x_1, x_2}^= = 1 - \delta_{x_1, x_2}$
Comparison	$\mathbf{V}^{\geq}$	$V_{\vec{y} \vec{x}}^{\geq} = \begin{cases} \delta_{y_1, 0} \delta_{y_2, 0} & \text{if } x_1 = x_2 \\ \delta_{y_1, 1} \delta_{y_2, 2} & \text{if } x_1 < x_2 \\ \delta_{y_1, 2} \delta_{y_2, 1} & \text{if } x_1 > x_2 \end{cases}$
Permutation	$\mathbf{V}^{\pi}$	$V_{\vec{y} \vec{x}}^{\pi} = \begin{cases} \delta_{y_1, 0} \delta_{y_2, 2} & \text{if } x_1 = 0 \\ \delta_{y_1, 1} \delta_{y_2, (x_2+2)\%3} & \text{if } x_1 = 1 \\ \delta_{y_1, 2} \delta_{y_2, (x_2+1)\%3} & \text{if } x_1 = 2 \end{cases}$
Difference	$\mathbf{V}^-$	$V_{\vec{y} \vec{x}}^- = \begin{cases} 1 & \text{if } y_1 = y_2 =  x_1 - x_2  \\ 0 & \text{otherwise} \end{cases}$
Communication Value	$\mathbf{V}^{\text{CV}}$	$V_{\vec{y} \vec{x}}^{\text{CV}} = \delta_{\vec{y}, \vec{x}}$

**TABLE XI:** Simulation games for  $33 \rightarrow 33$  multipoint communication networks. Each deterministic behavior  $\mathbf{V} \in \mathbb{V}_{\vec{y}|\vec{x}}$  cannot be simulated by the networks given in Fig. 21. Note that  $a\%b \equiv a \pmod b$ .

In Fig. 23 we plot our numerical results. We find that unassisted and entanglement-assisted quantum communication resources can broadly produce nonclassical behaviors in quantum networks. When unassisted classical signaling is used, no advantage is found in any of the considered simulation games  $(\gamma, \mathbf{V})$ , however we find violations to facet inequalities  $(\gamma, \mathbf{F})$  for all networks except the broadcast network. Thus, we show that quantum advantage can be demonstrated without entanglement in networks having multiple senders.

In the second row of Fig. 23, we consider entanglement-assisted receivers as shown in Fig. 22(b). In most cases, we find entanglement-assisted receivers to provide no advantage over unassisted quantum signaling. However, the hourglass (HG) network and butterfly (BF) network both show violations. Interestingly, the hourglass network shows an advantage in the communication value game  $(5, \mathbf{G}_{3,3}^{\text{CV}})$ , indicating that entanglement between the two receivers is able to increase the classical communication capacity of the network. For the butterfly network, the violation of the facet inequality  $\mathbf{F}^{\text{CV}}$  is also interesting because a larger score is achieved for entanglement-assisted receivers than entanglement-assisted senders. This indicates that the two sets  $\mathbb{Q}_{\text{ETx}}^{\text{Net}}$  and  $\mathbb{Q}_{\text{ERx}}^{\text{Net}}$  may have some mutually excluded regions.

In the third row of Fig. 23, we consider entanglement-assisted senders as shown in Fig. 22(c). We find that the entanglement-assisted senders broadly achieve larger violations than unassisted quantum signaling. Furthermore, we find the strongest violations for the multiaccess network MA(3,  $3^{2,2}9$ ), and entanglement-assisted senders in the quantum multiaccess network saturate the upper bounds. In nearly all examples, entanglement-assisted senders (ETx) can achieve larger violations than entanglement assisted receivers (ERx), while our findings for the butterfly network violation of  $\mathbf{F}^{\text{CV}}$  suggest that neither resource configuration can fully simulate the other.

Overall, we provide numerical evidence for operational advantages of quantum communication resources in multipoint networks. We show that entangled senders and receivers are able to demonstrate advantages in simula-



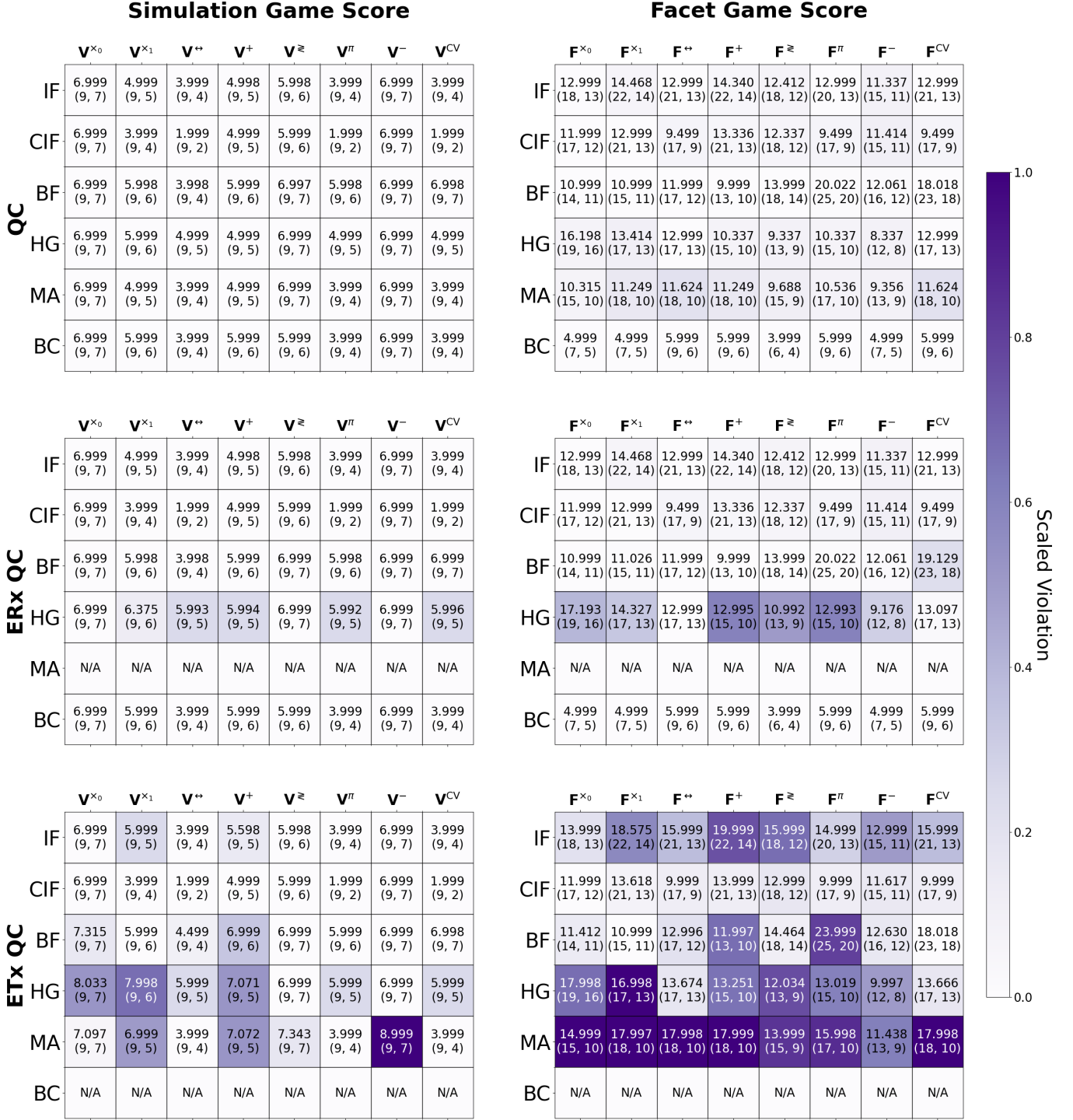


**FIG. 23: Quantum violation of classicality in  $3, 3 \overline{3}, 3, 3$  multipoint networks:** For the interference (IF), compressed interference (CIF), butterfly (BF), hourglass (HG), multiaccess (MA), and broadcast (BC) networks we consider quantum communication (QC), entanglement-assisted receiver quantum communication (ERx QC), and entanglement-assisted transmitter quantum communication (ETx QC) resource configurations as shown in shown in Fig. 22. The column of each plot corresponds to a different nonclassicality witness while each row corresponds to a different network DAG. The top number in each cell shows the largest numerical violation obtained via variational optimization. The lower tuple,  $(\gamma^*, \gamma)$ , shows the largest possible score  $\gamma^*$  and the classical bound  $\gamma$  for each linear black box game. In the left-hand column of plots, we show the quantum violations are listed for the simulation games listed in Table XI while the right-hand column of plots shows the quantum violations of the classical network polytope facet inequalities listed in Appendix D. In both cases, the cells are shaded according to the scaled violation.

tion games, implying that the deterministic tasks in Table XI can be performed with greater success probability. We also identify a large number of examples of nonclassicality witnessed with respect to facet inequalities of the classical network polytope. These violations pave the way for self-testing methods to characterize quantum resource configurations and causal structures.

#### IV. DISCUSSION

In this work we investigate the operational advantages attained using quantum communication resources communication networks. We employ nonclassicality as a quantifier of operational advantage, as it demonstrates a resource simulation advantage that can be observed in realistic quantum networks with limited quantum resources. In general, a quantum network’s nonclassicality implies that the network’s behavior cannot be simulated by a classical network using similar classical signaling resources. Indeed, we derive linear classicality inequalities that witness the nonsimulability of quantum behaviors and their explicit advantages in distributed information processing and communications tasks. To maximize the nonclassicality of a given quantum resource configuration, we apply variational optimization methods to our resource theoretic quantum circuit simulation of a quantum network.

We investigate a wide range of network nonclassicality witnesses and find that nonclassicality can be achieved ubiquitously across all considered networks that use entanglement to assist quantum or classical communication. Furthermore, we find that networks having multiple senders can achieve nonclassical behaviors using quantum communication unassisted by entanglement. We find that the amount of violation is distinct for each resource configuration, showing that different quantum resource configurations do not provide the same operational advantage. Indeed, in simple settings a strict hierarchy of resource advantage can be identified through relative simulability. In general, there may exist two resource configurations such that neither configuration can simulate the behaviors of the other with zero error.

Beyond the theoretical demonstration of operational quantum advantage in networks, the violations exhibited in this work also have practical applications such as self-testing, certification, and verification tasks for quantum resources and network configurations. Indeed, our framework for witnessing nonclassicality is semi-device-independent because the signaling dimension of each channel must be known. Thus our nonclassicality witnesses serve as semi-device-independent tests of LOCC and LOQC resources. Moreover, many of the violations cannot be achieved without the use of POVM measurements or nonunitary CPTP maps, indicating that the presence of certain operations at a device can also be certified. Our methods can also be used to help infer a network’s topology or resource configuration by ruling

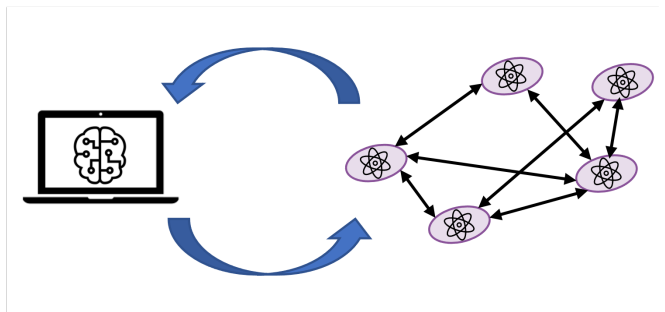


**FIG. 24:** Our variational quantum optimization methods could be used to automate quantum networking hardware to establish protocols using simulation games or certify quantum resources using nonclassicality.

out classes of networks that are unable to demonstrate the considered network’s black box behavior. Hence, in a device-independent manner, the internal causal structure and resources of a black box can be characterized to some degree.

From a fundamental physics perspective, our results provide new examples in which the classical concepts of locality, causality, and realism break down. By demonstrating these nonclassical signaling behaviors in the experimental setting, we can verify the correctness of quantum theory in new ways. Our results also reiterate what has been previously noted about Bell nonlocality [81]: the key requirement for nonclassicality is the local independence of network inputs. Note that the point-to-point and broadcast networks, which do not have locally independent inputs, are the only examples for which unassisted quantum signaling provides no witnessable advantage. Nevertheless, these networks demonstrate nonclassicality when assisted by entanglement where the entanglement is assumed to be locally independent from the classical input.

Our framework for quantum network simulation and optimization provides a few key advantages over standard classical methods. First, our quantum circuit model of a quantum network can be run on a quantum computer. As quantum computers improve, it is plausible that classical simulation software will be unable to simulate quantum networks with the same efficiency as the quantum computer. Second, our variational optimization framework can be extended to quantum networking hardware (see Fig. 24). Thus, Algorithm 2 provides a technique for optimizing quantum networks to perform a task encoded by the gain (or cost) function. These variational methods have been shown to successfully optimize quantum networks against uncharacterized noise models [46, 48, 68], as well as the ability to extract quantities such as the von Neumann entropy from quantum systems [67]. Furthermore, Algorithm 4 could be used to automatically establish communication protocols and distributed arithmetic operations on quantum networking hardware. Likewise, Algorithm 3 can be used to automatically establish nonclassical behaviors in quantum

networks, allowing the automation of self-testing and certification tasks.

The main drawbacks of our framework are scaling our computational methods. The facet derivation algorithms we apply push the limit of what can be computed on a typical laptop computer within a few hours. Extending our methods to larger networks will require high-performance computing and methods that exploit the permutation symmetry of the classical network polytope. For example, the adjacency decomposition algorithm [82] was used to compute signaling dimension witnesses in [26]. On the contrary, simulation games present a more scalable approach to witnessing nonclassicality. However, since simulation games do not tightly bound the classical network polytope, they are less sensitive to witnessing nonclassicality.

A second drawback is that our methods do not generally place an upper bound on the violations of quantum resources. Throughout this work, we only derive the classical bound, and the maximal possible score in a given black box game. We can therefore only confirm that a quantum resource configuration achieves the maximum if it saturates the maximal possible score for the given game. Otherwise, we can only assert that nonclassicality was demonstrated, but not if we actually achieved the maximum violation. Similarly, we find that maximal violations can depend on the number of ancilla qubits in network devices, and the considered postprocessing map. It is thus important to find ways to incorporate the postprocessing maps into the variational optimization, or investigate further how good postprocessing map can be selected. Another interesting question is to identify how the number of ancillary qubits relates to a network's ability to exhibit nonclassicality.

A third challenge is that our framework of black box behaviors requires a large number of samples to be collected for nonclassicality to be witnessed with confidence. As more parties or inputs are added to the network, the dimensions of the network's behavior matrix will scale exponentially. Therefore, it may not be feasible to collect a sufficient number of statistics to accurately construct a network's behavior matrix. This is a significant challenge faced by quantum technologies.

Overall, our work provides a broad analysis of the nonclassical behaviors that can emerge in quantum networks. However, there remains significant work to elucidate the details of these nonclassical behaviors. First, we note that improving our computational methods will be essential to scaling beyond the networks considered in this work. In essence, we apply standard algorithms to develop a novel framework, however, future researchers can tailor these algorithms so that they are better suited for the computational problems at hand.

We invite researchers to demonstrate the introduced nonclassical behaviors experimentally. To find optimal settings the variational ansatz can be tailored to resemble the free operations available in the experimental apparatus. Furthermore, Algorithm 3 can be extended to experimental apparatuses to automatically obtain nonclassical behaviors. From a theoretical point of view, it is important to derive upper bounds on each of the quantum resource configurations discussed in this work. This allows for our results to be validated further by showing convergence to an upper bound. We remark, however, that in all cases where the optimal settings are known, our variational optimization algorithm has converged to the maximal score. Thus, we provide strong numerical evidence that many of the results shown in this work also demonstrate maximal violations. Finally, our nonclassicality witnesses can be applied more generally to device-independent information processing, which may lead to new self-testing or device-independent protocols.

### Supplemental Code

We provide our supporting software, numerical methods, and data in a public GitHub repository to make our methods and results accessible, transparent, and reproducible [37].

### Acknowledgements

This research was supported by a grant through the IBM-Illinois Discovery Accelerator Institute.

- 
- [1] H. J. Kimble, *Nature* **453**, 1023 (2008), [arXiv:0806.4195 \[quant-ph\]](#).
  - [2] R. V. Meter, *IEEE Network* **26**, 59 (2012).
  - [3] S. Wehner, D. Elkouss, and R. Hanson, *Science* **362**, 10.1126/science.aam9288 (2018).
  - [4] A. Singh, K. Dev, H. Siljak, H. D. Joshi, and M. Magarini, *IEEE Communications Surveys & Tutorials* **23**, 2218 (2021), [arXiv:2101.04427 \[quant-ph\]](#).
  - [5] G. Brassard, *Foundations of Physics* **33**, 1593–1616 (2003), [arXiv:quant-ph/0101005](#).
  - [6] H. Buhrman, R. Cleve, S. Massar, and R. de Wolf, *Rev. Mod. Phys.* **82**, 665 (2010), [arXiv:0907.3584 \[quant-ph\]](#).
  - [7] C. Bennett, P. Shor, J. Smolin, and A. Thapliyal, *IEEE Transactions on Information Theory* **48**, 2637 (2002), [arXiv:quant-ph/0106052](#).
  - [8] A. Winter, *arXiv preprint* (2002), [arXiv:quant-ph/0208131](#).
  - [9] C. H. Bennett, I. Devetak, A. W. Harrow, P. W. Shor, and A. Winter, *IEEE Transactions on Information Theory* **60**, 2926 (2014), [arXiv:0912.5537 \[quant-ph\]](#).
  - [10] T. S. Cubitt, D. Leung, W. Matthews, and A. Winter, *IEEE Transactions on Information Theory* **57**, 5509 (2011), [arXiv:1003.3195 \[quant-ph\]](#).

- [11] S. Massar, D. Bacon, N. J. Cerf, and R. Cleve, *Phys. Rev. A* **63**, 052305 (2001), [arXiv:quant-ph/0009088](#).
- [12] D. Bacon and B. F. Toner, *Phys. Rev. Lett.* **90**, 157904 (2003), [arXiv:quant-ph/0208057](#).
- [13] B. F. Toner and D. Bacon, *Phys. Rev. Lett.* **91**, 187904 (2003), [arXiv:quant-ph/0304076](#).
- [14] O. Regev and B. Toner, *SIAM Journal on Computing* **39**, 1562 (2010), [arXiv:0708.0827 \[quant-ph\]](#).
- [15] K. Maxwell and E. Chitambar, *Phys. Rev. A* **89**, 042108 (2014), [arXiv:1405.3211 \[quant-ph\]](#).
- [16] N. Brunner, D. Cavalcanti, S. Pironio, V. Scarani, and S. Wehner, *Rev. Mod. Phys.* **86**, 419 (2014), [arXiv:1303.2849 \[quant-ph\]](#).
- [17] J. B. Brask and R. Chaves, *Journal of Physics A: Mathematical and Theoretical* **50**, 094001 (2017), [arXiv:1607.08182 \[quant-ph\]](#).
- [18] E. Zambrini Cruzeiro and N. Gisin, *Entropy* **21**, 171 (2019), [arXiv:1812.05107 \[quant-ph\]](#).
- [19] M. Alimuddin, A. Chakraborty, G. L. Sidhardh, R. K. Patra, S. Sen, S. R. Chowdhury, S. G. Naik, and M. Banik, *Phys. Rev. A* **108**, 052430 (2023), [arXiv:2303.06848 \[quant-ph\]](#).
- [20] P. E. Frenkel and M. Weiner, *Communications in Mathematical Physics* **340**, 563 (2015), [arXiv:1304.5723 \[quant-ph\]](#).
- [21] P. E. Frenkel and M. Weiner, *Quantum* **6**, 662 (2022), [arXiv:2103.08567 \[quant-ph\]](#).
- [22] M. Dall'Arno, S. Brandsen, A. Tosini, F. Buscemi, and V. Vedral, *Phys. Rev. Lett.* **119**, 020401 (2017), [arXiv:1609.09237 \[quant-ph\]](#).
- [23] T. Heinosaari and O. Kerppo, *Journal of Physics A: Mathematical and Theoretical* **52**, 395301 (2019), [arXiv:1903.04899 \[quant-ph\]](#).
- [24] T. Heinosaari, O. Kerppo, and L. Leppäjärvi, *Journal of Physics A: Mathematical and Theoretical* **53**, 435302 (2020), [arXiv:2003.05264 \[quant-ph\]](#).
- [25] D. Poderini, S. Brito, R. Nery, F. Sciarrino, and R. Chaves, *Phys. Rev. Res.* **2**, 043106 (2020).
- [26] B. Doolittle and E. Chitambar, *Phys. Rev. Res.* **3**, 043073 (2021), [arXiv:2102.12543 \[quant-ph\]](#).
- [27] A. Tavakoli, J. Pauwels, E. Woodhead, and S. Pironio, *PRX Quantum* **2**, 040357 (2021), [arXiv:2103.10748 \[quant-ph\]](#).
- [28] M. J. Renner, A. Tavakoli, and M. T. Quintino, *Phys. Rev. Lett.* **130**, 120801 (2023), [arXiv:2207.02244 \[quant-ph\]](#).
- [29] A. Grudka, M. Horodecki, R. Horodecki, and A. Wójcik, *Phys. Rev. A* **92**, 052312 (2015), [arXiv:1403.1295 \[quant-ph\]](#).
- [30] A. Tavakoli, A. Hameedi, B. Marques, and M. Bourennane, *Phys. Rev. Lett.* **114**, 170502 (2015), [arXiv:1504.08105 \[quant-ph\]](#).
- [31] T. Heinosaari and L. Leppäjärvi, *Journal of Physics A: Mathematical and Theoretical* **55**, 174003 (2022), [arXiv:2112.03781 \[quant-ph\]](#).
- [32] A. Piveteau, J. Pauwels, E. Håkansson, S. Muhammad, M. Bourennane, and A. Tavakoli, *Nature Communications* **13**, 10.1038/s41467-022-33922-5 (2022), [arXiv:2205.09602 \[quant-ph\]](#).
- [33] N. Sakharwade, M. Studziński, M. Eckstein, and P. Horodecki, *New Journal of Physics* **25**, 053038 (2023), [arXiv:2208.14422 \[quant-ph\]](#).
- [34] P. Lauand, D. Poderini, R. Nery, G. Moreno, L. Pollyceno, R. Rabelo, and R. Chaves, *PRX Quantum* **4**, 020311 (2023), [arXiv:2211.13349 \[quant-ph\]](#).
- [35] J. Bowles, N. Brunner, and M. Pawłowski, *Phys. Rev. A* **92**, 022351 (2015), [arXiv:1505.01736 \[quant-ph\]](#).
- [36] J. S. Bell, *Physics Physique Fizika* **1**, 195 (1964).
- [37] B. Doolittle, [Supplementary code for operational nonclassicality in quantum communication networks](#), <https://github.com/ChitambarLab/nonclassicality-in-quantum-communication-networks-supplemental-code> (2024).
- [38] F. V. Jensen and T. D. Nielsen, *Bayesian networks and decision graphs*, Vol. 2 (Springer, 2007).
- [39] J. Pearl, *Statistics Surveys* **3**, 10.1214/09-ss057 (2009).
- [40] A. Tavakoli, *Phys. Rev. Lett.* **125**, 150503 (2020), [arXiv:2003.03859 \[quant-ph\]](#).
- [41] G. Brassard, A. Broadbent, and A. Tapp, *Foundations of Physics* **35**, 1877 (2005), [arXiv:quant-ph/0407221](#).
- [42] J. Silman, S. Machnes, and N. Aharon, *Physics Letters A* **372**, 3796 (2008), [arXiv:0710.3322 \[quant-ph\]](#).
- [43] Y. Quek and P. W. Shor, *Phys. Rev. A* **95**, 052329 (2017), [arXiv:1701.03813 \[quant-ph\]](#).
- [44] F. Leditzky, M. A. Alhejji, J. Levin, and G. Smith, *Nature Communications* **11**, 10.1038/s41467-020-15240-w (2020), [arXiv:1909.02479 \[quant-ph\]](#).
- [45] J. Nötzel, *IEEE Journal on Selected Areas in Information Theory* **1**, 401 (2020), [arXiv:1910.03796 \[quant-ph\]](#).
- [46] B. Doolittle, T. R. Bromley, N. Killoran, and E. Chitambar, *IEEE Transactions on Quantum Engineering* , 1 (2023), [arXiv:2205.02891 \[quant-ph\]](#).
- [47] B. Doolittle and T. Bromley, [qnetvo: the quantum network variational optimizer](#), <https://github.com/ChitambarLab/qNetV0> (2022).
- [48] B. Doolittle, *Nonclassicality in Noisy Quantum Networks*, Phd thesis, University of Illinois Urbana-Champaign (2023), available at <https://hdl.handle.net/2142/121945>.
- [49] A. Tavakoli, A. Pozas-Kerstjens, M.-X. Luo, and M.-O. Renou, *Reports on Progress in Physics* **85**, 056001 (2022), [arXiv:2104.10700 \[quant-ph\]](#).
- [50] G. Ziegler, *Lectures on Polytopes*, Graduate Texts in Mathematics (Springer New York, 2012).
- [51] D. Rosset, J.-D. Bancal, and N. Gisin, *Journal of Physics A: Mathematical and Theoretical* **47**, 424022 (2014), [arXiv:1404.1306 \[quant-ph\]](#).
- [52] T. Christof and A. Löbel, *Porta*, <http://porta.zib.de/> (1997).
- [53] B. Doolittle and B. Legat, [Xporta.jl](#), <https://github.com/JuliaPolyhedra/XPORTA.jl> (2020).
- [54] B. Legat, R. Deits, G. Goretkin, T. Koolen, J. Huchette, D. Oyama, and M. Forets, [JuliaPolyhedra/polyhedra.jl](#) (2021).
- [55] Q. Huangfu and J. J. Hall, *Mathematical Programming Computation* **10**, 119 (2018), [arXiv:1503.01889 \[math.OC\]](#).
- [56] I. Dunning, J. Huchette, and M. Lubin, *SIAM Review* **59**, 295 (2017), [arXiv:1508.01982 \[math.OC\]](#).
- [57] V. Bergholm, J. Izaac, M. Schuld, C. Gogolin, S. Ahmed, V. Ajith, M. S. Alam, G. Alonso-Linaje, B. Akash-Narayanan, A. Asadi, *et al.*, [arXiv preprint](#) (2018), [arXiv:1811.04968 \[quant-ph\]](#).
- [58] M. A. Nielsen and I. L. Chuang, *Quantum Computation and Quantum Information* (Cambridge University Press, 2009).
- [59] D. E. Rumelhart, G. E. Hinton, and R. J. Williams, *Nature* **323**, 533 (1986).

- [60] M. Schuld, V. Bergholm, C. Gogolin, J. Izaac, and N. Killoran, *Phys. Rev. A* **99**, 032331 (2019), arXiv:1811.11184 [quant-ph].
- [61] A. Mari, T. R. Bromley, and N. Killoran, *Phys. Rev. A* **103**, 012405 (2021), arXiv:2008.06517 [quant-ph].
- [62] D. Wierichs, J. Izaac, C. Wang, and C. Y.-Y. Lin, *Quantum* **6**, 677 (2022), arXiv:2107.12390 [quant-ph].
- [63] O. Kyriienko and V. E. Elfving, *Phys. Rev. A* **104**, 052417 (2021), arXiv:2108.01218 [quant-ph].
- [64] S. Ruder, arXiv preprint (2016), arXiv:1609.04747 [cs.LG].
- [65] D. P. Kingma and J. Ba, arXiv preprint (2014), arXiv:1412.6980 [cs.LG].
- [66] M. Cerezo, A. Arrasmith, R. Babbush, S. C. Benjamin, S. Endo, K. Fujii, J. R. McClean, K. Mitarai, X. Yuan, L. Cincio, and P. J. Coles, *Nature Reviews Physics* **3**, 625–644 (2021), arXiv:2012.09265 [quant-ph].
- [67] D. T. Chen, B. Doolittle, J. M. Larson, Z. H. Saleem, and E. Chitambar, arXiv preprint (2022), arXiv:2212.07987 [quant-ph].
- [68] Z. Ma, P. Gokhale, T.-X. Zheng, S. Zhou, X. Yu, L. Jiang, P. Maurer, and F. T. Chong, in *2021 IEEE International Conference on Quantum Computing and Engineering (QCE)* (2021) pp. 419–430, arXiv:2010.08702 [quant-ph].
- [69] E. Chitambar, I. George, B. Doolittle, and M. Junge, *IEEE Transactions on Information Theory* **69**, 1660 (2023), arXiv:2109.11144 [quant-ph].
- [70] C. H. Bennett and S. J. Wiesner, *Phys. Rev. Lett.* **69**, 2881 (1992).
- [71] R. Gallego, N. Brunner, C. Hadley, and A. Acín, *Phys. Rev. Lett.* **105**, 230501 (2010), arXiv:1010.5064 [quant-ph].
- [72] A. Ambainis, D. Leung, L. Mancinska, and M. Ozols, arXiv preprint (2008), arXiv:0810.2937 [quant-ph].
- [73] M. Pawłowski and N. Brunner, *Phys. Rev. A* **84**, 010302 (2011), arXiv:1103.4105 [quant-ph].
- [74] H.-W. Li, Z.-Q. Yin, Y.-C. Wu, X.-B. Zou, S. Wang, W. Chen, G.-C. Guo, and Z.-F. Han, *Phys. Rev. A* **84**, 034301 (2011), arXiv:1108.1480 [quant-ph].
- [75] G. Moreno, R. Nery, C. de Gois, R. Rabelo, and R. Chaves, *Phys. Rev. A* **103**, 022426 (2021), arXiv:2102.02709 [quant-ph].
- [76] A. Tavakoli, J. m. k. Kaniewski, T. Vértesi, D. Rosset, and N. Brunner, *Phys. Rev. A* **98**, 062307 (2018), arXiv:1801.08520 [quant-ph].
- [77] M. Pawłowski and A. Winter, *Phys. Rev. A* **85**, 022331 (2012), arXiv:1106.2409 [quant-ph].
- [78] J. Pawwels, S. Pironio, E. Z. Cruzeiro, and A. Tavakoli, *Phys. Rev. Lett.* **129**, 120504 (2022), arXiv:2203.05372 [quant-ph].
- [79] S. Popescu and D. Rohrlich, *Foundations of Physics* **24**, 379–385 (1994).
- [80] J. F. Clauser, M. A. Horne, A. Shimony, and R. A. Holt, *Phys. Rev. Lett.* **23**, 880 (1969).
- [81] V. Scarani, *Acta Physica Slovaca* **62**, 347 (2012), arXiv:1303.3081 [quant-ph].
- [82] T. Christof and G. Reinelt, *International Journal of Computational Geometry & Applications* **11**, 423 (2001).
- [83] E. Chitambar and G. Gour, *Rev. Mod. Phys.* **91**, 025001 (2019), arXiv:1806.06107 [quant-ph].
- [84] S. G. A. Brito, B. Amaral, and R. Chaves, *Phys. Rev. A* **97**, 022111 (2018), arXiv:1709.04260 [quant-ph].

## Appendix A: List of Acronyms

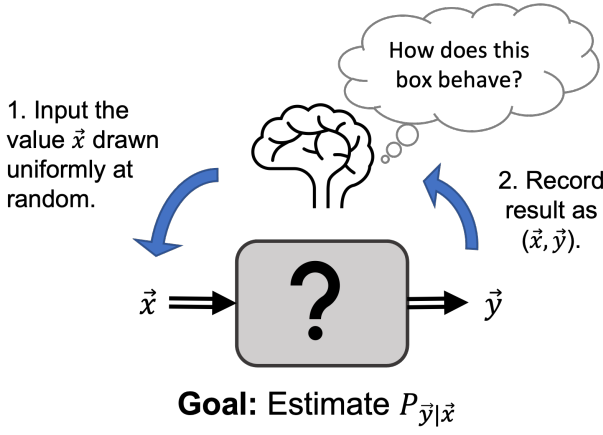
Acronym	Description
DAG	Directed Acyclic Graph
POVM	Positive Operator-Valued Measure
CPTP	Completely-Positive Trace-Preserving
QC	Quantum Communication
CC	Classical Communication
LOCC	Local Operations Classical Communication
LOQC	Local Operations Quantum Communication
GSR	Global Shared Randomness
EA	Entanglement-Assisted
GEA	Global Entanglement-Assisted
ETx	Entanglement-Assisted Senders
ERx	Entanglement-Assisted Receivers
VQO	Variational Quantum Optimization
CV	Communication Value
RAC	Random Access Coding
PM	Prepare and Measure
MA	Multiaccess
BC	Broadcast
IF	Interference
CIF	Compressed Interference
BF	Butterfly
HG	Hourglass
PR	Popescu and Rohrlich
CHSH	Clauser, Horne, Shimony, and Holt

TABLE XII: A list of acronyms used in this work.

## Appendix B: Black Box Models

### 1. Black Box Behaviors

A black box is a discrete and memoryless channel that models an unknown system or process. As shown in Fig. 25, an observer may query the black box with the input string  $\vec{x} \in \vec{\mathcal{X}} \equiv \mathcal{X}_1 \times \cdots \times \mathcal{X}_n$  where the black box returns the string  $\vec{y} \in \vec{\mathcal{Y}} \equiv \mathcal{Y}_1 \times \cdots \times \mathcal{Y}_m$  with probability  $P_{\vec{y}|\vec{x}} \geq 0$  where  $\sum_{\vec{y} \in \vec{\mathcal{Y}}} P_{\vec{y}|\vec{x}} = 1$ . The input is a string of  $n$  classical values  $\vec{x} = (x_i)_{i=1}^n$  where  $x_i \in \mathcal{X}_i = \{0, 1, \dots, |\mathcal{X}_i| - 1\}$  is drawn uniformly at ran-



**FIG. 25:** An observer characterizes a black box device by collecting data over many independent shot samples. In each shot, an input  $\vec{x} \in \vec{\mathcal{X}}$  is drawn from a uniformly random distribution and input into the black box device. The output  $\vec{y} \in \vec{\mathcal{Y}}$  is then recorded. After many shots, the transition probabilities  $P_{\vec{y}|\vec{x}}$  can be estimated.

dom. Likewise, the output is a string of  $m$  classical values  $\vec{y} = (y_j)_{j=1}^m$  where  $y_j \in \mathcal{Y}_j = \{0, 1, \dots, |\mathcal{Y}_j| - 1\}$ .

A black box is characterized by its *behavior*  $\mathbf{P} : \vec{\mathcal{X}} \rightarrow \vec{\mathcal{Y}}$ , which is represented by

$$\mathbf{P} \equiv \sum_{\vec{y} \in \vec{\mathcal{Y}}} \sum_{\vec{x} \in \vec{\mathcal{X}}} P_{\vec{y}|\vec{x}} |\vec{y}\rangle \langle \vec{x}| \quad (\text{B1})$$

with  $\mathbf{P} \in \mathbb{R}^{|\vec{\mathcal{Y}}| \times |\vec{\mathcal{X}}|}$  a column stochastic matrix and  $\{|\vec{y}\rangle\}_{\vec{y} \in \vec{\mathcal{Y}}}$  and  $\{|\vec{x}\rangle\}_{\vec{x} \in \vec{\mathcal{X}}}$  the computational bases for  $\mathbb{R}^{|\vec{\mathcal{Y}}|}$  and  $\mathbb{R}^{|\vec{\mathcal{X}}|}$ , respectively. For fixed input and output alphabets, the set of all black box behaviors is referred to as the *probability polytope*,

$$\mathbb{P}_{\vec{\mathcal{Y}}|\vec{\mathcal{X}}} \equiv \left\{ \mathbf{P} \in \mathbb{R}_{\geq 0}^{|\vec{\mathcal{Y}}| \times |\vec{\mathcal{X}}|} \mid \sum_{\vec{y} \in \vec{\mathcal{Y}}} P_{\vec{y}|\vec{x}} = 1 \forall \vec{x} \in \vec{\mathcal{X}} \right\}. \quad (\text{B2})$$

The probability polytope is convex such that  $\mathbb{P}_{\vec{\mathcal{Y}}|\vec{\mathcal{X}}} = \text{Conv} \left( \mathbb{V}_{\vec{\mathcal{Y}}|\vec{\mathcal{X}}} \right)$  where the extreme points  $\mathbb{V}_{\vec{\mathcal{Y}}|\vec{\mathcal{X}}}$  are the sets of deterministic behaviors

$$\mathbb{V}_{\vec{\mathcal{Y}}|\vec{\mathcal{X}}} \equiv \left\{ \mathbf{V} \in \mathbb{P}_{\vec{\mathcal{Y}}|\vec{\mathcal{X}}} \mid V_{\vec{y}|\vec{x}} \in \mathbb{B} \forall \vec{x} \in \vec{\mathcal{X}}, \vec{y} \in \vec{\mathcal{Y}} \right\} \quad (\text{B3})$$

with  $\mathbb{B} \equiv \{0, 1\}$  denoting the set of binary values.

Each behavior  $\mathbf{P} \in \mathbb{P}_{\vec{\mathcal{Y}}|\vec{\mathcal{X}}}$  describes a distinct operation that the black box device could apply. The probability polytope then contains all operations mapping the input  $\vec{\mathcal{X}}$  to the output  $\vec{\mathcal{Y}}$ . From a resource-theoretic perspective [83], we can say that  $\mathbb{P}_{\vec{\mathcal{Y}}|\vec{\mathcal{X}}}$  is the set of free operations that can be implemented by a black box device.

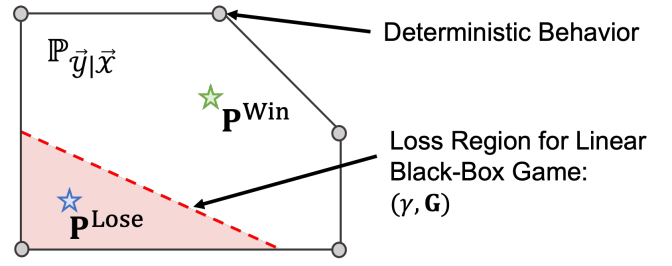


**FIG. 26:** A simplified depiction of the full probability polytope  $\mathbb{P}_{\vec{\mathcal{Y}}|\vec{\mathcal{X}}}$ . The abstraction shows key features of  $\mathbb{P}_{\vec{\mathcal{Y}}|\vec{\mathcal{X}}}$  such as its convexity and how its vertices (gray circles) are deterministic behaviors. The red dashed line depicts a linear black box game  $(\gamma, \mathbf{G})$  that separates the set of behaviors into a winning region (unshaded) and losing region (shaded red). Note that any behavior  $\mathbf{P}$  lying along the red dashed line satisfies  $\gamma = \langle \mathbf{G}, \mathbf{P} \rangle$ .

## 2. Black Box Games

We develop a game-theoretic framework for quantifying a black box's performance at a given task. Let a linear black box game be defined by the reward matrix  $\mathbf{G} \in \mathbb{R}^{|\vec{\mathcal{Y}}| \times |\vec{\mathcal{X}}|}$ . Given a behavior  $\mathbf{P} \in \mathbb{P}_{\vec{\mathcal{Y}}|\vec{\mathcal{X}}}$  and uniform prior, the average score of the game is evaluated as

$$\langle \mathbf{G}, \mathbf{P} \rangle := \text{Tr} [\mathbf{G}^T \mathbf{P}] = \sum_{\vec{y} \in \vec{\mathcal{Y}}} \sum_{\vec{x} \in \vec{\mathcal{X}}} G_{\vec{y}, \vec{x}} P_{\vec{y}|\vec{x}}. \quad (\text{B4})$$

**Lemma 3.** The maximal score  $\hat{\gamma}$  that can be achieved for a given black box game  $\mathbf{G}$  is

$$\hat{\gamma} \equiv \max_{\mathbf{P} \in \mathbb{P}_{\vec{\mathcal{Y}}|\vec{\mathcal{X}}}} \langle \mathbf{G}, \mathbf{P} \rangle = \sum_{\vec{x} \in \vec{\mathcal{X}}} \max_{\vec{y} \in \vec{\mathcal{Y}}} G_{\vec{y}, \vec{x}} \geq \gamma. \quad (\text{B5})$$

*Proof.* Since all behaviors  $\mathbf{P} \in \mathbb{P}_{\vec{\mathcal{Y}}|\vec{\mathcal{X}}}$  are column stochastic, it holds for all  $\vec{x} \in \vec{\mathcal{X}}$  that  $\sum_{\vec{y} \in \vec{\mathcal{Y}}} G_{\vec{y}, \vec{x}} P_{\vec{y}|\vec{x}} \leq \max_{\vec{y} \in \vec{\mathcal{Y}}} G_{\vec{y}, \vec{x}}$ . Then, summing over  $\vec{x} \in \vec{\mathcal{X}}$  as in Eq. (B4) yields the inequality in (B5). The upper bound  $\hat{\gamma}$  is achieved by the deterministic behavior  $\mathbf{V} \in \mathbb{V}_{\vec{\mathcal{Y}}|\vec{\mathcal{X}}}$  that satisfies  $V_{\vec{y}|\vec{x}} = \delta_{\vec{y}, g(\vec{x})}$  and  $g(\vec{x}) = \arg \max_{\vec{y} \in \vec{\mathcal{Y}}} G_{\vec{y}, \vec{x}}$  such that  $\langle \mathbf{G}, \mathbf{V} \rangle = \hat{\gamma}$ .  $\square$

**Lemma 4.** A linear black-box game  $(\gamma, \mathbf{G})$  can be rescaled into an equivalent game  $(0, \bar{\mathbf{G}})$  where

$$\bar{\mathbf{G}} = \frac{1}{\hat{\gamma} - \gamma} \left( \mathbf{G} - \frac{\gamma}{|\vec{\mathcal{X}}|} \mathbf{1}^{|\vec{\mathcal{Y}}| \times |\vec{\mathcal{X}}|} \right) \quad (\text{B6})$$

where  $\mathbf{1}^{|\vec{\mathcal{Y}}| \times |\vec{\mathcal{X}}|}$  is the ones matrix and  $\hat{\gamma}$  is defined in Eq. (B5). It follows that the average score of all winning behaviors is bounded as

$$1 \geq \langle \bar{\mathbf{G}}, \mathbf{P} \rangle \geq 0. \quad (\text{B7})$$

*Proof.* Consider a behavior that wins the game  $(\gamma, \mathbf{G})$  such the inequality  $\hat{\gamma} \geq \langle \mathbf{G}, \mathbf{P} \rangle \geq \gamma$  is satisfied. Then by algebraic manipulation we find

$$\hat{\gamma} - \gamma \geq \langle \mathbf{G}, \mathbf{P} \rangle - \gamma \geq 0 \quad (\text{B8})$$

$$1 \geq \frac{\langle \mathbf{G}, \mathbf{P} \rangle - \gamma}{\hat{\gamma} - \gamma} \geq 0 \quad (\text{B9})$$

$$1 \geq \frac{\langle \mathbf{G} - \frac{\gamma}{|\vec{\mathcal{X}}|} \mathbf{1}^{|\vec{\mathcal{Y}}| \times |\vec{\mathcal{X}}|}, \mathbf{P} \rangle}{\hat{\gamma} - \gamma} \geq 0 \quad (\text{B10})$$

$$1 \geq \langle \bar{\mathbf{G}}, \mathbf{P} \rangle \geq 0 \quad (\text{B11})$$

where the ones matrix satisfies  $\langle \mathbf{1}^{|\vec{\mathcal{Y}}| \times |\vec{\mathcal{X}}|}, \mathbf{P} \rangle = |\vec{\mathcal{X}}|$ .  $\square$

Although each reward matrix  $\mathbf{G} \in \mathbb{R}^{|\vec{\mathcal{Y}}| \times |\vec{\mathcal{X}}|}$  encodes a task whose performance is measured by the average score  $\langle \mathbf{G}, \mathbf{P} \rangle$ , it is not always clear how to interpret the task. However, given a Boolean reward matrix that satisfies  $\mathbf{G} \in \mathbb{B}^{|\vec{\mathcal{Y}}| \times |\vec{\mathcal{X}}|}$ , the game describes a task where for each input  $\vec{x}$  there is a set of ‘‘correct’’ outputs  $\vec{f}(\vec{x}) \subseteq |\vec{\mathcal{Y}}|$  such that

$$G_{\vec{y}, \vec{x}} = \begin{cases} 1 & \text{if } \vec{y} \in \vec{f}(\vec{x}) \\ 0 & \text{otherwise} \end{cases}. \quad (\text{B12})$$

For a uniform input distribution  $P_{\vec{x}} = \frac{1}{|\vec{\mathcal{X}}|}$ , we define the success probability as

$$P_{\text{Success}} = \frac{1}{|\vec{\mathcal{X}}|} \sum_{\vec{x} \in \vec{\mathcal{X}}} \sum_{\vec{y} \in \vec{f}(\vec{x})} P_{\vec{y}|\vec{x}} = 1 - P_{\text{Error}} \quad (\text{B13})$$

where  $P_{\text{Success}}, P_{\text{Error}} \in [0, 1]$ . The following Lemma draws a connection between the score of a Boolean black box game and the corresponding success probability.

**Lemma 5.** Consider a Boolean black box game  $(\gamma, \mathbf{G})$  satisfying  $\mathbf{G} \in \mathbb{B}^{|\vec{\mathcal{Y}}| \times |\vec{\mathcal{X}}|}$ . For any behavior  $\mathbf{P} \in \mathbb{P}_{\vec{\mathcal{Y}}|\vec{\mathcal{X}}}$ , the success probability relates to the average score as

$$P_{\text{Success}} = \frac{1}{|\vec{\mathcal{X}}|} \langle \mathbf{G}, \mathbf{P} \rangle. \quad (\text{B14})$$

*Proof.* Let  $\vec{f}(\vec{x}) \subseteq |\vec{\mathcal{Y}}|$  be the set of rows containing nonzero elements in the  $\vec{x}^{\text{th}}$  column of  $\mathbf{G}$ . Inserting the Boolean black box game defined in Eq. (B12) into Eq. (B4) yields

$$\langle \mathbf{G}, \mathbf{P} \rangle = \sum_{\vec{x} \in \vec{\mathcal{X}}} \sum_{\vec{y} \in \vec{f}(\vec{x})} P_{\vec{y}|\vec{x}}. \quad (\text{B15})$$

Then, multiplying Eq. (B15) by the uniform prior distribution  $1/|\vec{\mathcal{X}}|$  recovers the success probability in Eq. (B13).  $\square$

### 3. Simulating Black Boxes

Having introduced behaviors and games, we can now incorporate the concept of simulability into our black box model. Since the internals of a black box are hidden, a simulation of a black box only needs to reproduce the behavior  $\mathbf{P}$  that characterizes the black box. Recall that a black box behavior corresponds to a point in the probability polytope  $\mathbb{P}_{\vec{\mathcal{Y}}|\vec{\mathcal{X}}}$ . Following the approach taken by Britto *et al.* in reference [84], the distance between two black box behaviors  $\mathbf{P}, \mathbf{P}' \in \mathbb{P}_{\vec{\mathcal{Y}}|\vec{\mathcal{X}}}$  can be defined as the variational distance for probability distributions

$$D(\mathbf{P}, \mathbf{P}') = \frac{1}{2|\vec{\mathcal{X}}|} \sum_{x \in \vec{\mathcal{X}}} \sum_{y \in \vec{\mathcal{Y}}} |P_{\vec{y}|x} - P'_{\vec{y}|x}|, \quad (\text{B16})$$

where the scalar factor of  $1/|\vec{\mathcal{X}}|$  results from the assumption that the inputs  $\vec{x} \in \vec{\mathcal{X}}$  are drawn with uniform probability.

We formalize black box simulation using the variational distance in Eq. (B16). A black box behavior  $\mathbf{P}'$  achieves an *approximate simulation* of  $\mathbf{P}$  if  $D(\mathbf{P}, \mathbf{P}') \leq \epsilon$  where  $0 < \epsilon \ll 1$  is the allowable tolerance for error. Furthermore, a *zero-error simulation* of the black box behavior requires that  $\epsilon = 0$ . Although zero-error simulation is an important theoretical concept, it pertains to an idealized scenario. Black boxes are generally stochastic in nature and only a finite number of shots can be taken, and hence in practical settings the presence of sampling noise leads to approximate simulations.

For certain black box games, referred to as *simulation games*, we find that the distance measure in Eq. (B16), reduces to a linear black box game (see Lemma 6). A simulation game takes the form  $(\gamma, \mathbf{V})$  where  $\mathbf{V} \in \mathbb{V}_{\vec{\mathcal{Y}}|\vec{\mathcal{X}}}$  is a deterministic behavior. As we show in the following lemma, the score of a simulation game precisely measures the distance  $D(\mathbf{V}, \mathbf{P})$ , hence the objective of a simulation game is to simulate the deterministic behavior  $\mathbf{V}$ . That is, if  $\langle \mathbf{V}, \mathbf{P} \rangle / |\vec{\mathcal{X}}| = P_{\text{Success}} \rightarrow 1$  then  $\mathbf{P} \approx \mathbf{V}$  and approximate simulation is achieved with  $\epsilon \rightarrow 0$ .

**Lemma 6.** The distance between a deterministic behavior  $\mathbf{V} \in \mathbb{V}_{\vec{\mathcal{Y}}|\vec{\mathcal{X}}}$  and any other behavior  $\mathbf{P} \in \mathbb{P}_{\vec{\mathcal{Y}}|\vec{\mathcal{X}}}$  is

$$D(\mathbf{V}, \mathbf{P}) = P_{\text{Error}} = 1 - \frac{1}{|\vec{\mathcal{X}}|} \langle \mathbf{V}, \mathbf{P} \rangle. \quad (\text{B17})$$

*Proof.* Let  $g(\vec{x}) \in |\vec{\mathcal{Y}}|$  be the function that indexes the nonzero row in the  $\vec{x}^{\text{th}}$  column of the deterministic be-

havior  $\mathbf{V}$ , that is,  $V_{\vec{y}|\vec{x}} = \delta_{\vec{y},g(\vec{x})}$ . Then using Eq. (B16),

$$D(\mathbf{V}, \mathbf{P}) = \frac{1}{2^{|\mathcal{X}|}} \sum_{\vec{y}} \sum_{\vec{x}} |\delta_{\vec{y},g(\vec{x})} - P_{\vec{y}|\vec{x}}| \quad (\text{B18})$$

$$= \frac{1}{2^{|\mathcal{X}|}} \sum_{\vec{x}} \left( 1 - P_{g(\vec{x})|\vec{x}} + \sum_{\vec{y} \neq g(\vec{x})} P_{\vec{y}|\vec{x}} \right) \quad (\text{B19})$$

$$= \frac{1}{2^{|\mathcal{X}|}} \sum_{\vec{x}} (1 - P_{g(\vec{x})|\vec{x}} + 1 - P_{g(\vec{x})|\vec{x}}) \quad (\text{B20})$$

$$= \frac{2}{2^{|\mathcal{X}|}} \left( |\mathcal{X}| - \langle \mathbf{V}, \mathbf{P} \rangle \right) \quad (\text{B21})$$

$$= 1 - \frac{1}{|\mathcal{X}|} \langle \mathbf{V}, \mathbf{P} \rangle \quad (\text{B22})$$

$$= 1 - P_{\text{Success}} = P_{\text{Error}} \quad (\text{B23})$$

where we used that  $\sum_{\vec{x}} P_{g(\vec{x})|\vec{x}} = \langle \mathbf{V}, \mathbf{P} \rangle$  in Eq. (B21).  $\square$

### Appendix C: Modeling Classical Communication Networks

In this section, we open up the black box to expose its internal causal structure and communication resources (see Fig. 27(c)). We model the system as a collection of independent black boxes linked into a network by one-way classical communication. The causal structure of the network is represented as a directed acyclic graph (DAG). We refer to the DAG of an arbitrary network as *Net*. If more detail is needed, we use the notation  $\text{Net}(\vec{\mathcal{X}} \xrightarrow{\vec{d}} \vec{\mathcal{Y}})$  to specify the input and output alphabets for the network and the signaling dimension of each link  $\vec{d}$ . The causal structure and communication resources impose constraints on the network's behaviors  $\mathbf{P}^{\text{Net}}: \vec{\mathcal{X}} \rightarrow \vec{\mathcal{Y}}$ . Our aim is to characterize the set of classical network behaviors  $\mathbb{C}^{\text{Net}}$  for general classical communication networks.

Without loss of generality, a network's DAG can be organized into a sequence of time steps that we refer to as a *layers*. In each layer, a collection of nonsignaling devices  $\vec{A} = (A_j)_{j=1}^{|\vec{A}|}$  each operate independently on their local information where we order network layers alphabetically  $\vec{A}, \vec{B}, \vec{C}, \dots$ . Although devices in the same layer are nonsignaling, one-way communication can occur from one layer to another. Since the network layers represent time steps, the layer of the sender device must precede the layer of the receiver, implying a strict causal structure. We assume that communicating devices are connected by a noiseless one-way classical channel  $\mathbb{I}_{\vec{d}}^{\text{Tx} \rightarrow \text{Rx}}$  where Tx and Rx label the respective sender and receiver devices. The signaling dimension  $d$  corresponds to the size of the message alphabet and quantifies the possible amount of information contained in a single message. Unless otherwise specified, we assume that  $d = 2$  such that one bit is sent from the sender to the receiver. The total amount of communication used across one shot of

the network is then characterized by the set of channels in the network's DAG  $\{\mathbb{I}_{\vec{d}_i}^{\text{Tx}_i \rightarrow \text{Rx}_i}\}_{i=1}^M$ .

A network's DAG describes the tensor decomposition of the network's behaviors. Let each device in the network be characterized by a black box behavior  $\mathbf{P}^{A_j}: \mathcal{X}_j \rightarrow \mathcal{A}_j$  where  $x_j \in \mathcal{X}_j$  and  $a_j \in \mathcal{A}_j$  are the classical inputs and outputs passed to the device. Devices within the same layer are combined using the tensor product as follows:

$$\mathbf{P}^{\vec{A}} = \bigotimes_{j=1}^{|\vec{A}|} \mathbf{P}^{A_j} \quad \text{where } \mathbf{P}^{\vec{A}}: \vec{\mathcal{X}} \rightarrow \vec{\mathcal{A}} \quad (\text{C1})$$

where  $\vec{\mathcal{X}} = \mathcal{X}_1 \times \dots \times \mathcal{X}_{|\vec{A}|}$  are the inputs to the layer and  $\vec{\mathcal{A}} = \mathcal{A}_1 \times \dots \times \mathcal{A}_{|\vec{A}|}$  are the layer's outputs (see Fig. 27(a)). Note that all outputs from one layer are input to the next, where communication may pass through a layer without being operated upon by a device. In this case, we model the pass-through communication as a device that performs the identity map  $\mathbf{P}^{A_j} = \mathbb{I}^{A_j}$ . If we let the final layer be labeled as  $\vec{M}$ , the total behavior  $\mathbf{P}^{\text{Net}}$  of the network is given by the matrix product of the sequential layers' behaviors (see Fig. 27(b)),

$$\mathbf{P}^{\text{Net}} = \mathbf{P}^{\vec{M}} \dots \mathbf{S}^{\vec{B} \rightarrow \vec{C}} \mathbf{P}^{\vec{B}} \mathbf{S}^{\vec{A} \rightarrow \vec{B}} \mathbf{P}^{\vec{A}}. \quad (\text{C2})$$

Note that  $\mathbf{S}^{\vec{A} \rightarrow \vec{B}}$  represents the noiseless one-way channels that map each output from one layer to its respective input of the next layer. The network behavior  $\mathbf{P}^{\text{Net}}$  is then the composition of behavior maps

$$\mathbf{P}^{\text{Net}}: \vec{\mathcal{X}} \rightarrow \vec{\mathcal{A}} \rightarrow \vec{\mathcal{B}} \rightarrow \dots \vec{\mathcal{M}} \rightarrow \vec{\mathcal{Y}} \quad (\text{C3})$$

with transition probabilities

$$P_{\vec{y}|\vec{x}}^{\text{Net}} = \dots \sum_{\vec{c} \in \vec{\mathcal{C}}} \sum_{\vec{b} \in \vec{\mathcal{B}}} \sum_{\vec{a} \in \vec{\mathcal{A}}} \dots P_{\vec{c}|\vec{b}}^{\vec{C}} P_{\vec{b}|\vec{a}}^{\vec{B}} P_{\vec{a}|\vec{x}}^{\vec{A}}. \quad (\text{C4})$$

Without loss of generality, the network's input  $\vec{\mathcal{X}}$  is passed to the first layer and the network's output  $\vec{\mathcal{Y}}$  is output by the last layer because the inputs and outputs can be passed through layers using identity maps.

The set of classical network behaviors is defined as

$$\mathbb{C}^{\text{Net}} \equiv \left\{ \mathbf{P}^{\text{Net}} \in \mathbb{P}_{\vec{\mathcal{Y}}|\vec{\mathcal{X}}} \mid \mathbf{P}^{\text{Net}} \text{ satisfies Eq. (C2)} \right\} \quad (\text{C5})$$

where each network DAG gives a unique tensor decomposition for the behavior  $\mathbf{P}^{\text{Net}}$ . Taking a resource-theoretic perspective [83], the links in a network's DAG describe a fixed set of communication resources on which the nodes may freely apply local operations. The set of classical network behaviors  $\mathbb{C}^{\text{Net}}$  then characterizes the set of operations that can be implemented using the fixed set of resources and free operations local to each device. Since each device in the network is modeled as a black box, the free operations of device  $A_j$  are the probability polytope  $\mathbb{P}_{\mathcal{A}_j|\mathcal{X}_j}$ . Hence, no restrictions are placed on the local free operations of each device, and any constraints on the set of classical network behaviors  $\mathbb{C}^{\text{Net}}$  result from constraints on the network's communication resources.



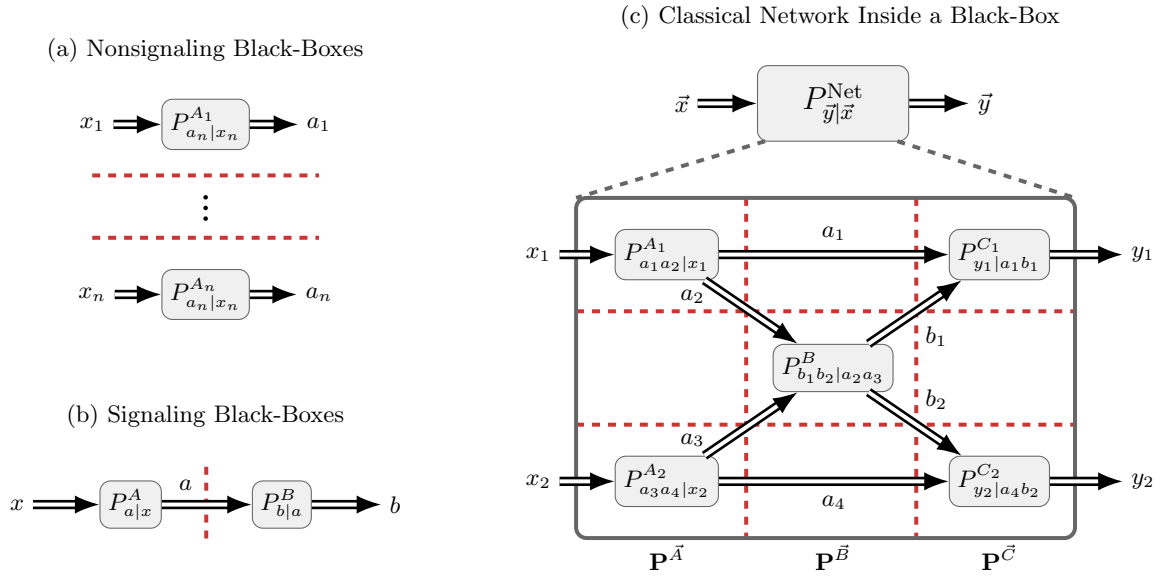


**FIG. 27:** DAGs depicting classical communication networks and their associated tensor calculus. (a) The behaviors of the nonsignaling devices in each layer combine via the tensor product  $\mathbf{P}^{\vec{A}} = \bigotimes_{i=1}^n \mathbf{P}^{A_i}$ . (b) The behaviors of one device signaling to another combine via the matrix product  $\mathbf{P}^{AB} = \mathbf{P}^B \mathbf{P}^A$ . (c) The causal structure inside of a black-box is exposed as a DAG. Time flows from left to right where vertical red dashed lines separate the network into layers and the horizontal dashed red lines show the independence of devices in each layer. The behavior for this network decomposes as

$$\mathbf{P}^{\text{Net}} = (\mathbf{P}^{C_1} \otimes \mathbf{P}^{C_2})(\mathbb{I}_{d_1} \otimes \mathbf{P}^B \otimes \mathbb{I}_{d_4})(\mathbf{P}^{A_1} \otimes \mathbf{P}^{A_2}).$$

#### Appendix D: Facet Inequalities for Multipoint Networks

$$\begin{array}{l}
13 \geq \mathbf{F}_{\text{IF}}^{\times_0} = \begin{bmatrix} 1 & 2 & 1 & 3 & 0 & 1 & 0 & 0 & 1 \\ 1 & 0 & 0 & 1 & 3 & 0 & 0 & 1 & 2 \\ 1 & 0 & 0 & 1 & 1 & 3 & 0 & 2 & 0 \\ 0 & 1 & 1 & 0 & 1 & 2 & 1 & 1 & 2 \\ 0 & 1 & 1 & 0 & 1 & 2 & 1 & 1 & 2 \\ 0 & 1 & 1 & 1 & 1 & 2 & 1 & 1 & 2 \\ 1 & 0 & 0 & 1 & 3 & 1 & 0 & 0 & 2 \\ 1 & 1 & 0 & 1 & 1 & 2 & 0 & 1 & 2 \\ 1 & 1 & 1 & 2 & 2 & 2 & 1 & 1 & 1 \end{bmatrix} \\
14 \geq \mathbf{F}_{\text{IF}}^+ = \begin{bmatrix} 3 & 0 & 1 & 0 & 2 & 1 & 1 & 0 & 1 \\ 0 & 3 & 0 & 2 & 0 & 0 & 1 & 0 & 1 \\ 0 & 0 & 4 & 0 & 2 & 1 & 2 & 0 & 0 \\ 2 & 1 & 2 & 0 & 0 & 3 & 0 & 2 & 0 \\ 1 & 0 & 3 & 1 & 1 & 2 & 1 & 1 & 1 \\ 1 & 2 & 2 & 1 & 1 & 2 & 0 & 1 & 1 \\ 2 & 1 & 2 & 0 & 2 & 1 & 0 & 0 & 1 \\ 1 & 1 & 3 & 0 & 2 & 1 & 1 & 0 & 1 \\ 2 & 2 & 3 & 1 & 1 & 2 & 1 & 1 & 0 \end{bmatrix} \\
12 \geq \mathbf{F}_{\text{IF}}^{\searrow} = \begin{bmatrix} 2 & 0 & 0 & 0 & 3 & 0 & 0 & 0 & 1 \\ 0 & 1 & 1 & 1 & 0 & 3 & 1 & 1 & 0 \\ 1 & 1 & 1 & 0 & 0 & 3 & 0 & 1 & 0 \\ 0 & 2 & 1 & 0 & 2 & 2 & 1 & 0 & 1 \\ 1 & 1 & 1 & 0 & 0 & 3 & 1 & 1 & 0 \\ 0 & 3 & 1 & 0 & 1 & 3 & 1 & 0 & 0 \\ 1 & 2 & 1 & 1 & 1 & 2 & 0 & 0 & 1 \\ 0 & 1 & 2 & 2 & 0 & 1 & 1 & 1 & 0 \\ 1 & 2 & 2 & 1 & 2 & 2 & 1 & 0 & 0 \end{bmatrix} \\
13 \geq \mathbf{F}_{\text{IF}}^{\leftrightarrow} = \begin{bmatrix} 3 & 0 & 0 & 0 & 2 & 0 & 1 & 0 & 1 \\ 1 & 1 & 2 & 2 & 0 & 0 & 1 & 0 & 1 \\ 0 & 1 & 3 & 0 & 1 & 1 & 2 & 0 & 0 \\ 0 & 3 & 0 & 2 & 0 & 0 & 0 & 1 & 1 \\ 1 & 1 & 2 & 0 & 2 & 0 & 0 & 1 & 1 \\ 1 & 0 & 3 & 1 & 0 & 1 & 0 & 2 & 0 \\ 0 & 0 & 4 & 1 & 1 & 0 & 1 & 1 & 0 \\ 1 & 2 & 2 & 0 & 0 & 2 & 1 & 1 & 0 \\ 2 & 2 & 3 & 1 & 1 & 1 & 1 & 1 & 0 \end{bmatrix}
\end{array}$$

$$\begin{array}{l}
13 \geq \mathbf{F}_{\text{IF}}^{\times_1} = \begin{bmatrix} 3 & 0 & 1 & 0 & 2 & 1 & 1 & 0 & 1 \\ 0 & 3 & 0 & 2 & 0 & 0 & 1 & 0 & 1 \\ 0 & 0 & 4 & 0 & 2 & 1 & 2 & 0 & 0 \\ 2 & 1 & 2 & 0 & 2 & 1 & 0 & 1 & 1 \\ 2 & 1 & 2 & 1 & 1 & 2 & 0 & 1 & 1 \\ 2 & 1 & 2 & 0 & 0 & 3 & 0 & 2 & 0 \\ 2 & 1 & 2 & 0 & 2 & 1 & 0 & 0 & 1 \\ 2 & 1 & 2 & 0 & 2 & 1 & 0 & 0 & 1 \\ 2 & 2 & 3 & 1 & 1 & 2 & 1 & 1 & 0 \end{bmatrix} \\
11 \geq \mathbf{F}_{\text{IF}}^- = \begin{bmatrix} 2 & 0 & 0 & 0 & 2 & 0 & 1 & 0 & 1 \\ 0 & 0 & 2 & 1 & 1 & 2 & 1 & 0 & 1 \\ 1 & 0 & 2 & 0 & 0 & 2 & 1 & 0 & 1 \\ 0 & 0 & 2 & 1 & 1 & 2 & 1 & 0 & 1 \\ 0 & 0 & 2 & 2 & 0 & 2 & 0 & 1 & 0 \\ 0 & 0 & 2 & 2 & 1 & 2 & 0 & 0 & 1 \\ 1 & 0 & 2 & 0 & 0 & 2 & 1 & 0 & 1 \\ 0 & 0 & 2 & 2 & 1 & 2 & 0 & 0 & 1 \\ 1 & 1 & 3 & 1 & 1 & 2 & 1 & 0 & 0 \end{bmatrix} \\
13 \geq \mathbf{F}_{\text{IF}}^{\pi} = \begin{bmatrix} 3 & 0 & 0 & 0 & 1 & 1 & 0 & 1 & 1 \\ 0 & 3 & 2 & 1 & 0 & 1 & 0 & 0 & 1 \\ 0 & 0 & 4 & 1 & 1 & 1 & 0 & 1 & 0 \\ 1 & 1 & 2 & 1 & 2 & 0 & 0 & 1 & 1 \\ 1 & 2 & 2 & 1 & 0 & 3 & 0 & 1 & 0 \\ 1 & 2 & 2 & 2 & 0 & 0 & 0 & 0 & 1 \\ 1 & 2 & 2 & 1 & 1 & 1 & 0 & 1 & 1 \\ 0 & 1 & 3 & 0 & 1 & 2 & 1 & 0 & 0 \\ 2 & 2 & 3 & 1 & 1 & 2 & 0 & 1 & 0 \end{bmatrix} \\
13 \geq \mathbf{F}_{\text{IF}}^{\text{CV}} = \begin{bmatrix} 3 & 0 & 0 & 0 & 2 & 0 & 1 & 0 & 1 \\ 0 & 3 & 0 & 2 & 0 & 0 & 0 & 1 & 1 \\ 0 & 0 & 4 & 1 & 1 & 0 & 1 & 1 & 0 \\ 1 & 1 & 2 & 2 & 0 & 0 & 1 & 0 & 1 \\ 1 & 1 & 2 & 0 & 2 & 0 & 0 & 1 & 1 \\ 1 & 2 & 2 & 0 & 0 & 2 & 1 & 1 & 0 \\ 0 & 1 & 3 & 0 & 1 & 1 & 2 & 0 & 0 \\ 1 & 0 & 3 & 1 & 0 & 1 & 0 & 2 & 0 \\ 2 & 2 & 3 & 1 & 1 & 1 & 1 & 1 & 0 \end{bmatrix}
\end{array}$$

**TABLE XIII:** Derived nonclassicality witnesses for the interference network. Each inequality  $(\gamma, \mathbf{G})$  is expressed as  $\gamma \geq \mathbf{G}$ .



$$\begin{array}{l}
11 \geq \mathbf{F}_{\text{BF}}^{\times_0} = \begin{bmatrix} 1 & 3 & 1 & 1 & 0 & 0 & 1 & 0 & 0 \\ 0 & 0 & 0 & 1 & 2 & 0 & 1 & 0 & 1 \\ 0 & 1 & 0 & 0 & 0 & 1 & 0 & 2 & 0 \\ 0 & 2 & 1 & 0 & 1 & 1 & 0 & 1 & 1 \\ 0 & 1 & 0 & 1 & 2 & 0 & 0 & 0 & 2 \\ 0 & 2 & 1 & 1 & 1 & 1 & 0 & 1 & 1 \\ 0 & 2 & 1 & 0 & 1 & 1 & 0 & 1 & 1 \\ 0 & 0 & 0 & 1 & 1 & 0 & 1 & 0 & 1 \\ 1 & 2 & 1 & 1 & 1 & 1 & 1 & 1 & 1 \end{bmatrix} \\
11 \geq \mathbf{F}_{\text{BF}}^{\times_1} = \begin{bmatrix} 2 & 0 & 1 & 1 & 0 & 0 & 0 & 0 & 0 \\ 0 & 1 & 1 & 3 & 0 & 0 & 0 & 0 & 0 \\ 0 & 0 & 1 & 1 & 0 & 0 & 2 & 0 & 0 \\ 1 & 0 & 1 & 0 & 1 & 1 & 0 & 1 & 0 \\ 0 & 1 & 1 & 1 & 0 & 2 & 0 & 1 & 0 \\ 0 & 0 & 1 & 1 & 0 & 2 & 0 & 2 & 0 \\ 1 & 1 & 1 & 1 & 1 & 1 & 0 & 0 & 1 \\ 0 & 1 & 0 & 2 & 1 & 1 & 1 & 0 & 1 \\ 1 & 1 & 1 & 2 & 1 & 1 & 1 & 1 & 1 \end{bmatrix} \\
10 \geq \mathbf{F}_{\text{BF}}^+ = \begin{bmatrix} 1 & 0 & 1 & 0 & 1 & 1 & 1 & 1 & 0 \\ 0 & 2 & 0 & 1 & 0 & 0 & 0 & 0 & 2 \\ 1 & 1 & 2 & 0 & 1 & 1 & 1 & 1 & 1 \\ 0 & 1 & 1 & 0 & 0 & 2 & 1 & 1 & 0 \\ 0 & 1 & 0 & 0 & 0 & 0 & 0 & 0 & 2 \\ 0 & 1 & 2 & 0 & 0 & 1 & 1 & 1 & 1 \\ 1 & 0 & 1 & 0 & 1 & 1 & 1 & 1 & 1 \\ 0 & 1 & 0 & 1 & 0 & 0 & 0 & 0 & 2 \\ 1 & 1 & 2 & 0 & 1 & 1 & 1 & 1 & 1 \end{bmatrix} \\
12 \geq \mathbf{F}_{\text{BF}}^- = \begin{bmatrix} 3 & 0 & 0 & 0 & 2 & 0 & 0 & 1 & 1 \\ 1 & 0 & 0 & 1 & 1 & 0 & 0 & 1 & 1 \\ 2 & 0 & 0 & 0 & 1 & 0 & 0 & 0 & 1 \\ 2 & 0 & 1 & 0 & 0 & 2 & 0 & 1 & 0 \\ 1 & 0 & 1 & 2 & 0 & 1 & 0 & 2 & 0 \\ 2 & 1 & 1 & 1 & 1 & 2 & 0 & 1 & 0 \\ 1 & 0 & 0 & 0 & 0 & 1 & 0 & 1 & 1 \\ 0 & 0 & 1 & 1 & 0 & 2 & 0 & 1 & 1 \\ 2 & 1 & 2 & 1 & 1 & 2 & 1 & 1 & 0 \end{bmatrix} \\
14 \geq \mathbf{F}_{\text{BF}}^{\curvearrowright} = \begin{bmatrix} 3 & 0 & 0 & 0 & 2 & 0 & 1 & 0 & 1 \\ 2 & 1 & 0 & 0 & 1 & 0 & 1 & 1 & 1 \\ 2 & 1 & 1 & 0 & 0 & 1 & 0 & 1 & 0 \\ 1 & 1 & 2 & 0 & 0 & 2 & 0 & 1 & 1 \\ 0 & 2 & 2 & 0 & 0 & 2 & 0 & 1 & 1 \\ 0 & 3 & 2 & 0 & 0 & 3 & 0 & 0 & 0 \\ 1 & 1 & 2 & 0 & 1 & 1 & 1 & 1 & 0 \\ 1 & 2 & 2 & 1 & 1 & 1 & 1 & 1 & 0 \\ 2 & 2 & 3 & 1 & 1 & 2 & 1 & 1 & 0 \end{bmatrix} \\
20 \geq \mathbf{F}_{\text{BF}}^{\pi} = \begin{bmatrix} 2 & 1 & 0 & 1 & 3 & 0 & 1 & 1 & 2 \\ 1 & 5 & 2 & 0 & 0 & 2 & 1 & 1 & 0 \\ 0 & 3 & 3 & 1 & 3 & 3 & 0 & 2 & 0 \\ 1 & 2 & 0 & 1 & 4 & 0 & 1 & 0 & 2 \\ 0 & 3 & 1 & 1 & 1 & 3 & 1 & 1 & 0 \\ 0 & 3 & 3 & 2 & 1 & 2 & 0 & 1 & 0 \\ 1 & 0 & 0 & 1 & 3 & 0 & 1 & 1 & 1 \\ 0 & 3 & 1 & 0 & 0 & 2 & 2 & 1 & 1 \\ 2 & 3 & 3 & 1 & 3 & 3 & 1 & 2 & 0 \end{bmatrix} \\
12 \geq \mathbf{F}_{\text{BF}}^{\leftrightarrow} = \begin{bmatrix} 2 & 0 & 1 & 0 & 0 & 1 & 0 & 1 & 0 \\ 0 & 0 & 1 & 2 & 0 & 1 & 0 & 1 & 0 \\ 1 & 0 & 1 & 1 & 1 & 1 & 1 & 1 & 1 \\ 0 & 2 & 0 & 0 & 0 & 1 & 1 & 0 & 0 \\ 0 & 0 & 1 & 0 & 2 & 0 & 1 & 0 & 0 \\ 0 & 1 & 1 & 1 & 1 & 1 & 0 & 1 & 1 \\ 0 & 0 & 3 & 0 & 0 & 2 & 0 & 1 & 0 \\ 0 & 0 & 2 & 0 & 0 & 3 & 0 & 1 & 0 \\ 1 & 1 & 2 & 1 & 1 & 2 & 1 & 1 & 1 \end{bmatrix} \\
18 \geq \mathbf{F}_{\text{BF}}^{\text{CV}} = \begin{bmatrix} 3 & 0 & 1 & 0 & 3 & 1 & 0 & 0 & 0 \\ 1 & 3 & 0 & 0 & 3 & 1 & 0 & 0 & 0 \\ 0 & 0 & 3 & 0 & 4 & 1 & 0 & 0 & 1 \\ 1 & 0 & 1 & 3 & 2 & 1 & 0 & 0 & 0 \\ 3 & 1 & 1 & 1 & 3 & 0 & 0 & 0 & 0 \\ 3 & 1 & 2 & 0 & 0 & 2 & 0 & 0 & 1 \\ 0 & 0 & 1 & 0 & 3 & 1 & 2 & 1 & 1 \\ 2 & 0 & 1 & 0 & 0 & 1 & 2 & 1 & 1 \\ 4 & 1 & 2 & 1 & 4 & 1 & 1 & 0 & 0 \end{bmatrix}
\end{array}$$

**TABLE XV:** Derived nonclassicality witnesses for the butterfly network. Each inequality  $(\gamma, \mathbf{G})$  is expressed as  $\gamma \geq \mathbf{G}$ .

$$\begin{array}{l}
16 \geq \mathbf{F}_{\text{HG}}^{\times_0} = \begin{bmatrix} 2 & 2 & 2 & 2 & 1 & 0 & 2 & 0 & 2 \\ 1 & 1 & 1 & 1 & 2 & 0 & 1 & 1 & 2 \\ 0 & 0 & 0 & 0 & 0 & 2 & 0 & 2 & 0 \\ 1 & 1 & 1 & 1 & 1 & 1 & 2 & 1 & 2 \\ 1 & 2 & 1 & 1 & 2 & 0 & 1 & 0 & 3 \\ 1 & 2 & 1 & 1 & 1 & 1 & 1 & 1 & 2 \\ 0 & 0 & 1 & 1 & 2 & 0 & 1 & 0 & 2 \\ 1 & 1 & 1 & 2 & 2 & 1 & 2 & 1 & 2 \\ 1 & 2 & 2 & 2 & 2 & 1 & 2 & 1 & 2 \end{bmatrix} \\
13 \geq \mathbf{F}_{\text{HG}}^{\times_1} = \begin{bmatrix} 3 & 0 & 0 & 1 & 1 & 0 & 0 & 0 & 1 \\ 0 & 3 & 0 & 2 & 0 & 0 & 0 & 0 & 1 \\ 1 & 1 & 2 & 1 & 0 & 0 & 1 & 1 & 1 \\ 2 & 1 & 0 & 0 & 1 & 1 & 0 & 1 & 1 \\ 0 & 2 & 0 & 1 & 0 & 1 & 0 & 1 & 1 \\ 1 & 1 & 1 & 0 & 0 & 2 & 1 & 2 & 0 \\ 2 & 0 & 0 & 1 & 1 & 1 & 0 & 1 & 1 \\ 0 & 2 & 0 & 1 & 1 & 0 & 0 & 1 & 1 \\ 2 & 2 & 2 & 1 & 1 & 1 & 1 & 1 & 1 \end{bmatrix} \\
13 \geq \mathbf{F}_{\text{HG}}^{\leftrightarrow} = \begin{bmatrix} 2 & 0 & 0 & 0 & 1 & 0 & 0 & 0 & 1 \\ 0 & 0 & 0 & 2 & 0 & 0 & 0 & 0 & 1 \\ 0 & 1 & 0 & 0 & 1 & 0 & 2 & 2 & 1 \\ 0 & 2 & 0 & 1 & 0 & 0 & 0 & 0 & 1 \\ 0 & 0 & 0 & 0 & 2 & 0 & 0 & 0 & 1 \\ 1 & 0 & 0 & 1 & 0 & 0 & 2 & 2 & 1 \\ 0 & 0 & 2 & 1 & 1 & 2 & 0 & 0 & 1 \\ 1 & 1 & 2 & 0 & 0 & 2 & 0 & 0 & 1 \\ 1 & 1 & 2 & 1 & 1 & 2 & 2 & 2 & 0 \end{bmatrix} \\
10 \geq \mathbf{F}_{\text{HG}}^+ = \begin{bmatrix} 2 & 0 & 0 & 0 & 0 & 2 & 0 & 1 & 0 \\ 0 & 2 & 0 & 2 & 1 & 0 & 0 & 0 & 1 \\ 0 & 1 & 2 & 1 & 2 & 1 & 1 & 0 & 0 \\ 2 & 0 & 0 & 0 & 0 & 2 & 0 & 1 & 0 \\ 0 & 2 & 0 & 1 & 1 & 1 & 0 & 0 & 1 \\ 0 & 1 & 2 & 1 & 1 & 1 & 1 & 0 & 0 \\ 2 & 0 & 0 & 0 & 0 & 2 & 0 & 1 & 0 \\ 0 & 1 & 0 & 2 & 1 & 0 & 0 & 0 & 1 \\ 1 & 1 & 2 & 1 & 2 & 1 & 1 & 0 & 0 \end{bmatrix} \\
9 \geq \mathbf{F}_{\text{HG}}^{\triangleright} = \begin{bmatrix} 2 & 0 & 0 & 0 & 2 & 0 & 0 & 0 & 1 \\ 0 & 0 & 1 & 1 & 1 & 1 & 0 & 1 & 0 \\ 1 & 0 & 0 & 0 & 1 & 2 & 1 & 0 & 0 \\ 1 & 0 & 0 & 0 & 0 & 2 & 0 & 0 & 1 \\ 0 & 0 & 1 & 1 & 0 & 2 & 0 & 1 & 0 \\ 1 & 1 & 1 & 0 & 1 & 2 & 1 & 0 & 0 \\ 1 & 0 & 0 & 0 & 1 & 1 & 0 & 0 & 1 \\ 0 & 0 & 1 & 2 & 0 & 1 & 0 & 1 & 0 \\ 1 & 1 & 1 & 1 & 1 & 2 & 1 & 0 & 0 \end{bmatrix} \\
10 \geq \mathbf{F}_{\text{HG}}^{\pi} = \begin{bmatrix} 2 & 0 & 0 & 1 & 1 & 1 & 0 & 0 & 1 \\ 0 & 2 & 0 & 0 & 0 & 2 & 1 & 0 & 0 \\ 1 & 0 & 2 & 1 & 1 & 1 & 0 & 1 & 0 \\ 1 & 0 & 0 & 1 & 2 & 0 & 0 & 0 & 1 \\ 0 & 2 & 0 & 0 & 0 & 2 & 1 & 0 & 0 \\ 1 & 1 & 2 & 2 & 1 & 1 & 0 & 1 & 0 \\ 1 & 0 & 0 & 1 & 2 & 0 & 0 & 0 & 1 \\ 0 & 2 & 0 & 0 & 0 & 2 & 1 & 0 & 0 \\ 1 & 1 & 2 & 2 & 1 & 1 & 0 & 1 & 0 \end{bmatrix} \\
8 \geq \mathbf{F}_{\text{HG}}^- = \begin{bmatrix} 2 & 0 & 0 & 0 & 1 & 0 & 0 & 0 & 1 \\ 1 & 0 & 0 & 1 & 0 & 1 & 0 & 0 & 1 \\ 1 & 0 & 0 & 0 & 0 & 1 & 0 & 0 & 1 \\ 1 & 0 & 0 & 1 & 0 & 1 & 0 & 0 & 1 \\ 0 & 0 & 1 & 2 & 0 & 1 & 0 & 1 & 0 \\ 0 & 0 & 1 & 1 & 0 & 2 & 0 & 0 & 0 \\ 1 & 0 & 0 & 0 & 0 & 1 & 0 & 0 & 1 \\ 0 & 0 & 1 & 1 & 0 & 2 & 0 & 0 & 0 \\ 1 & 1 & 1 & 1 & 0 & 2 & 1 & 0 & 0 \end{bmatrix} \\
13 \geq \mathbf{F}_{\text{HG}}^{\text{CV}} = \begin{bmatrix} 2 & 0 & 0 & 0 & 1 & 0 & 0 & 0 & 1 \\ 0 & 2 & 0 & 1 & 0 & 0 & 0 & 0 & 1 \\ 0 & 0 & 2 & 1 & 1 & 2 & 0 & 0 & 1 \\ 0 & 0 & 0 & 2 & 0 & 0 & 0 & 0 & 1 \\ 0 & 0 & 0 & 0 & 2 & 0 & 0 & 0 & 1 \\ 1 & 1 & 2 & 0 & 0 & 2 & 0 & 0 & 1 \\ 0 & 1 & 0 & 0 & 1 & 0 & 2 & 2 & 1 \\ 1 & 0 & 0 & 1 & 0 & 0 & 2 & 2 & 1 \\ 1 & 1 & 2 & 1 & 1 & 2 & 2 & 2 & 0 \end{bmatrix}
\end{array}$$

**TABLE XVI:** Facet inequalities for the hourglass (HG) network. Each inequality  $(\gamma, \mathbf{F})$  is presented as  $\gamma \geq \mathbf{F}$ .